

## AN ABSTRACT OF THE THESIS OF

Maureen Anne Mathias for the degree of Master of Science in Civil Engineering presented on September 26, 2002. Title: Modeling Cometabolic Transformation of a CAH Mixture by a Butane Utilizing Culture.

Abstract approved: ✓

Redacted for privacy

✓ Lewis Semprini ✓

The goal of this research was to mathematically simulate the ability of bioaugmented microorganisms to aerobically cometabolize a mixture of chlorinated aliphatic hydrocarbon (CAH) compounds during in-situ treatment. Parameter values measured from laboratory experiments were applied to the transport model with biotransformation processes included. In laboratory microcosm studies, a butane-grown, enriched culture was inoculated in soil and groundwater microcosms and exposed to butane and several repeated additions of 1,1,1-trichloroethane (TCA), 1,1-dichloroethylene (DCE), and 1,1-dichloroethane (DCA) at aqueous concentrations of 200 µg/L, 100 µg/L, and 200 µg/L, respectively. Microcosms containing the bioaugmented culture showed 1,1-DCE to be rapidly transformed, followed by slower transformation of 1,1-DCA and 1,1,1-TCA. After most of the butane had been consumed, transformation of these latter CAHs increased, indicating strong inhibition by butane. With repeat biostimulations, butane utilization and CAH transformation accelerated, showing the increase in cell mass. These trends occurred in two sets of microcosm triplicates. No stimulation was observed in controls containing only the microorganisms indigenous to Moffett Field, confirming that activity seen in the bioaugmented microcosms was a result of the introduced culture's activity.

Batch reactor results were simulated using differential equations accounting for Michaelis-Menten kinetics, transformation product toxicity, substrate inhibition, butane utilization, and CAH transformation. The equations were solved simultaneously by

Runge-Kutta numerical integration with parameter values adjusted to match the microcosm data.

Having defined the parameter values from laboratory studies, the biotransformation model was combined with 1-D advective-dispersive transport to simulate behavior of the culture and the substrates within an aquifer. The model was used to simulate the results of field studies where the butane-utilizing culture was injected into a 7 m subsurface test site and exposed to alternating pulses of oxygen and butane, along with the contaminant mixture studied in the microcosms. Monitoring wells spaced at 1 m, 2.2 m, and 4 m from the injection well allowed temporal and spatial changes in substrate concentrations to be determined. Model simulations of the field demonstration were performed to determine how well the biotransformation/solute transport model predicted actual field observations.

To model the influences of solute transport, simulations were run and compared to breakthrough test data (prior to bioaugmentation) to determine the values for advection, dispersion, and sorption. The simulations showed that flow ranged from 1.0 to 1.5 m<sup>3</sup>/day (average linear velocity of 2.0 m/day). Dispersion was estimated as 0.31 m<sup>2</sup>/day. Sediment sorption partitioning coefficients for 1,1-DCE, 1,1,-DCA, and 1,1,1,-TCA were determined to be approximately 0.69, 0.50, and 0.50 L/kg, respectively. It was more difficult to determine an appropriate value of the mass transfer rate coefficient for non-equilibrium sorption, so simulations were run to compare equilibrium and non-equilibrium cases. Results indicated that non-equilibrium (with mass transfer rate coefficient of approximately 0.2 day<sup>-1</sup>) better simulated the field data.

Using these transport parameters and the biotransformation values determined from the laboratory experiments, simulations of the field data showed that the model was capable of simulating the effects of transformation rates, butane inhibition, and 1,1-DCE product toxicity. Simulations for varying pulsing cycles and durations provided possible improvements for future field demonstrations.

Overall, this work proved that there is good potential in extrapolating laboratory based kinetics to simulate biotransformation at a field scale. Although the complexity of such systems makes modeling difficult, such simulations are useful in understanding and interpreting field data.

Modeling Cometabolic Transformation of a CAH Mixture by a Butane Utilizing  
Culture

by  
Maureen Anne Mathias

A THESIS

submitted to

Oregon State University

in partial fulfillment of  
the requirements for the  
degree of

Master of Science

Presented September 26, 2002

Commencement June, 2003

Master of Science thesis of Maureen Anne Mathias presented on September 26, 2002

APPROVED:

<sup>^</sup>  
Redacted for privacy

\_\_\_\_\_  
Major Professor, representing Civil Engineering

Redacted for privacy

\_\_\_\_\_  
Head of Department of Civil, Construction, and Environmental Engineering

Redacted for privacy

\_\_\_\_\_  
Dean of the Graduate School

I understand that my thesis will become part of the permanent collection of Oregon State University libraries. My signature below authorizes release of my thesis to any reader upon request.

Redacted for privacy

\_\_\_\_\_  
Maureen Anne Mathias, Author

## ACKNOWLEDGEMENTS

“All you need is confidence and ignorance, and success is assured.”

-Albert Einstein

“The sun shines not on us, but in us.”

-John Muir

These are two quotes which inspired me throughout my thesis work, stated by two very different individuals whose reputation for fascination and mischievousness have inspired me throughout my life.

Along with these highly-motivated individuals, I would like to recognize Dr. Lewis Semprini, who not only provided me an opportunity to delve into my secret passion of manipulating differential equations, but kept me laughing and challenged throughout the experience. Thank you for sharing your knowledge and enthusiasm for bioremediation strategies. You have continuously impressed me with your memory, intuition, and persistence.

Thank you also to Dr. Mark Dolan, whose approachable manner and sharp mind kept me confident and sane throughout the oh-so-long hours of laboratory experiments and data analysis. Thank you for your patience in sharing your knowledge of laboratory methods and equipment. Thank you, also, for proving as a great mentor in being practical and helping me focus on positive outcome, rather than fretting over mistakes that have been made.

I would also like to thank Dr. Brian Wood for assisting in my defense and thesis work. Thank you for helping me appreciate attention to detail and view organization as a “talent”. I believe the department made a great choice in bringing you on as a new professor. A sure sign of great things to come.

Thank you to Dr. Jon Kimerling for acting as graduate representative on my committee.

Great recognition is due to all of Dr. Semprini's graduate students, particularly Seung Ho, George, Sarun, and Hee Lim, and Dr. Young Kim and Dr. Mohammad Azizinan for sharing their knowledge (and equipment!) in the laboratory. You are all extraordinary people, and I have so much enjoyed getting to know you and sharing stories, whether or not they be about biotransformation!

I would like to acknowledge my fellow Merryfield peers, who sympathized with me when I needed it, laughed at me when I didn't, and in most other cases took me out for beers to celebrate life. Thank you for sharing your projects, homework, interests and life stories with me. Happy adventures to you all.

Last but not least (that phrase is for Mom), I thank my family for being all that you are: hopeful, caring, practical, and goofy. Mom, Dad, Beth, John, and Lee, thank you for your never-ending love, support, understanding, and encouragement. And all the chocolate you've shared with me over the years!

## TABLE OF CONTENTS

	<u>Page</u>
CHAPTER 1: INTRODUCTION AND LITERATURE REVIEW.....	1
1.1 Overview.....	1
1.2 Why CAHs are of Concern.....	2
1.3 Aerobic Cometabolism of CAHs by Microorganisms.....	3
1.3.1 Butane as an Electron Donor/Primary Growth Substrate.....	4
1.3.2 Transformation of 1,1-DCE, 1,1-DCA, and 1,1,1-TCA.....	5
1.4 Processes Influencing Cometabolism and Bioremediation.....	6
1.4.1 Product Toxicity.....	6
1.4.2 Substrate Inhibition.....	7
1.4.3 Solute Transport.....	8
1.5 Combined Biotransformation and Transport Models.....	9
1.6 Objectives of This Thesis.....	10
CHAPTER 2: MODEL PRESENTATION.....	12
2.1 Modeling Biotransformation.....	13
2.1.1 Monod/Michaelis-Menten Kinetics.....	13
2.1.2 Modeling Substrate Inhibition.....	15
2.1.3 Modeling Product Toxicity.....	17
2.2 Modeling Contaminant Transport.....	18
2.3 Combined Biotransformation and Transport Model.....	19
2.4 Verification of Model Performance.....	23
2.4.1 Comparison of Model Output for Contaminant Transport.....	24
2.4.2 Comparison of Model Output for Biotransformation in Batch Reactors.....	28

## TABLE OF CONTENTS, CONTINUED

	<u>Page</u>
CHAPTER 3: LABORATORY METHODS FOR MEDIA AND MICROCOSM EXPERIMENTS.....	33
3.1 Chemical Sources.....	33
3.2 Growth of the Butane Culture for Bioaugmentation.....	34
3.3 Batch Transformation Kinetic Tests in Media.....	36
3.4 Batch Transformation Kinetic Tests in Microcosm.....	36
3.4.1 Preparation.....	37
3.4.2 Biotransformation Analysis.....	39
3.4.3 Mass Transfer Limitation Study.....	40
3.4.4 1,1-DCE Product Toxicity Experiment.....	41
3.5 Headspace Gas Analysis.....	43
CHAPTER 4: RESULTS OF MEDIA AND MICROCOSM EXPERIMENTS AND MODEL SIMULATIONS.....	44
4.1 Comparison of Laboratory Data and Model Simulation from Media Experiments .....	44
4.2 Comparison of Laboratory Data and Model Simulation from Microcosm Experiments.....	51
4.2.1 Results from Microcosms with Indigenous Microorganisms (M1) and Mercury Killed Controls (M4).....	51
4.2.2 Laboratory Data from Bioaugmented Culture Exposed to Butane and CAHs (M2, M3).....	54
4.2.3 1,1-DCE Transformation Capacity Experiments in Microcosm.....	57
4.2.4 Results of the Mass Transfer Limitation Studies.....	64
4.2.5 Results and Modeling of Butane in the Absence of CAHs.....	67
4.2.6 Model Simulations for Biotransformation in Microcosm M2B.....	73
4.3 Summary of Laboratory Experiments and Simulations.....	81



## TABLE OF CONTENTS, CONTINUED

	<u>Page</u>
CHAPTER 5: RESULTS OF MODELING FIELD DATA.....	83
5.1 Field Experiment.....	83
5.2 Determination of Flow.....	86
5.3 Determination of Sorption Parameter Values.....	90
5.4 Interpretation of Biotransformation/Transport Field Data.....	96
5.5 Modeling of Biotransformation/Transport Field Data.....	109
5.5.1 Simulation of Field Bioaugmentation Data.....	112
5.5.2 Simulations to Predict Activity after Bioaugmentation.....	119
5.5.3 Sensitivity Analysis of 1,1-DCE Product Toxicity.....	123
5.5.4 Sensitivity of 1,1-DCE Transformation Rate.....	127
5.5.5 Sensitivity of First Order Mass Transfer Rate and Pulsing Cycles.....	130
5.6 Summary of Field Modeling.....	136
CHAPTER 6: CONCLUSIONS.....	138
BIBLIOGRAPHY.....	142
APPENDICES.....	147

## LIST OF FIGURES

<u>FIGURE</u>		<u>PAGE</u>
1.1	Fate of 1,1,1-TCA	5
2.1	Comparison of Model Output for Solute Transport	27
2.2	Comparison of Model Output for Biotransformation	31
2.3	Comparison of Model Output for Biotransformation with High 1,1-TCA Product Toxicity	32
4.1	Media Biotransformation Experiment Data	45
4.2	Biotransformation Activity in Media Reactors	46
4.3a	Media Experiment Data and Model Output using Kim's ( <i>in press</i> ) Data	50
4.3b	Media Data and Model Output using Adjusted Input Values	50
4.4	Laboratory Data for M1 (Indigenous Culture)	52
4.5	Laboratory Data for M4 (Mercury Killed Control)	53
4.6	Microcosm M2B Experimental Data	55
4.7	Results of Biotransformation Experiments for Microcosms M2 and M3	56
4.8	Simulations of Butane Utilization prior to 1,1-DCE Transformation Capacity Experiments	58
4.9	Results of Transformation Capacity Experiments of 1,1-DCE	60
4.10	Simulations for Various $k_{mDCE}$ Values Compared to Laboratory Data	63
4.11	Mass Transfer Limitation Study Results for Microcosm M2	66
4.12	Butane Utilization within Microcosms M5	67

## LIST OF FIGURES, CONTINUED

<u>FIGURE</u>		<u>PAGE</u>
4.13a	Mass Transfer Limitation Model for Microcosm M5A, 0 to 800 hrs	71
4.13b	Mass Transfer Limitation Model for Microcosm M5A, 800 to 1500 hrs	72
4.14a	Comparison of Laboratory Data versus Model Output for M2B, 0 to 1700 hrs	76
4.14b	Comparison of Laboratory Data versus Model Output for M2B, 1900 to 2300 hrs	77
4.14c	Cell Concentrations Calculated by the Stella Model for M2B Biotransformation	78
4.15	Comparison Plot of M2B Data and Model Output Assuming Low $k_{mDCE}$ (0.1 mol/mg/hr)	80
5.1	Conceptual Model of Moffett Field Test Aquifer	85
5.2	Bromide Tracer Test Data at the Three Monitoring Wells S1 (1m); S2 (2.2m); S3 (4m) and the Injection Well	87
5.3	Comparison of Tracer Data to Model Output	89
5.4	Breakthrough Curves of 1,1-DCE, 1,1-DCA, and 1,1,1-TCA	91
5.5	Comparison of CAH Breakthrough Data with Model Output for Varying Mass Transfer Rate Coefficient ( $F_k$ ) at S1 (1m)	95
5.6a	Butane and Oxygen Concentrations Measured at S1 (1m), S3 (4m), and Injection Well during First Twenty Days of the Field Experiments	100
5.6b	1,1-DCE and 1,1,1-TCA Concentrations Measured at S1 (1m), S3 (4m), and the Injection Well the during First Twenty Days of the Field Experiments	101

## LIST OF FIGURES, CONTINUED

<u>FIGURE</u>		<u>PAGE</u>
5.6c	1,1-DCA Concentrations Measured at S1 (1m), S3 (4m), and the Injection Well during the First Twenty Days of the Field Experiments	102
5.7a	Butane and Oxygen Concentrations Measured at S1 (1m), S3 (4m), and the Injection Well during the First Forty Days of the Field Experiments	103
5.7b	1,1-DCE and 1,1,1-TCA Concentrations Measured at S1 (1m), S3 (4m), and the Injection Well during the First Forty Days of Field Experiments	104
5.7c	1,1-DCA Concentrations Measured at S1 (1m), S3 (4m), and the Injection Well during the First Forty Days of Field Experiments	105
5.8a	Butane and Oxygen Concentrations Measured at S1 (1m) and the Injection Well during the Field Experiments (Days 0-75)	106
5.8b	1,1-DCE and 1,1,1-TCA Concentrations Measured at S1 (1m) and the Injection Well during the Field Experiments (Days 0-75)	107
5.8c	1,1-DCA Concentrations Measured at S1 (1m) and the Injection Well during the Field Experiments (Days 0-75)	108
5.9a	Comparison of Butane and Oxygen Field Data and Model Output at S1 (1m)	114
5.9b	Comparison of 1,1-DCE and 1,1,1-TCA Field Data and Model Output at S1 (1m)	115
5.9c	Comparison of 1,1-DCA Field Data and Model Output at S1 (1m)	116
5.9d	Model Output of Cell Concentration at S1 (1m)	117
5.9e	Model Output of Cell Distribution over the First 2.6 m of the Test Zone on Day 20 and Day 75	118

## LIST OF FIGURES, CONTINUED

<u>FIGURE</u>		<u>PAGE</u>
5.10	Model Output for Simulating Utilization and Transformation at S1 (1m) if 25 mg/L Oxygen Is Injected between days 75 and 90	121
5.11	Model Output for Simulating Utilization and Transformation at S1 (1m) if 50 mg/L Butane and Oxygen Are Injected between Days 75 and 90	122
5.12a	Butane and Oxygen Output from Sensitivity Analysis of 1,1-DCE Product Toxicity at S1 (1m)	124
5.12b	1,1-DCE and 1,1,1-TCA Output from Sensitivity Analysis of 1,1-DCE Product Toxicity at S1 (1m)	125
5.12c	Biomass Results from Sensitivity Analysis of 1,1-DCE Product Toxicity	126
5.13a	Comparison of Butane and Oxygen Utilizations from Field Biotransformation Assuming Different 1,1-DCE Transformation Rate	128
5.13b	Comparison of 1,1-DCE and 1,1,1-TCA Transformation from Field Biotransformation Assuming Different 1,1-DCE Transformation Rate	129
5.14a	Comparison of Butane Utilization at S1 (1m) for Equilibrium ( $F_k = 2.0 \text{ day}^{-1}$ ) and Non-equilibrium ( $F_k = 0.2 \text{ day}^{-1}$ ) Sorption	132
5.14b	Comparison of Oxygen Utilization at S1 (1m) for Equilibrium ( $F_k = 2.0 \text{ day}^{-1}$ ) and Non-equilibrium ( $F_k = 0.2 \text{ day}^{-1}$ ) Sorption with Elongated Butane and Oxygen Pulsing Durations	133
5.14c	Comparison of 1,1-DCE Transformation S1 (1m) for Equilibrium ( $F_k = 2.0 \text{ day}^{-1}$ ) and Non-equilibrium ( $F_k = 0.2 \text{ day}^{-1}$ ) Sorption with Elongated Butane and Oxygen Pulsing Durations	134
5.14d	Comparison of 1,1,1-TCA Transformation S1 (1m) for Equilibrium ( $F_k = 2.0 \text{ day}^{-1}$ ) and Non-equilibrium ( $F_k = 0.2 \text{ day}^{-1}$ ) Sorption with Elongated Butane and Oxygen Pulsing Durations	135

## LIST OF TABLES

<u>TABLE</u>		<u>PAGE</u>
1.1	Physical and Chemical Properties of 1,1-DCA, 1,1-DCE, and 1,1,1-TCA.	3
2.1	Features of the Contaminant Transport/Biotransformation Model	13
2.2	Input Values for Transport Comparison	25
2.3	Stella Input Values for Biotransformation Comparison	29
2.4	Fortran Input Values for Biotransformation Comparison	30
3.1	Growth Media Composition	35
3.2	Microcosm Descriptions	38
3.3	Biotransformation Experiment Descriptions	39
3.4	Mass Transfer Limitation Experiment Descriptions	41
4.1	Input Parameters for Modeling Biotransformation in Media	49
4.2	Input Parameters for Modeling 1,1-DCE Product Toxicity	61
4.3	Input Values for Simulating MTL during Different Spikes	69
4.4	Initial Cell Concentrations and $K_{Ga}$ Used in Simulation MTL	70
4.5	Input Values for Simulating Biotransformation in M2 and M3	74
4.6	Initial Cell Concentration for Simulating Biotransformation in M2 and M3	75
5.1	Aquifer Hydraulic Characteristics	85
5.2	Retardation Factors and Solids Partition Coefficients	93
5.3	Butane and Oxygen Injection Pulsing Durations and Concentrations	97

## LIST OF TABLES, CONTINUED

<u>TABLE</u>		<u>PAGE</u>
5.4	1,1-DCE, 1,1-DCA, and 1,1,1-TCA Injection Concentrations	97
5.5	Biotransformation Values for Simulating Field Data	110
5.6	Transport Parameter Values for Simulating Field Data	111

## LIST OF APPENDICES

<u>APPENDIX</u>		<u>PAGE</u>
A	Nomenclature and Units for Biotransformation/Transport Model	148
B	Stella Biotransformation Model for Batch Reactors	152
C	Nomenclature and Units for Stella Biotransformation Model	156
D	Moffett Field Soil Cores Used for Microcosms	159
E	Derivation of Mass Transfer of Volatile Compounds in a Batch Reactor	160
F	Mass Transfer Limitation in M3 Microcosms	161
G	Mass Transfer Limitation Model	162
H	Biotransformation/Transport Model Input for Flow (Q) Determination	164
I	Biotransformation/Transport Model Input for Mass Transfer Rate Coeff. Determination ( $F_k$ )	166
J	Biotransformation/Transport Model Input for Transformation at S1	167
K	Parameter Descriptions for Biotransformation/Transport Model	169
L	Initial Microbial Distribution Assumed within Aquifer for Bioaugmentation Modeling	175
M	1,1-DCE Transformation Capacity ( $T_{cDCE}$ ) Input Values for Sensitivity Analysis of Biotransformation/Transport Model	176
N	Biotransformation/Transport Model Input for First Order Mass Transport Sorption Rate and Pulsing Durations	177



## LIST OF APPENDIX TABLES

<u>TABLE</u>		<u>PAGE</u>
D.1	Core Material Used in Microcosms	151
H.1	Input Values for Flow Determination at S1 (1m)	164
H.2	Input Values for Flow Determination at S3 (1m)	165
I.1	Input Values for $F_k$ at S1 (1m)	166
J.1	Input Values for 1,1-DCE and 1,1,1-TCA Simulation at S1	167
J.2	Input Values for 1,1-DCE and 1,1-DCA Simulation at S1	168
L.1	Initial Microbial Distribution of Biotransformation Simulations	175
M.1	$T_{cDCE}$ Input Values for Sensitivity Analysis	176
N.1	Input Values for Variations in Mass Transfer Sorption and Butane and Oxygen Pulsing Durations	177

# **Modeling Cometabolic Transformation of a CAH Mixture by a Butane Utilizing Culture**

## **CHAPTER 1 INTRODUCTION AND LITERATURE REVIEW**

---

### **1.1 OVERVIEW**

Complex mechanisms such as solute transport and biodegradation may be simulated by mathematically assigning selective processes to approximate system performance. Modeling enhances design and application of systems such as those developed to treat sites contaminated with chlorinated aliphatic hydrocarbons (CAHs). CAHs are of great concern due to the potential health hazards they pose, combined with their wide-spread use in industry. Recent studies have shown butane to be an effective growth substrate for biodegrading CAH mixtures by inducing aerobic cometabolism (Hamamura et al., 1997; Kim et al., 1997, Jitnuyanont et al., 2000; Kim et al., 2000, 2002, *in press*; Rungkamol, 2001). The success of these studies was the inspiration for this thesis.

This study used butane as the primary growth substrate for aerobic cometabolism of the CAH mixture 1,1-dichloroethane (1,1-DCA), 1,1-dichloroethylene (1,1-DCE), and 1,1,1-trichloroethane (1,1,1-TCA), extrapolating a model developed from laboratory experiments to field-scale application. The model simulated biodegradation and solute transport of the CAH mixture within a groundwater aquifer.

The work included growing a pure culture in the laboratory and testing its degradation ability in growth media and soil/groundwater microcosm experiments. A biotransformation model adapted from Kim et al. (2002, *in press*) was used to simulate media and microcosm tests and define kinetic parameters specific to our culture and the compounds of interest. Having defined the biotransformation parameters, the model was expanded to include contaminant transport with non-equilibrium sorption. This

combined model was run to simulate a field test during which the bioaugmented culture was inoculated into a groundwater aquifer containing the same compounds studied in the laboratory experiments. Model output of concentration profiles over time was then compared with actual field data.

## 1.2 WHY CAHS ARE OF CONCERN

Many CAHs are defined as possible human carcinogens by the United States Environmental Protection Agency (USEPA, IRIS, 2001). Material Safety Data Sheets (MSDS) list potential health hazards from CAH exposure such as dizziness, fatigue, skin and eye irritation, gastrointestinal problems, liver damage, respiratory and nervous system depression, unconsciousness, and even death (MSDS, 2001).

These compounds are frequently present in groundwater and soil systems due to their widespread use in factory processing, as fumigants and pesticides, and as degreasing agents and solvents (Fetter, 1993, pg. 309). They may enter the environment through accidental spills and leaks or illegal dumping.

Our study focused on a CAH mixture consisting of 1,1-dichloroethane (DCA), 1,1-dichloroethylene (DCE), and 1,1,1-trichloroethane (TCA), as these three compounds are often found together at contaminated sites. In a groundwater survey of 158 sites, Westrick et al. (1984) found that 1,1-DCA, 1,1-DCE, and 1,1,1-TCA existed in 1.8, 6.3, and 16.5% of their samples, respectively. Squillace et al. (2002) ranked these CAHs among the top 14 compounds that contributed to greater than 95% of the detections in the 402 most common mixtures identified in their survey.

Their relatively high solubility in water and low affinity for sediment sorption make CAHs easily transported through soils and groundwater. Table 1.1 presents the physical and chemical properties of the CAHs investigated in this study as well as the maximum contaminant levels (MCLs) defined by the US EPA.

**Table 1.1 Physical and chemical properties of 1,1-DCA, 1,1-DCE, and 1,1,1-TCA.**

CAH	Mol. Wt. (g/mol)	Specific Gravity <sup>a</sup>	Water Solubility <sup>b</sup> (mg/L)	Vapor Pressure <sup>b</sup> (mm Hg @ 20°C)	MCL <sup>c</sup> (µg/L)
1,1-DCA	98.96	1.174	5500	182	-
1,1-DCE	96.94	1.218	2250	600	7
1,1,1-TCA	133.4	1.35	1500	123	200

a. Fetter (1993)

b. US EPA (1990)

c. US EPA (2001)

### 1.3 AEROBIC COMETABOLISM OF CAHS BY MICROORGANISMS

Aerobic cometabolism has been shown to be an effective treatment method in reducing CAH contamination (Hopkins and McCarty, 1995; McCarty et al., 1998). Cometabolic transformation results from nonspecific enzymes fortuitously catalyzing reactions. Because these reactions do not provide energy or carbon, a primary growth substrate must be (at least) intermittently available to maintain a viable microbial population. In oxidative cometabolism, the enzymes use the primary growth substrate as an electron donor and oxygen as an electron acceptor.

The performance of several cultures capable of cometabolic oxidative dechlorination has been studied for a variety of contaminants and primary growth substrates. Trichloroethylene (TCE) transformation was studied by Hopkins et al. (1993), Chang and Criddle (1997), and Lee et al. (2000) by phenol-oxidizers, methanotrophs, and phenol-oxidizers, respectively. Chang and Alvarez-Cohen (1996) measured and modeled aerobic degradation of CAH mixtures (including TCE, 1,1-DCE, 1,2-DCA, 1,1,1-TCA, *cis*-DCE, *trans*-DCE, chloroform, etc.) by methane oxidizing cultures. Mixtures of TCE, 1,1-DCE, *cis*-DCE, *trans*-DCE, and vinyl chloride were degraded by a toluene-induced enzyme introduced by Shim et al. (2001).

Butane utilizers capable of aerobically degrading chloroform (CF) were observed by Kim et al. (1997) and Hamamura et al. (1997).

Biodegradation is influenced by the specific growth and non-growth substrates present. Our study built upon past research using butane as the electron donor for inducing 1,1-DCA, 1,1-DCE, and 1,1,1-TCA aerobic cometabolism.

#### 1.3.1 Butane as an Electron Donor/Primary Growth Substrate

Kim et al. (1997) reported that butane had great potential for dechlorination of methanes, ethanes, and ethenes. This growth substrate proved to be one of the best (compared to propane, methane, ammonia, phenol, etc.) for transforming chloroform (CF) and 1,1,1-TCA. In concurrence with transformation, they observed utilization of butane and oxygen and reasoned that a monooxygenase enzyme likely initiated degradation. From their work, they concluded that organisms using butane as the primary growth substrate may be advantageous over methanotrophs in transforming 1,1-DCA, 1,1-DCE, and 1,1,1-TCA.

Other studies showed butane to be an effective growth substrate for transforming some of the most recalcitrant chlorinated compounds. Hamamura et al. (1997) first reported the success of CF degradation by butane-utilizing bacteria. Work done by Jitnuyanont et al. (2000) suggested that in-situ bioremediation by butane utilizing cultures is effective for 1,1,1-TCA removal. Kim et al. (2000) looked at a butane-utilizing culture's ability to aerobically degrade a range of chlorinated compounds, noting 86-100% oxidative transformation of chloro-ethane, VC, and *cis*-DCE. Rungkamol (2001) presented a kinetic analysis of a butane-grown culture which successfully degraded 1,1,1-TCA.

### 1.3.2 Transformation of 1,1-DCA, 1,1-DCE and 1,1,1-TCA

Although most chlorinated contamination consists of CAH mixtures, few studies have been conducted on such compositions (Shim et al., 2001). Modeling a more realistic occurrence (i.e. a combination of CAHs) improves remediation design because the presence of one compound may inhibit or inactivate biotransformation of others (Alvarez-Cohen and Speitel, 2001; Strand et al., 1990; Kindred and Celia, 1989; Chang and Alvarez-Cohen, 1995 and 1996). Studies focusing on merely one contaminant may therefore lack any influences the presence of other contaminants cause and ultimately be incomplete or incorrect.

Our study investigated the transformation of 1,1-DCA, 1,1-DCE and 1,1,1-TCA, three CAHs that are frequently found together due to biotic and abiotic transformation of the latter into the former two, respectively. Vogel and McCarty (1987) provided a detailed report of the transformation processes. A schematic of the breakdown mechanisms is show in Figure 1.1.

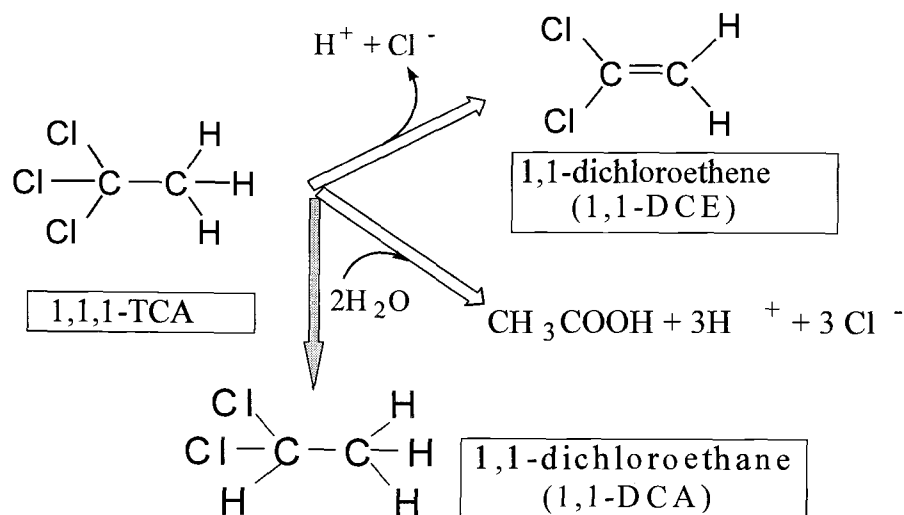


**Figure 1.1 Fate of 1,1,1-TCA.** *Vogel and McCarty, 1987*

The schematic shows that 1,1,1-TCA is abiotically transformed into 1,1-DCE and acetic acid. The pseudo-first order rate constant for transformation to 1,1-DCE was reported as  $0.04 \text{ yr}^{-1}$ . 1,1-DCA can simultaneously be produced through reductive dehalogenation.

## 1.4 PROCESSES INFLUENCING COMETABOLISM AND BIOREMEDIATION

Cometabolic biotransformation models most often stem from Michaelis-Menten and Monod enzyme kinetics. These expressions have been expanded to include processes such as substrate inhibition (Kindred and Celia, 1989; Broholm et al., 1992; Keenan et al., 1994; Ely et al., 1995; and Kim et al., 2002), product toxicity (Chang and Criddle, 1997; Alvarez-Cohen and McCarty, 1991; Kim et al., 2000), and reducing energy limitations (Chang and Alvarez-Cohen, 1995; Sipkema et al., 2000). Alvarez-Cohen and Speitel (2001) provided a review and discussion of these processes and the models representing them. For *in situ* bioremediation, contaminant transport models have been incorporated as well.

The models used in this study incorporated product toxicity, substrate inhibition, and contaminant transport with Michaelis-Menten/Monod kinetics.

### 1.4.1 Product Toxicity

During transformation reactions, products may develop that pose toxic threats to cells or enzymes, thereby inactivating them. This phenomenon is termed *product toxicity* and may be assigned one of several parameters to account for cell/enzyme death in mathematical models. Transformation capacity ( $T_c$ ) represents one such parameter, defined as the quantity of a compound that a specific mass of microorganisms can degrade before they are destroyed by toxicity from transformation

products. Units of transformation capacity are typically mass of degrading substrate per mass of cells. (Rittman and McCarty, 2001)

Various assumptions are made in using such parameters to simulate product toxicity. Alvarez-Cohen and Speitel (2001) reviewed interpretations for approximating inactivation, separating them into two classes. One class represents loss of full cellular function, while the other class assumes the loss of specific enzyme activity. The first class is the most commonly used in modeling biodegradation and was incorporated in our study.

#### 1.4.2 Substrate Inhibition

Substrate inhibition describes the hindrance of substrate transformation or utilization due to competition for or alteration of degradative enzymes. There are several types of inhibition, including self-inhibition, competitive, noncompetitive, and mixed. *Self-inhibition*, or *Haldane inhibition*, may result when the growth substrate itself is inhibitory at high concentrations. When an enzyme lacks specificity, *competitive inhibition* may occur in which another substrate binds to the catalytic site of the enzyme, thus preventing another substrate from reacting. A substrate may also bind to a non-reactive site on the enzyme, altering its conformation and creating *noncompetitive inhibition* which reduces the utilization of another substrate. Competitive and noncompetitive inhibition may occur simultaneously, causing a condition termed *mixed inhibition*. (Rittman and McCarty, 2001). Competitive inhibition is the most frequent form of inhibition addressed in mathematically modeling cometabolic biotransformation (Broholm et al., 1992; Chang and Alvarez-Cohen, 1995; Chang and Criddle, 1997; Lee et al., 2000).

The competitive inhibition constant (Section 2.1.2) has often been approximated using a value equal to that of the competing substrate's half-saturation constant. Kim et al. (2002, *in press*), however, noted various studies where this appeared to be an



incorrect assumption and, in response, presented a method for determining inhibition type and respective constants. As with our study, Kim et al. (*in press*) focused on butane utilization by a mixed culture with cometabolic transformation of 1,1-DCE, 1,1-DCA, and 1,1,1-TCA, and, using techniques presented in earlier reports (Kim et al., 2002), observed that competitive and mixed inhibition occurred. CAHs competitively inhibited the other CAHs and butane, while butane showed mixed inhibitory effects toward the CAHs. Since Kim's culture was a parent of our culture, we assumed that these inhibition types were appropriate in our modeling work.

#### 1.4.3 Solute Transport

When a chemical enters the subsurface, the compound may sorb to particle surfaces and/or be transported via advective and dispersive forces. Advective transport results from the flow of water in which mass is dissolved. Advection is therefore dependent on groundwater velocity and direction of flow. Dispersive transport results from a mixing process which creates an interface between two fluids of differing compositions.

Sorption is the process in which compounds adhere to soil particles, causing transport of the compound mass to be temporarily detained. Sorption is dependent on a soil's bulk density and porosity. Equilibrium sorption refers to a constant rate of equal masses adhering to and being released from particle surfaces. Non-equilibrium sorption refers to an inconsistent rate of sorption onto and release from sediments. Modeling non-equilibrium sorption includes a mass transfer rate and partitioning coefficient. Thorough reviews of contaminant transport are available by Freeze and Cherry (1979), Domenico and Schwartz (1990), and Fetter (1993). Our model incorporates mathematics describing advection, dispersion, and non-equilibrium sorption that will be presented in Chapter 2.

## 1.5 COMBINED BIOTRANSFORMATION AND TRANSPORT MODELS

There have been many publications of work done to model the phenomena of solute transport with biotransformation. Most models are based on Michaelis-Menten/Monod kinetics and advection/dispersion as described above, with variations as to inhibition, sorption, spatial dimensions, microbial profiles, boundary conditions, iterative solutions, etc. (Borden and Bedient, 1986; MacQuarrie et al., 1990; Schäfer et al., 1998; Unice and Logan, 2000; Kaluarachchi et al., 2000; Clement et al., 2000). A trend toward improving these models as predictive sources is to include mixed inhibition, aerobic and anaerobic transformation, multi-substrate tracking, and/or growth and transport of microbes (Waddill and Widdowson, 1998; Kindred and Celia, 1989). Kindred and Celia (1989) introduced a model capable of simulating aerobic and anaerobic metabolism, aerobic cometabolism, and competitive and noncompetitive inhibition. Their work demonstrated "the feasibility of modeling biological systems involving complex interactions between a variety of nutrients and substrates." (p. 1157). Sun et al. (1998) introduced a model following dual-substrate Monod kinetics, accounting for microbial growth and migration and found that non-instantaneous reactions and microbial transport were key mechanisms in field scale biodegradation. The United States Geological Survey (USGS, 1998) provided a solute-transport and biodegradation model capable of tracking multi-species in two dimensions and included noncompetitive, competitive, and Haldane inhibition. It is primarily used for simulating the metabolism of petroleum hydrocarbons.

Semprini and McCarty (1991, 1992) presented a two part series of a combined, non-steady state biotransformation-transport model for cometabolism. In Part 1 they defined the basic features of the model with regards to biostimulation, including differential equations tracking concentrations of electron acceptor, electron donor, and biomass, as well as non-equilibrium sorption influences. In their model, the mathematics of the Michaelis-Menten/Monod kinetics were expanded, assuming that the rate of microbial growth depends on both electron donor (primary growth substrate)

and electron acceptor. Part 2 introduced the cometabolism of two contaminants including effects of competitive inhibition. CAH transformation was approximated using the ratio of half-saturation constants to estimate inhibition parameters.

Semprini and McCarty's model was expanded upon in our study to include more influential mechanisms such as mixed inhibition and product toxicity, extrapolating from biotransformation experiments and models reported by Kim et al. (2002, *in press*). Because Kim's culture was the parent culture of the one used in our study, the parameter values reported by Kim were deemed as appropriate starting estimates for mathematically modeling CAH transformation by our culture. Some parameters were adjusted during simulation of batch laboratory results from the enrichment culture used in our studies.

## 1.6 OBJECTIVES OF THIS THESIS

As described above, this thesis built upon past studies involving cometabolic transformation of CAH mixtures and application of a combined biotransformation-transport model. The objectives of this thesis were:

- 1) to evaluate in batch reactors the transformation of CAH mixtures consisting of 1,1-DCA, 1,1-DCE, and 1,1,1-TCA, by a butane enrichment culture in growth media.
- 2) to evaluate in batch soil/groundwater microcosms the culture's ability to transform the CAH mixtures and utilize butane upon bioaugmentation to the microcosm.
- 3) to mathematically simulate the biotransformation seen in both the media and microcosm experiments by using the cometabolic transformation and inhibition

parameter values reported by Kim et al. (2002, *in press*) and adjusting a few values as appropriate.

4) to modify the existing biotransformation-transport model of Semprini and McCarty (1991, 1992) by incorporating the competitive and mixed inhibition model reported by Kim et al. (2002, *in press*), and including transformation capacity for each of the CAHs.

5) to compare the model output (using the parameter values identified from microcosm tests) to actual data collected from field experiments in which the culture was bioaugmented and then biostimulated.

## CHAPTER 2

### MODEL PRESENTATION

---

Building upon the theories and concepts discussed in Chapter 1, our study focused on recreating the phenomena of aerobic cometabolism, mixed inhibition, product toxicity, etc., and developing a mathematical model to simulate observed laboratory and field performance. Two models were used to do this. Laboratory data were simulated using the biotransformation model developed by Kim et al. (*in press*). The model is presented in Appendix B with nomenclature and units provided in Appendix C. The model was operated using Stella ® software (High Performance System, Inc., Hanover, NH) with Runge-Kutta integration. It is referred to as the Stella model throughout this thesis. The field data were simulated using a modified form of the combined biotransformation/transport model presented by Semprini and McCarty (1991, 1992), with nomenclature and units in Appendix A. This model is referred to as the Fortran or combined model throughout this thesis. The features of the combined model used in our study are presented in Table 2.1. The biotransformation features listed in Table 2.1 are also relevant to the model created by Kim.

**Table 2.1: Features of the contaminant transport/biotransformation model**


---

Monod/Michaelis-Menten Kinetics

Competitive Inhibition of CAHs on CAH Transformation

Competitive Inhibition of CAHs on Butane Utilization

Mixed Inhibition of Butane on CAH Transformation\*

Transformation Product Toxicity

1-D Advective/Dispersive Transport

Equilibrium and Non-Equilibrium Sorption

Cyclic Pulsing of Electron Donor and Electron Acceptor at Boundaries

---

*\*The transport model also allowed for mixed inhibition of butane and CAHs by CAHs. However, Kim et al. (in press) only butane mixed inhibition on 1,1-DCE to be relevant, so mixed inhibition of butane on 1,1-DCA and 1,1,1-TCA was omitted from our study.*

---

## 2.1 MODELING BIOTRANSFORMATION

Biotransformation for both models used in our studies followed that introduced by Kim et al. (2002, *in press*). The combined biotransformation/transport model expanded upon Kim's mathematics to include the influence of an electron acceptor. The model presented below describes the expanded version. The Stella model used for simulating laboratory results (Appendix B) omits parameters and equations relevant to the electron acceptor.

### 2.1.1 Monod/Michaelis-Menten Kinetics

Michaelis-Menten/Monod kinetics provide the backbone mathematics for modeling biotransformation. The differential equations representing substrate utilization and microbial growth are:

$$\frac{dX}{dt} = Y \frac{dS}{dt} - bX \quad (2.1) \quad \frac{dS}{dt} = -X \frac{k_m S}{K_s + S} \quad (2.2)$$

where: S = substrate aqueous concentration (mg/L)

X = microbial concentration (mg/L)

$k_m$  = maximum utilization rate of substrate (mg substrate/mg cells/day)

Y = yield coefficient (mg cells/mg growth substrate)

$K_s$  = half-saturation constant of substrate (mg/L)

b = decay coefficient ( $\text{day}^{-1}$ )

Semprini and McCarty (1991) found that for aerobic cometabolism, the rate of microbial growth depends on both electron donor (primary growth substrate) and electron acceptor, and, therefore, provided dual Monod terms to equation 2.1 to describe this. The resulting equation is:

$$\frac{dX}{dt} = \left[ X k_{mD} Y \left( \frac{C_D}{K_{sD} + C_D} \right) - bX \right] \left( \frac{C_A}{K_{sA} + C_A} \right) \quad (2.3)$$

where:  $C_D$  = aqueous concentration of electron donor (ED) (mg/L)

$C_A$  = aqueous concentration of electron acceptor (EA) (mg/L)

$k_{mD}$  = maximum utilization rate of ED (mg ED/mg cells/day)

$K_{sD}$  = half-saturation constant of ED (mg ED/L)

$K_{sA}$  = half-saturation constant of EA (mg/L)

In their model, utilization of the electron donor (primary growth substrate) and electron acceptor were also represented by expanding equation 2.2 for dual Monod kinetics:

$$\frac{dC_D}{dt} = -k_{mD} X \left( \frac{C_D}{K_{sD} + C_D} \right) \left( \frac{C_A}{K_{SA} + C_A} \right) \quad (2.4)$$

$$\begin{aligned} \frac{dC_A}{dt} = & -k_{mD} F_a X \left( \frac{C_D}{K_{sD} + C_D} \right) \left( \frac{C_A}{K_{SA} + C_A} \right) \\ & - d_c f_d b X \left( \frac{C_A}{K_{SA} + C_A} \right) \end{aligned} \quad (2.5)$$

where:  $F_a$  = stoichiometric ratio of electron acceptor per electron donor utilized for cell synthesis (mg EA/mg ED)

$d_c$  = cell decay oxygen demand (mg  $O_2$ / mg cells)

$f_d$  = fraction of biodegradable cells

### 2.1.2 Modeling Substrate Inhibition

Kim et al. (2002) presented the following mathematics for modeling competitive, noncompetitive, and mixed inhibition. Competitive inhibition is the most frequent inhibition type included in mathematical simulations. Incorporating this into substrate utilization mathematics, equation 2.2 becomes:

$$\frac{dS}{dt} = \frac{-Xk_m S}{K_s \left( 1 + \frac{I_c}{K_{Ic}} \right) + S} \quad (2.6)$$

where:  $I_c$  = aqueous concentration of inhibitor (mg/L)

$K_{Ic}$  = const. for competitive inhibition (mg inhibitor/L)

Note that in competitive inhibition, the half-saturation portion of the equation becomes as function of the inhibitor concentration.



Noncompetitive inhibition more specifically influences the maximum utilization rate, and equation 2.2 may be transformed to:

$$\frac{dS}{dt} = \frac{-Xk_m}{1 + I_u/K_{lu}} \left( \frac{S}{K_s + S} \right) \quad (2.7)$$

where:  $I_u$  = aqueous concentration of noncompetitive inhibitor (mg/L)

$K_{lu}$  = constant for noncompetitive inhibition (mg inhibitor/L)

For the case of mixed inhibition, the mathematics have a combined form of equations 2.6 and 2.7, resulting in:

$$\frac{dS}{dt} = \frac{-Xk_m}{1 + I_u/K_{lu}} \left( \frac{S}{\frac{K_s}{1 + I_u/K_{lu}} \left( 1 + I_c/K_{lc} \right) + S} \right) \quad (2.8)$$

Competitive and noncompetitive inhibition may or may not be caused by the same inhibitor. Terms for competitive and noncompetitive inhibition are additive, and equation 2.8 may be extended to include several inhibitors. For example, transformation of 1,1,1-TCA may be inhibited by the presence of 1,1-DCE, butane, and 1,1-DCA through competitive, mixed, and competitive fashions, respectively. Expansion of the transformation equation would be:

$$\frac{dC_{TCA}}{dt} = \left( \frac{-Xk_{mTCA}}{1 + \frac{C_B}{K_{Iu,B,TCA}}} \right) \left( \frac{C_A}{K_{sA} + C_A} \right)^* \quad (2.9)$$

$$\left( \frac{\frac{K_{sTCA}}{1 + \frac{C_B}{K_{Iu,B,TCA}}} \left( 1 + \frac{C_B}{K_{Ic,B,TCA}} + \frac{C_{DCE}}{K_{Ic,DCE,TCA}} + \frac{C_{DCA}}{K_{Ic,DCA,TCA}} \right) + C_{TCA}}{C_{TCA}} \right)$$

where: C = aqueous concentration of substrate (mg/L)

$k_m$  = maximum utilization rate of 1,1,1-TCA (mg TCA/mg cells/day)

$K_{sTCA}$  = half-saturation constant of 1,1,1-TCA (mg TCA/L)

$K_{Iu,S,TCA}$  = constant for noncompetitive inhibition of 1,1,1-TCA by inhibitor "S"  
(mg inhibitor/L)

$K_{Ic,S,TCA}$  = constant for competitive inhibition of 1,1,1-TCA by inhibitor "S"  
(mg inhibitor/L)

### 2.1.3 Modeling Product Toxicity

The model in this study incorporates transformation capacity ( $T_c$ ) into the differential term for cell growth (equation 2.3) to account for product toxicity. Competitive inhibition of butane by CAHs in the form of equation 2.6 is included also:

$$\frac{dX}{dt} = \left[ XYk_{mD} \left( \frac{C_D}{K_{sD} \left( 1 + \frac{I_c}{K_{Ic}} \right) + C_D} \right) - bX - \frac{1}{T_{cS}} \frac{dC_S}{dt} \right] * \quad (2.10)$$

$$\left( \frac{C_A}{K_{SA} + C_A} \right)$$

where:  $T_{cS}$  = transformation capacity of non-growth substrate "S"  
(mg substrate/ mg cells)

$T_c$  is specific for any parent compound and the culture exposed to it. Product toxicity from several non-growth substrates may be incorporated by adding a  $T_c$  term for each compound (Alvarez-Cohen and McCarty, 1991).

## 2.2 MODELING CONTAMINANT TRANSPORT

Non-equilibrium sorption for one dimensional transport was defined in our model as a first-order rate process:

$$\frac{dS}{dt} = D_h \frac{\partial^2 S}{\partial x^2} - \frac{Q}{A\phi} \frac{dS}{dx} - \frac{\rho_b}{\phi} F_k (k_d S - S^*) \quad (2.11)$$

$$\frac{dS^*}{dt} = F_k (k_d S - S^*) \quad (2.12)$$

where:  $S^*$  = sorbed-phase concentration of substrate (mg substrate/kg soil)

$S$  = aqueous concentration of substrate (mg/L)

$F_k$  = rate coeff. for mass transfer between aqueous and sorbed phases ( $\text{day}^{-1}$ )

$D_h$  = hydrodynamic dispersion coefficient ( $\text{m}^2/\text{day}$ )

$Q$  = average groundwater flow (m<sup>3</sup>/day)

$A$  = cross-sectional area of aquifer, width x thickness (m<sup>2</sup>)

$\rho_b$  = bulk density of the aquifer solids (kg/L)

$k_d$  = partition coefficient of sorbed substrate (L/kg)

$\phi$  = aquifer porosity

This form was chosen to provide a simple, non-equilibrium sorption process. Equilibrium sorption conditions may be simulated by assigning the mass transfer rate coefficient ( $F_k$ ) a very high value.

### 2.3 COMBINED BIOTRANSFORMATION AND TRANSPORT MODEL

The biotransformation and contaminant transport models presented above were combined to create separate equations for tracking the aqueous concentrations of the electron donor (butane), electron acceptor (oxygen), and CAHs (1,1-DCE, 1,1-DCA, and 1,1,1-TCA). Equation 2.11 was added to equations 2.4, 2.5, and 2.8 to represent utilization/transformation and transport of each compound. The latter term of equation 2.11 was omitted from the combined equations for the electron donor and acceptor because of limited sorption capacity for butane and oxygen.

A Haldane constant was incorporated into the electron donor utilization equation, as some substrates can pose inhibition on themselves. For substrates such as butane for which this is not the case, a large value input for the Haldane constant can cancel out the effect of this parameter.

The combined biotransformation-transport equation for butane and oxygen utilization are presented below (equations 2.13 and 2.14, respectively).

$$\frac{dC_{BUT}}{dt} = -Xk_{mBUT} \left( \frac{C_A}{K_{sA} + C_A} \right)^* \quad (2.13)$$

$$\left( \frac{C_{BUT}}{K_{sBUT} \left( 1 + \frac{C_{DCE}}{K_{Ic,DCE,BUT}} + \frac{C_{DCA}}{K_{Ic,DCA,BUT}} + \frac{C_{TCA}}{K_{Ic,TCA,BUT}} \right) + \frac{C_{BUT}^2}{K_{HAL}} + C_{BUT}} \right) + D_h \frac{\partial^2 C_{BUT}}{\partial x^2} - \frac{Q}{A\phi} \left( \frac{dC_{BUT}}{dx} \right)$$

$$\frac{dC_{O2}}{dt} = -F_a Xk_{mBUT} \left( \frac{C_{O2}}{K_{sO2} + C_{O2}} \right)^* \quad (2.14)$$

$$\left( \frac{C_{BUT}}{K_{sBUT} \left( 1 + \frac{C_{BUT}}{K_{HAL}} + \frac{C_{DCE}}{K_{Ic,DCE,BUT}} + \frac{C_{DCA}}{K_{Ic,DCA,BUT}} + \frac{C_{TCA}}{K_{Ic,TCA,BUT}} \right) + C_{BUT}} \right) - d_c f_d bX \left( \frac{C_{O2}}{K_{sO2} + C_{O2}} \right) + D_h \frac{\partial^2 C_{O2}}{\partial x^2} - \frac{Q}{A\phi} \left( \frac{dC_{O2}}{dx} \right)$$

Transformation of 1,1-DCE, 1,1-DCA, and 1,1,1-TCA including mixed inhibition by butane and competitive inhibition by CAHs are:

$$\begin{aligned} \frac{dC_1}{dt} = & -X \left( \frac{k_{m1}}{1 + C_{BUT}/K_{lu,BUT,1}} \right) \left( \frac{C_{O2}}{K_{sO2} + C_{O2}} \right) \\ & \left( \frac{C_1}{\frac{K_{s1}}{1 + C_{BUT}/K_{lu,BUT,1}} \left( 1 + C_{BUT}/K_{lc,BUT,1} + C_2/K_{lc,2,1} + C_3/K_{lc,3,1} \right) + C_1} \right) \\ & + D_h \frac{\partial^2 C_1}{\partial x^2} - \frac{Q}{A\phi} \left( \frac{dC_1}{dx} \right) - \frac{\rho_b}{\phi} F_{k1} (k_{d1} C_1 - C_1^*) \end{aligned} \quad (2.15)$$

where:  $C_1$  = aqueous concentration of transforming CAH (mg/L)

$C_1^*$  = sorbed phase concentration of transforming CAH (mg CAH/kg soil)

$C_2$  = aqueous concentration of second CAH (mg/L)

$C_3$  = aqueous concentration of third CAH (mg/L)

$K_{lu,BUT,1}$  = uncompetitive inhibition constant of transforming CAH by butane (mg butane/L)

$K_{lc,BUT,1}$  = competitive inhibition constant of transforming CAH by butane (mg butane/L)

$K_{lc,2,1}$  = competitive inhibition constant of transforming CAH by second CAH (mg CAH#2/L)

$K_{lc,3,1}$  = competitive inhibition constant of transforming CAH by third CAH (mg CAH#3/L)

$k_{d1}$  = partition coefficient of transforming CAH (L/kg)

$F_{k1}$  = rate coefficient for mass transfer between aqueous and solids (day<sup>-1</sup>)

The microbial culture was assumed to be an immobile, distributed mass. Therefore transport (equation 2.11) was not included in defining microbial concentration profiles. Equation 2.10 was used alone, with expanded terms for product toxicity of all three CAHs studied. The resulting mathematical equation for microbial growth with competitive inhibition by CAHs is:

$$\begin{aligned} \frac{dX}{dt} = & XYk_{mBUT} \left( \frac{C_{O_2}}{K_{sO_2} + C_{O_2}} \right) * \\ & \left( \frac{C_{BUT}}{K_{sBUT} \left( 1 + \frac{C_{DCE}}{K_{Ic,DCE,BUT}} + \frac{C_{DCA}}{K_{Ic,DCA,BUT}} + \frac{C_{TCA}}{K_{Ic,TCA,BUT}} \right) + C_{BUT}} \right) \\ & - bX \left( \frac{C_{O_2}}{K_{sO_2} + C_{O_2}} \right) \\ & - \left( \frac{dC_{DCE}}{dt} \frac{1}{T_{cDCE}} + \frac{dC_{DCA}}{dt} \frac{1}{T_{cDCA}} + \frac{dC_{TCA}}{dt} \frac{1}{T_{cTCA}} \right) \left( \frac{C_{O_2}}{K_{sO_2} + C_{O_2}} \right) \end{aligned} \quad (2.16)$$

where:  $T_{cDCE}$  = transformation capacity of 1,1,1-DCE (mg DCE/mg cells)

$T_{cDCA}$  = transformation capacity of 1,1,1-DCA (mg DCA/mg cells)

$T_{cTCA}$  = transformation capacity of 1,1,1-TCA (mg TCA/mg cells)

$K_{Ic,DCE,BUT}$  = competitive inhibition constant of by 1,1-DCE  
(mg DCE/L)

$K_{Ic,DCA,BUT}$  = competitive inhibition constant of butane by 1,1-DCA  
(mg DCA/L)

$K_{Ic,TCA,BUT}$  = competitive inhibition constant of butane by 1,1,1-TCA  
(mg TCA/L)

$dC_{TCA}/dt$  = Overall 1,1,1-TCA transformation rate for biotransformation only,  
as defined in equation 2.15 and omitting terms for transport and sorption  
(mg/L/day)

$dC_{DCA}/dt$  = Overall 1,1-DCA transformation rate for biotransformation only  
as defined in equation 2.15 and omitting terms for transport and sorption  
(mg/L/day)

$dC_{DCE}/dt$  = Overall 1,1-DCE transformation rate for biotransformation only  
as defined in equation 2.15 and omitting terms for transport and sorption  
(mg/L/day)

Equations 2.13 through 2.16 were solved simultaneously using Runge-Kutta numerical integration as described by Semprini and McCarty (1991,1992). Input for various parameters were a conglomeration of values obtained from field tests, laboratory experiments, and literature. The combined model allows for cyclic additions of electron donor and acceptor at varying concentrations and duration periods.

## 2.4 VERIFICATION OF MODEL PERFORMANCE

To ensure that our combined biodegradation/transport model was performing appropriately, simulations were run and the output was compared to that from other models. Comparisons included simulations for contaminant transport without biodegradation and biodegradation in batch systems.



### 2.4.1 Comparison of Model Output for Contaminant Transport

The transport portion of our model was tested for adequate description of advection, dispersion, and sorption by comparing output from our model to the Ogatta-Banks (OB) approximation (Domenico and Schwartz, 1990. pg 375). The OB approximation defines solute transport with linear sorption as:

$$\frac{dC}{dt} = D_x \frac{d^2 C}{R_f dx^2} - v_x \frac{dC}{R_f dx} \quad (2.17)$$

$$R_f = 1 + \left[ \frac{1 - \phi}{\phi} \right] \rho_b k_d \quad (2.18)$$

where: C = aqueous-phase concentration (mg/L)

$v_x$  = average pore-water velocity (m/day)

$$v_x = Q / (\Phi * A)$$

Q = average flow within aquifer (m<sup>3</sup>/day)

A = cross sectional area of aquifer, width \* thickness (m<sup>2</sup>)

$D_h$  = hydrodynamic dispersion coefficient (m<sup>2</sup>/day)

$\rho_b$  = bulk density of solid matrix (kg/L)

$R_f$  = retardation coefficient for linear sorption

$k_d$  = partitioning coefficient from aqueous phase to solids phase (L/kg)

$\Phi$  = porosity

For solute transport with no sorption,  $R_f$  is set equal to 1. Solving for concentration as a function of time and distance, the Ogatta-Banks approximation becomes:

$$C = \frac{C_o}{2} \operatorname{erfc} \left[ \frac{R_f x - v_x t}{2(\alpha_d v_x t R_f)^{1/2}} \right] \quad (2.19)$$

where:  $C_o$  = initial aqueous concentration (mg/L)

$\alpha_d$  = dispersivity (m)

$\operatorname{erfc}$  = complementary error function

Simulations were run using our model (equations 2.13 through 2.16) and the Ogatta-Banks approximation (equation 2.19) for advective and dispersive transport of butane, oxygen, and 1,1,1-TCA. For our model, the transformation rate of 1,1,1-TCA ( $k_{mTCA}$ ) was set to zero, thus shutting off biotransformation. Equilibrium sorption of 1,1,1-TCA was assumed by setting the solids' mass transfer rate coefficient ( $F_k$ ) to a very high value (200 day<sup>-1</sup>), thus forcing equilibrium conditions. It was assumed that butane and oxygen would not be retarded. For the OB model, retardation was omitted by setting  $R_f$  to 1 for these substrates. Our model excludes sorption for the electron donor and acceptor, so no adaptation was necessary.

The input values are presented in Table 2.2 and represent approximate conditions at the Moffett Field Test Facility.

**Table 2.2: Input values for transport comparison**

Average flow*, Q (m/day)	Aquifer Thickness, b (m)	Porosity, $\Phi$ (-)	Bulk Density, $\rho_b$ (kg/L)	Dispersivity, $\alpha_d$ (m)	1,1,1-TCA Partitioning Coeff., $k_d$ (L/kg)	1,1,1-TCA Retardation Factor, $R_f$ (-)
2.16	1.5	0.333	1.6	.31	.2	1.96

\*Based on this flow average linear velocity,  $v_x$  of 4.32 m/day was input into the Ogatta Banks Approx.

In running the simulation, concentrations/masses were recorded at distances 1.17 m, 2.3 m, and 3.5 m from the injection well with 1 hour time increments. The results are presented in Figure 2.1.

The plots show aqueous concentrations of butane, oxygen, and 1,1,1-TCA over time for simulations by both the Ogatta-Banks approximation and our model. Note that there is excellent comparison for transport of all three substrates at all three locations. The minor shifts between the curves may be attributed to omitting a second term of the Ogatta-Banks approximation and the differences in boundary conditions between the two models. The close comparison confirmed that the transport portion of our model was performing adequately.

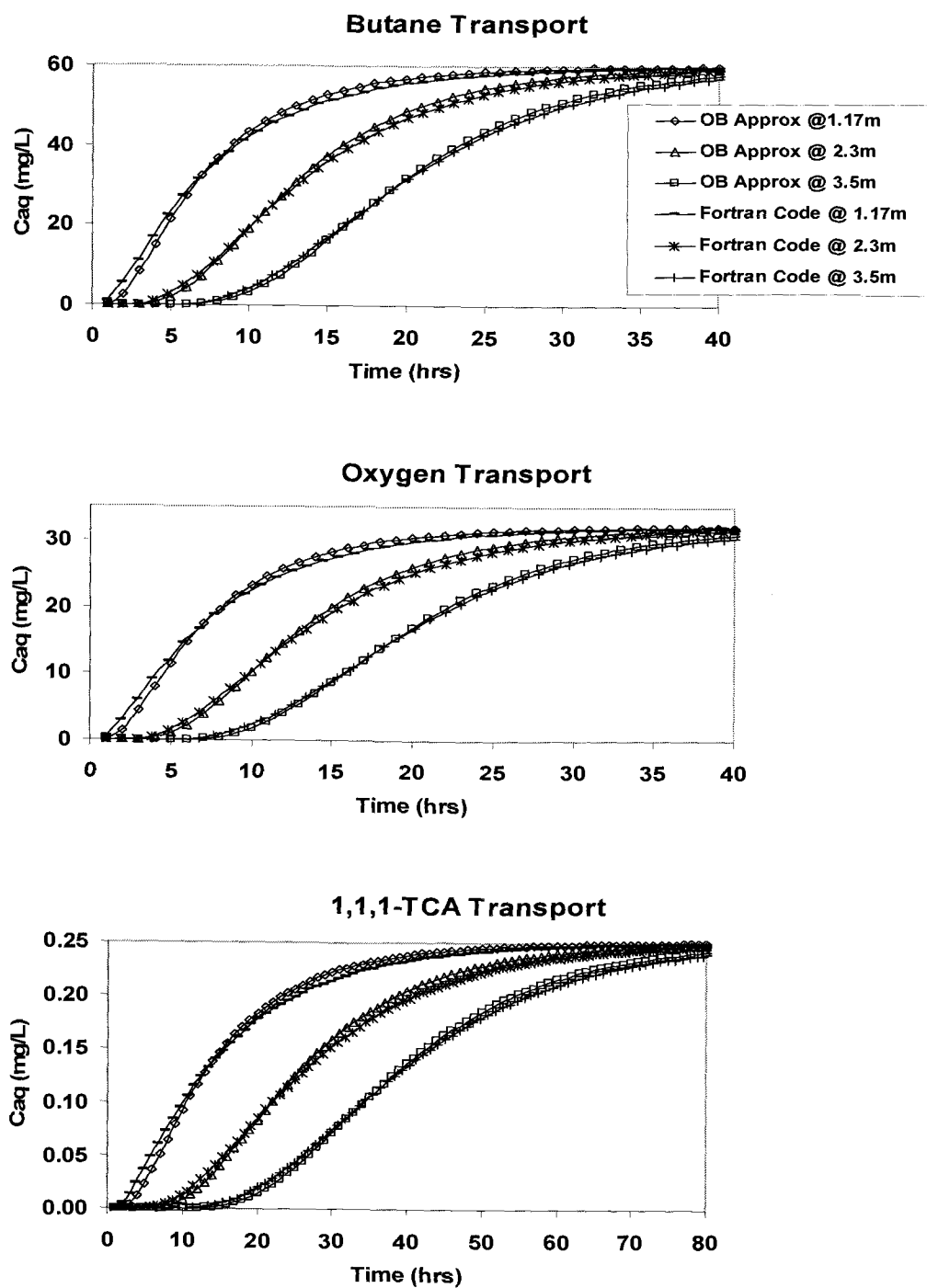


**Figure 2.1 Comparison of model output for solute transport.**  
*OB Approx refers to Ogatta-Banks approximations output.*  
*Fortran Code refers to our model's output.*

#### 2.4.2 Comparison of Model Output for Biotransformation in Batch Reactors

The biotransformation portion of our combined code was evaluated by shutting down transport and comparing the biotransformation results to that of the cometabolism model introduced by Kim et al. (2002, *in press*). Simulations were run by each model for biotransformation of 1,1-DCE and 1,1,1-TCA with butane as the electron donor.

Simulations were run for a 49.5 L volume of liquid (no gas phase present). This volume was based on an aquifer 2.4 m long, 1 m wide, and 1.5 m thick with porosity of 0.333. These characteristics represented settings for the Moffett Field Test Facility site where actual field experiments of transport with biodegradation were to be modeled (Chapter 5). A batch system in which only biodegradation occurred (no transport) was approximated in our model by setting flow, dispersion, and sorption values to zero. The voids surrounding the solids therefore provided an all liquid “batch” reactor.

Kinetic input values as defined by Kim et al. (*in press*) were assumed and are presented in Tables 2.3 and 2.4. These tables list input for the Stella model and the Fortran model. Specific details on chosen values are discussed in Section 4.1.

**Table 2.3 Stella input values for biotransformation comparison**

Parameter	Units	Value	Parameter	Units	Value
K <sub>ic</sub> DCEBUT	μmol/L	8.7	K <sub>max</sub> BUT	μmol /mg/ hr	2.5
K <sub>ic</sub> DCETCA	μmol /L	1.1	K <sub>max</sub> DCE	μmol /mg/ hr	2.8
			K <sub>max</sub> TCA	μmol /mg/ hr	0.2
K <sub>iu</sub> BUTDCE	μmol /L	6.9			
K <sub>iu</sub> BUTTCA	μmol /L	0.5	K <sub>s</sub> BUT	μmol /L	19.2
			K <sub>s</sub> DCE	μmol /L	1.48
K <sub>ic</sub> TCABUT	μmol /L	313	K <sub>s</sub> TCA	μmol /L	12.2
K <sub>ic</sub> TCADCE	μmol /L	17			
			T <sub>c</sub> DCE	μmol /mg	0.52
K <sub>ic</sub> BUTDCE	μmol /L	0.33	T <sub>c</sub> TCA	μmol /mg	0.82*
X <sub>0</sub>	mg/L	12	H <sub>cc</sub> BUT	-	38
Y	mg/μmol	0.046	H <sub>cc</sub> DCE	-	0.86
b	hr-1	.0042	H <sub>cc</sub> TCA	-	0.55
V <sub>L</sub>	L	49.5	V <sub>G</sub>	L	0

Nomenclature is provided in Appendix C. \* The value given was input for the shown in Figure 2.2.  $T_{cTCA} = 0.08$  was input for simulation of the comparison shown in Figure 2.3.

**Table 2.4 Fortran input values for biotransformation comparison**

Parameter	Units	Value	Parameter	Units	Value
K <sub>ic</sub> DCEBUT	mg/L	0.84	kmaxBUT	mg/mg/d	3.48
K <sub>ic</sub> DCETCA	mg/L	0.11	KmaxDCE	mg/mg/d	6.51
			KmaxTCA	mg/mg/d	0.64
K <sub>iu</sub> BUTDCE	mg/L	0.40			
K <sub>iu</sub> BUTTCA	mg/L	0.03	KsBUT	mg/L	1.11
			KsDCE	mg/L	0.14
K <sub>ic</sub> TCABUT	mg/L	41.75	KsTCA	mg/L	1.63
K <sub>ic</sub> TCADCE	mg/L	2.27			
			TcDCE*	mg/mg	19.8
K <sub>ic</sub> BUTDCE	mg/L	0.02	TcTCA*	mg/mg	9.1
X <sub>0</sub>	mg/L	12	f <sub>d</sub>	-	0.8
Y	mg/mg	0.79	F <sub>a</sub>	g EA/g ED	4.0
B	d-1	0.10	d <sub>c</sub>	g EA/ g cells	1.42
V <sub>L</sub>	L	49.5	V <sub>G</sub>	L	0

Nomenclature is provided in Appendix A. \*Input values for transformation capacity are the inverse of the convention used; units here are in mg cells per mg substrate. The value given was input for simulation of the comparison shown in Figure 2.2.  $T_{cTCA} = 91.0$  was input for simulation of the comparison shown in Figure 2.3.

To assure that the simulated batch bioreactor was uniform throughout the aquifer zone, output from our model was recorded at distances of 1 m, 1.5 m, and 2 m from the injection well. Results from all three locations were exactly the same.

Figure 2.2 compares output from both the Stella simulation and the Fortran model's simulation as total substrate mass and cell concentration remaining over time. Overall there is good comparison between the two models, indicating that the transport code adequately simulates biotransformation.

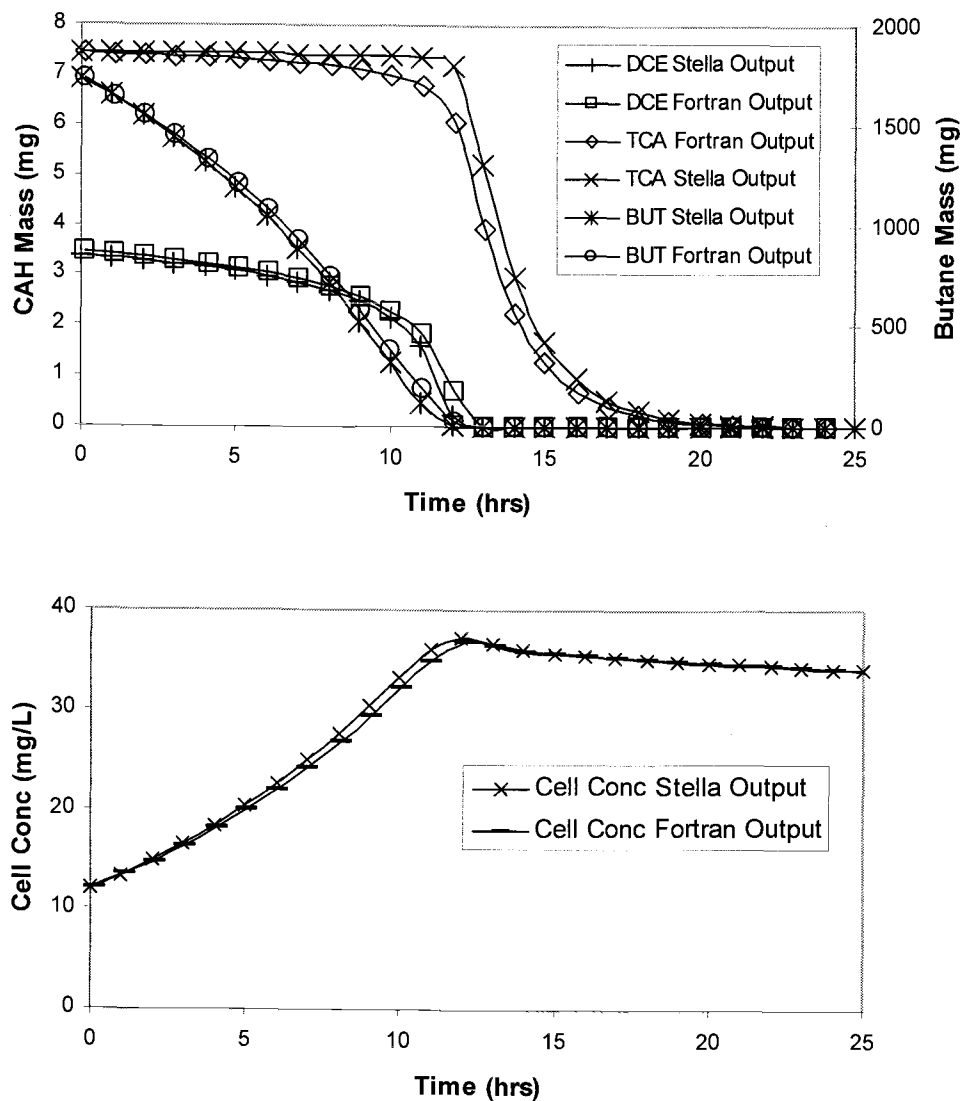


**Figure 2.2 Comparison of model output for biotransformation.**  
*Fortran Output refers to our model results*

To stress the model, product toxicity of 1,1,1-TCA was assumed to be high ( $T_{cTCA} = 91.0 \text{ mg cells/ } \mu\text{mol TCA} = 0.08 \text{ } \mu\text{mol TCA/ mg cells}$ ). This  $T_{cTCA}$  value compares to an order of magnitude difference in that used for laboratory and field data modeling (Chapters 4 and 5;  $T_{cTCA} = 9.10 \text{ mg cells/} \mu\text{mol TCA} = 0.082 \mu\text{mol TCA/mg}$



cells). Figure 2.3 shows similar comparisons for these simulations as those presented in Figure 2.2. ( $T_{cTCA} = 9.1 \text{ mg cells}/\mu\text{mol}$ /  $TCA = 0.82 \mu\text{mol TCA}/\text{mg cells}$ ). Thus the model appeared to be simulating the transformation capacity term well.

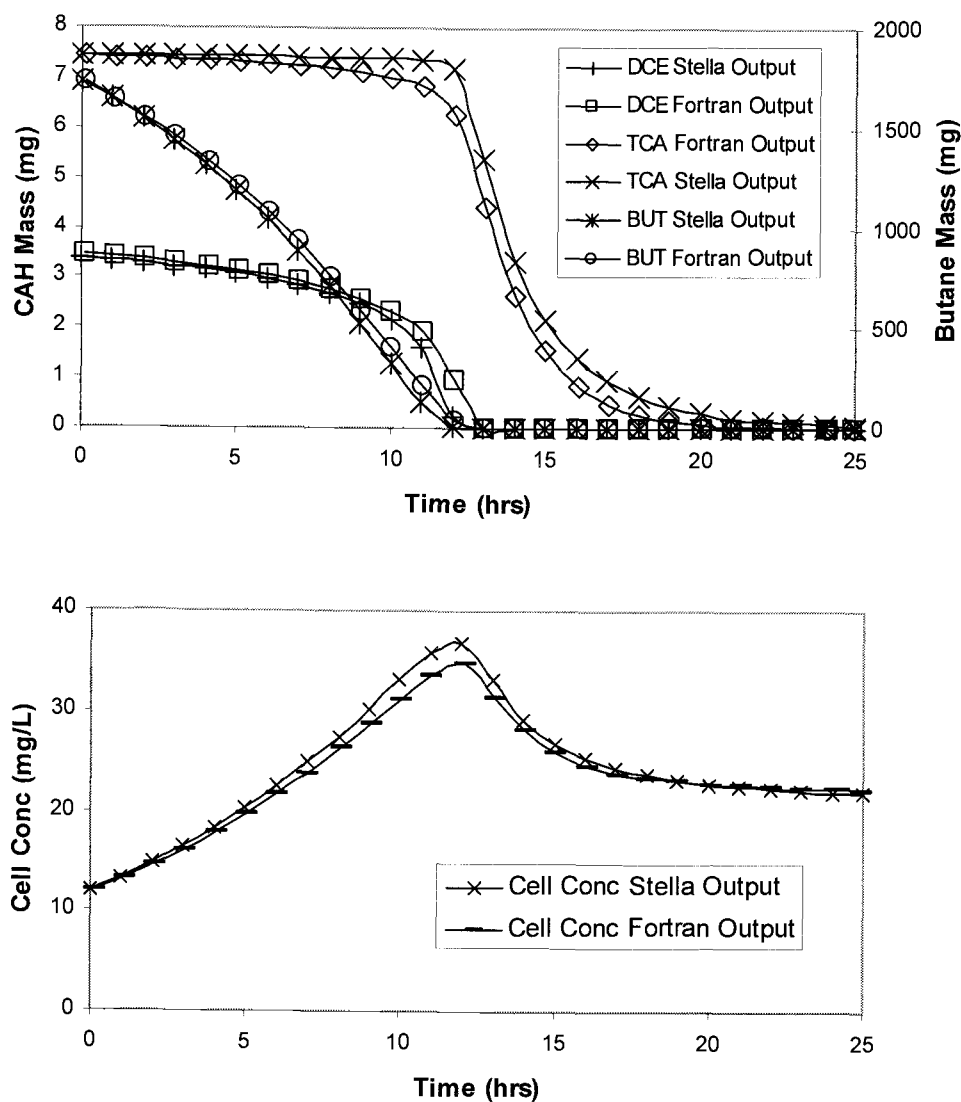


**Figure 2.3 Comparison of model output for biotransformation with high 1,1,1-TCA product toxicity.**

*Fortran Output refers to our model results.*

### CHAPTER 3

## LABORATORY METHODS FOR MEDIA AND MICROCOSM EXPERIMENTS

---

This chapter presents the material and methods used in performing laboratory studies. Experiments included bioaugmentation of the culture using butane as the growth substrate, biotransformation kinetic tests of butane, 1,1-DCE, 1,1-DCA, and 1,1,1-TCA in media and soil/groundwater batches, gaseous/aqueous phase butane mass transfer limitation studies, and 1,1-DCE product toxicity tests.

### 3.1 CHEMICAL SOURCES

Chemicals used in all laboratory experiments included butane, 1,1-dichloroethylene (1,1-DCE), 1,1-dichloroethane (1,1-DCA), and 1,1,1-trichloroethane (1,1,1-TCA). N-Butane (Grade CP) was obtained from Airgas Co. (Corvallis, OR). 1,1,1-TCA (99.5%), 1,1-DCE (99%) and 1,1-DCA (>99%) were all purchased from Aldrich Chemical Co. (Milwaukee, WI).

Concentrations of 1,1-DCE, 1,1-DCA, and 1,1,1-TCA were added during experiments using a saturated solution of each CAH. These solutions were made by injecting the stock solutions listed above into 27 mL vials containing approximately 25 mL of deionized water. Volumes of each CAH stock solution were added so that total mass in the saturated solution volume exceeded the solubility limit (Table 1.1) of each CAH. This created dissolved CAH saturation solution in the deionized water. Each saturated solution was lightly shaken by hand 5 minutes before injecting a sample of the aqueous phase into a reactor.

### 3.2 GROWTH OF THE BUTANE CULTURE FOR BIOAUGMENTATION

The culture used in this study was grown in batch and stored frozen for use as inoculum in laboratory experiments (Section 3.4) and the field tests. Growth occurred in several batches.

The butane-utilizing culture used in this study was isolated from a mixture of samples obtained from the Hanford DOE site, WA, and Moffett Federal Airfield, CA. The mixed culture was inoculated onto agar plates containing mineral salts media and incubated in a chamber with a 3% butane-in-air headspace. Individual colonies were serially streaked through 4 generations before being re-introduced to liquid media and grown for harvesting and storage in liquid nitrogen. The bioaugmentation culture consisted of an isolate with a terminal restriction fragment length of 183 base pairs when digested with restriction enzyme *MnII*. Microscopic observation of a DAPI-stained sample of the culture showed a single morphology consisting of small rods approximately 1 micron wide by 1.5 microns long often grouped in pairs. Culture characterization is on-going.

The bioaugmentation culture was then inoculated in 707 mL clear glass bottles containing growth media and capped with gray butyl rubber septa (Wheaton Glass Co., Millville, NJ). Composition of the growth media followed that used by Rungkamol (2001) and is presented in Table 3.1. Before inoculation the bottles and media were autoclaved. Growth media was checked for neutral pH (7.0-7.2). After inoculation, 15-30 mL of headspace (air) was removed and replaced with an equivalent volume of butane. Bottles were incubated at 20°C and shaken at approximately 200 rpm. All growth reactors were periodically fed oxygen to maintain atmospheric pressure within, and to ensure that oxygen limitation would not occur. Butane concentrations and optical densities (600 nm) were read periodically from representative bottles using gas chromatography (Section 3.5) and spectroscopy, respectively.

**Table 3.1: Growth media composition.**

<i>Stock Solution</i>	<i>Compound</i>	<i>Concentration</i>
Phosphate Buffer	$K_2HPO_4 \cdot 3H_2O$	2030.9 (mg/L)
	$NaH_2PO_4 \cdot H_2O$	739.0 (mg/L)
Sulfate Solution	$MgSO_4$	60.2 (mg/L)
Chloride Solution	$CaCl_2$	11.1 (mg/L)
Nitrate Solution	$NaNO_3$	153.0 (mg/L)
Trace Element Solution	$FeSO_4 \cdot 7H_2O$	6283.0 ( $\mu$ g/L)
	$MnCl_2 \cdot 4H_2O$	300.8 ( $\mu$ g/L)
	$ZnSO_4 \cdot 7H_2O$	146.6 ( $\mu$ g/L)
	$H_3BO_3$	61.8 ( $\mu$ g/L)
	$Na_2MoO_4 \cdot 2H_2O$	108.9 ( $\mu$ g/L)
	$NiCl_2 \cdot 6H_2O$	23.8 ( $\mu$ g/L)
	$CuCl_2 \cdot 2H_2O$	17.0 ( $\mu$ g/L)
	$CoCl_2 \cdot 6H_2O$	23.8 ( $\mu$ g/L)

Source: Rungkamol et al., 2001

When most of the butane had been utilized and optical density at 600 nm reached approximately 1.0, the cells were harvested. The aqueous cell mixture was centrifuged at 8000 rpm (Du pont Sorvall RC-5B) for 30 minutes. Supernatant was decanted and the concentrated cells were transferred into a 50 mL beaker. Glycerol was stirred in with the harvested cells at approximately 15% by volume to prevent cell damage during freezing. The cells/glycerol mixture was stored in cryogenic vials in a dewar filled with liquid nitrogen. Prior to freezing, a dry weight test was performed using a 1 mL sample of the harvested, condensed cells to determine approximate cell concentration. Four batches were grown with final, harvested concentrations ranging from 11 to 39 g/L.

### 3.3 BATCH TRANSFORMATION KINETIC TESTS IN MEDIA

The culture's ability to degrade 1,1,1-TCA, 1,1-DCE, and 1,1-DCA while utilizing butane as a carbon/energy source was measured in growth media (Table 3.1). 27 mL vials containing 10 mL of bioaugmented cells in growth media, 17 mL of air, and concentrations of 1,1-DCE, 1,1-DCA, 1,1,1-TCA, and butane served as the media reactors. Degradation of the substrates over time was recorded to develop transformation profiles.

From each of 8 reactors representing the first bioaugmented batch, 10 mL of bioaugmented cells were collected directly from the first growth batch (Section 3.2) and placed into the 27 mL vials with a septa cap. Volumes of 1,1-DCE (1  $\mu$ L), 1,1-DCA (0.5  $\mu$ L), and 1,1,1-TCA (2.4  $\mu$ L) were injected to obtain approximate aqueous concentrations of 100, 200, and 200  $\mu$ g/L, respectively. Approximate cell concentrations ranged 170 to 200 mg/L. Butane (0.7 mL) was injected to obtain approximately 4% volume headspace. The vials were shaken on a table at 200 rpm. Gas samples were taken periodically using a 100  $\mu$ L gas-tight syringe, and compound masses were measured by gas chromatography (Section 3.5).

### 3.4 BATCH TRANSFORMATION KINETIC TESTS IN MICROCOSMS

Butane utilization and transformation of the CAH mixture were studied in microcosms to better analyze the culture's behavior in an aquifer environment. Microcosms consisted of 707 mL clear-glass bottles containing soil, groundwater, air, the bioaugmented culture, and aqueous and gaseous concentrations of butane, 1,1-DCE, 1,1-DCA, and 1,1,1-TCA. A mass-remaining-over-time profile was developed for each microcosm by headspace analysis (Section 3.5).

This section provides the preparation and composition of the microcosms and the biotransformation experiments of butane and the CAH mixture. The latter

experiments include laboratory tests for butane mass transfer limitation between the aqueous and gaseous phases (Section 3.4.3) and 1,1-DCE product toxicity experiments (Section 3.4.4).

### 3.4.1 Preparation

Microcosm solids were obtained by mixing several core soil samples from Moffett Field Test Facility, CA (Appendix D). Large gravel was removed, and the soil was stirred to obtain a fairly homogenous material consisting of pea-sized gravel, sand, and silt. Fifteen 707 mL clear-glass bottles were autoclaved, cooled, and filled with approximately 100 mL of soil mixture, with approximate weight of 120 g. Groundwater (400 mL) taken from Moffett Field was added, and the bottles were capped with (autoclaved) gray butyl rubber septa. Headspace volume was approximately 267 mL.

Reactors were divided in to five groups of triplicates, described in Table 3.2. Group M1 represented the organisms indigenous to Moffett Field, provided by the site's groundwater and core sediment samples. Groups M2, M3, M4, and M5 contained the bioaugmented culture. All five groups were exposed to butane, but only groups M2, M3, and M4 were injected with the CAH mixture. M3 is distinguished from M2 and M4 by a 12 hour lag time between butane and CAH injections. This was done to study the effect of the butane pre-exposure on the thawed cells. Group M4 served as a mercury killed control set. M5 provided data on cell growth when fed only butane. Table 3.2 also notes which microcosms were involved in each laboratory experiment. Details for each experiment are provided in the following sections of this chapter.

**Table 3.2: Microcosm descriptions.**

<i>Microcosm Group</i>	<i>Culture<sup>a</sup></i>	<i>Compound included</i>				<i>Experiment</i>		
		<i>BUT</i>	<i>1,1-DCE</i>	<i>1,1-DCA</i>	<i>1,1,1-TCA</i>	<i>BioT<sup>b</sup></i>	<i>MTL<sup>c</sup></i>	<i>TcDCE<sup>c</sup></i>
M1	I	x	x	x	x	x	-	-
M2	B	x	x	x	x	x	x	x
M3	B	x	x	x	x	x	x	x
M4 <sup>e</sup>	B	x	x	x	x	x	-	-
M5	B	x	-	-	-	x	-	-

*a. I represents the indigenous culture. B represents the bioaugmentation culture.*

*b. Biotransformation Experiment (Section 3.4.2)*

*c. Mass Transfer Limitation Experiment (Section 3.4.3)*

*d. 1,1-DCE Product Toxicity Experiment (Section 3.4.4)*

*e. Mercury killed control*

The bioaugmented culture was inoculated into microcosm groups M2, M3, M4, and M5 using a resuspended solution of previously frozen, concentrated cells (Section 3.2). A cryogenic vial containing the frozen cells was removed from liquid nitrogen and allowed to thaw to room temperature for about 1 hour. 2.5 mL of the thawed cells were transferred into eppendorf aliquots and spun at 14,000 rpm for 3 minutes in an Eppendorf 5415C centrifuge. Supernatant was decanted and replaced with autoclaved growth media (Table 3.1). The centrifuging and washing were repeated 2 times. The rinsed seed culture was diluted in 100 mL of growth media (Table 3.1). A 1 mL sample of this solution was injected into each microcosm. Dilution and dry weight analysis of the frozen culture indicated cell concentration within the reactors was approximately 1.5 mg/L.

### 3.4.2 Biotransformation Analysis

This section describes the methods used to add compounds into the microcosms. For microcosm groups M1 through M4, saturated solution (Section 3.1) volumes of 1,1-DCE (20  $\mu\text{L}$ ), 1,1-DCA (16  $\mu\text{L}$ ), and 1,1,1-TCA (65  $\mu\text{L}$ ) were injected using glass syringes to achieve aqueous concentrations of 100, 200, and 200  $\mu\text{g/L}$ , respectively. These concentrations were in the range used in later field experiments. Four mL of butane (9.6 mg total mass, 0.91 mg/L aqueous concentration at equilibrium) was injected with a plastic syringe into all microcosm reactors. Table 3.3 provides a summary of total mass injected into each microcosm.

**Table 3.3: Biotransformation experiment descriptions.**

<i>Microcosm Group</i>	<i>Culture</i>	<i>Mass Injected (<math>\mu\text{g}</math>)</i>			
		<i>Butane</i>	<i>1,1-DCE</i>	<i>1,1-DCA</i>	<i>1,1,1-TCA</i>
M1*	indigenous	9600	58	105	91
M2**	bioaugmented	9600	58	105	91
M3**	bioaugmented	9600	58	105	91
M4***	bioaugmented	9600	58	105	91
M5*	bioaugmented	9600	-	-	-

\* M1 and M5 were shaken at 100 rpm until the time of the 4<sup>th</sup> compound addition to microcosms M2 and M3. At this time M1 and M5 were shaken at 150 rpm. \*\*During transformation of 1<sup>st</sup>, 2<sup>nd</sup>, & 3<sup>rd</sup> compound addition, M2 and M3 were shaken at 100 rpm. See Table 3.4 for shaker speeds during transformation of 4<sup>th</sup> compound addition. After 5<sup>th</sup> compound addition these microcosms were shaken at 150 rpm. \*\*\* Mercury killed control. M4 was shaken at 100 rpm until the time of the 4<sup>th</sup> compound addition to microcosms M2 and M3. At this time M4 was shaken at 150 rpm

Immediately after substrate injection, each bottle was hand shaken for five minutes, and then sampled to determine compound headspace concentrations using gas chromatography (Section 3.5). The reactors were incubated at 20°C and stored upright



on a shaker table at 100 rpm with periodic headspace sampling. Oxygen was added to the reactors according to stoichiometric oxygen demand for butane consumption (4 mol O<sub>2</sub>: 1 mol butane). This was done by filling a glass syringe with oxygen and allowing headspace in the reactors to equilibrate to atmospheric pressure. These methods were followed for five repeat additions of butane and the CAH mixture. The first spike occurred at time zero. The second, third, fourth, and fifth additions occurred at approximately 1220, 1485, 1920, and 2210 hours after start-up, respectively.

### 3.4.3 Mass Transfer Limitation Study

Calculation of a total mass balance from headspace analysis (Section 3.5) may be inaccurate if incomplete equilibrium partitioning exists between the aqueous and gaseous phases within a reactor. This may be caused by shaking reactors too slow during incubation. Such non-equilibrium conditions result in *mass transfer limitations*, in which transfer of mass between the phases is limited.

Mass transfer limitations were suspected in our microcosms after the third spike of compounds because actual laboratory biotransformation rates were slower than those predicted by our biotransformation model. To examine this, reactors from microcosm groups M2 and M3 were divided onto three separate shaker tables, each set at differing speeds, after injecting with a fourth spike of butane and CAHs (1485 hours after start-up). M2A and M3A were shaken at 100 rpm, M2B and M3B were shaken at 150 rpm, and M2C and M3C were shaken at 200 rpm. This is summarized in Table 3.4. Transformation profiles indicated that mass transfer limitations were occurring at the lower shaking speed; the two higher speeds showed greater transformation rates than the lower, with no difference between them. For all future tests the reactors were incubated at 150 rpm. Mass transfer limitations were included in modeling biotransformation for the first three compound additions. ( See Appendix G for model development.)

**Table 3.4: Mass transfer limitations experiment descriptions.**

<i>Microcosm Group</i>	<i>Shaker Speed (rpm)</i>	<i>Mass Injected (<math>\mu\text{g}</math>)</i>			
		<i>Butane</i>	<i>1,1-DCE</i>	<i>1,1-DCA</i>	<i>1,1,1-TCA</i>
M2A	100	9600	58	105	91
M2B	150	9600	58	105	91
M2C	200	9600	58	105	91
M3A	100	9600	58	105	91
M3B	150	9600	58	105	91
M3C	200	9600	58	105	91

*MTL experiments occurred during the fourth biotransformation experiment (Section 3.4.2)*

#### 3.4.4 1,1-DCE Product Toxicity Experiment

Product toxicity experiments for 1,1-DCE were performed to determine transformation capacity ( $T_{\text{cDCE}}$ ). The experiments included adding butane to the microcosms and running model simulations to determine an approximate cell mass within the microcosm. An elevated mass of 1,1-DCE was then added to the microcosms to determine  $T_{\text{cDCE}}$ , followed by another mass of butane to check that cell activity had terminated. Further description is provided below.

Product toxicity of 1,1-DCE was studied after the biotransformation experiments (Section 3.4.2) in microcosm groups M2 and M3. Because so many biotransformation experiments had been performed, it was suspected that nutrients within the reactors may have become limited. To ensure sufficient nutrients were available, groundwater was exchanged by removing most of the groundwater from each microcosm and replacing it with an equivalent volume of fresh groundwater. Microcosms were then set uncapped under a laminar flow hood to equilibrate the headspace to atmospheric pressure.

Because the microcosms had been inactive for a long period (approximately 2800 hours since the last biotransformation experiment), butane was injected into the reactors to stimulate cellular activity. Microcosms M2A, M2B, M3A, and M3B were first exposed to 4 mL butane (9.6 mg total mass, 0.91 mg/L aqueous concentration at equilibrium). After butane had been fully utilized, 1 mL of butane (2.4 mg, 0.23 mg/L aqueous concentration at equilibrium) was injected into the microcosms, followed by another 0.5 mL of butane (1.2 mg, 0.11 mg/L aqueous concentration at equilibrium). After each butane addition, the reactors' headspaces were periodically sampled (Section 3.5). Reactors were incubated at 20°C at 150 rpm.

After determining the required 1,1-DCE mass to terminate active transformation (Section 4.2.3), residual butane was purged from the reactors with helium for 30 minutes. Microcosms M2B, M2C, M3B, and M3C were then exposed to 1.5 mg 1,1-DCE (determined in Section 4.2.3) and 105 µg (200 µg/L) 1,1,1-TCA (saturated solution, Section 3.1). The mass of 1,1,1-TCA was the same as in the previous biotransformation experiments. The microcosms were incubated at 20°C at 150 rpm, and headspaces were periodically sampled (Section 3.5).

When CAH transformation appeared to have stopped, the microcosms were purged with helium for 30 to 120 minutes, allowed to equilibrate with ambient air for 30 minutes, and injected with 3 mg butane. This served as a check that the 1,1-DCE mass previously added did in fact terminate cell activity. Microcosms were incubated at 20°C at 150 rpm. Butane mass was checked periodically using headspace analysis (Section 3.5).

### 3.5 HEAD SPACE GAS ANALYSIS

Partitioning between gaseous and aqueous phases within the media and microcosm reactors allowed compound masses to be determined. Gaseous concentrations within the reactors were measured based on gas chromatography analysis using calibration curves from external standards. Mass balances incorporating these gaseous concentrations, published Henry's constants (Mackay and Shiu, 1981; Gossett, 1987), and solution volumes were used to determine mass remaining in the bottle (Appendix E). This method is further described by Kim (2000) and Rungkamol (2001).

To determine gaseous concentrations, 100  $\mu$ L headspace samples were taken from reactors and injected into gas chromatographs. Butane and 1,1-DCA gaseous concentrations were determined using a flame ionization detector (FID) from a Hewlett Packard (Wilmington, DE) 6890 gas chromatograph. The FID was connected in series to a photo ionization detector (PID). The PID allowed determination of 1,1-DCE gaseous concentration. Separation was obtained through a GS-Q 30m x 0.53mm PLOT column (J&W Scientific, Folsom, CA). The column temperature was ramped after 1.5 minutes at 145°C to 205°C at an increasing rate of 40°C/min. Carrier gas was helium at a flow rate of 15 mL/min.

1,1,1-TCA was measured using a Hewlett Packard (Wilmington, DE) 5890 gas chromatograph equipped with a  $^{63}\text{Ni}$  electron capture detector (ECD). Chromatographic separation was achieved using a HP-624 capillary, 30m x 0.25mm x 1.4mm film thickness. This column was operated isothermally at 100°C. The carrier gas was helium at a flow rate of 1.5 mL/min with an argon/methane mixture (95%:5%) make-up gas.

## CHAPTER 4

### RESULTS OF MEDIA AND MICROCOSM EXPERIMENTS AND MODEL SIMULATIONS

---

This chapter discusses the results of laboratory experiments including biotransformation in growth media and microcosms, 1,1-DCE product toxicity, and mass transfer limitations. Model simulations of the experimental results are also presented. Mass profiles of the CAHs and butane over time were simulated using the model described in Appendix B.

#### 4.1 COMPARISON OF LABORATORY DATA AND MODEL SIMULATION FROM MEDIA EXPERIMENTS

Media experiments showed that the bioaugmented culture was capable of butane utilization and biotransformation of the CAH mixture. Figure 4.1 presents laboratory data for one of the reactors. The plot shows the total mass of each compound within the reactor versus time. Total mass was determined by measuring the headspace concentrations and assuming equilibrium partitioning between the aqueous and gaseous phases (Section 3.5). 1,1-DCE was quickly transformed, followed by butane, 1,1-DCA, and 1,1,1-TCA. The slower transformation of 1,1-DCA and 1,1,1-TCA may be attributed to inhibition by butane, with faster transformation of these CAHs occurring once about half the butane had been utilized.

All other reactors produced similar results, as seen in Figure 4.2. Note that there is good reproducibility in these trends. For example, the reactors which showed slower butane utilization (183G-1A and B) also had slower transformation of all three CAHs

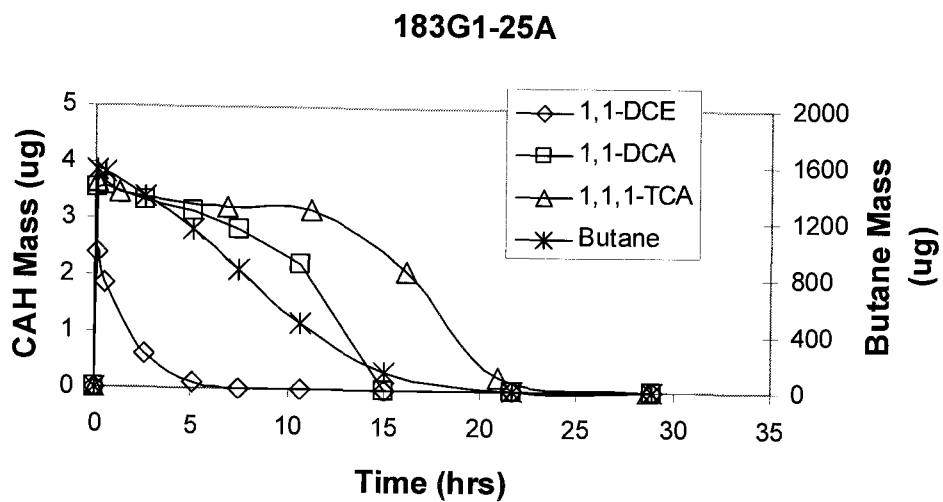


**Figure 4.1 Media biotransformation experiment data.**

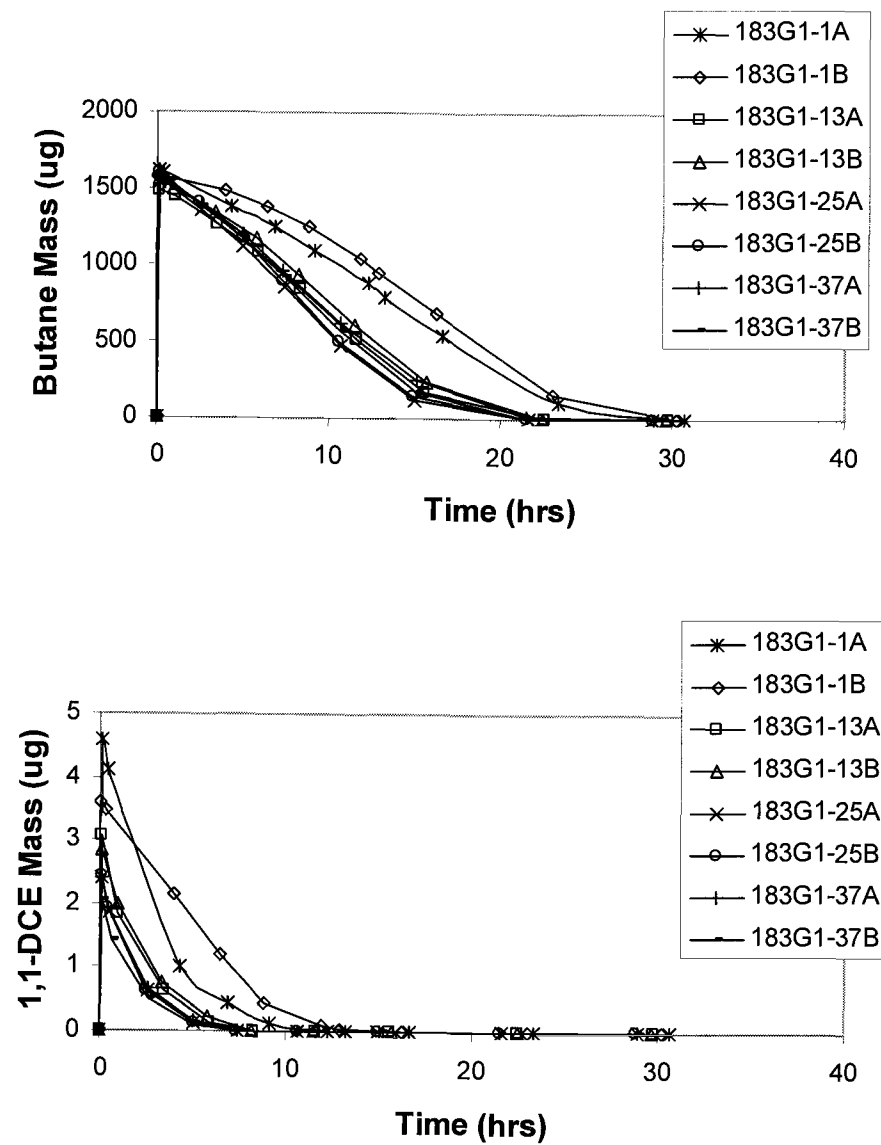


**Figure 4.2 Biotransformation activity in media reactors.**  
(continued on next page)

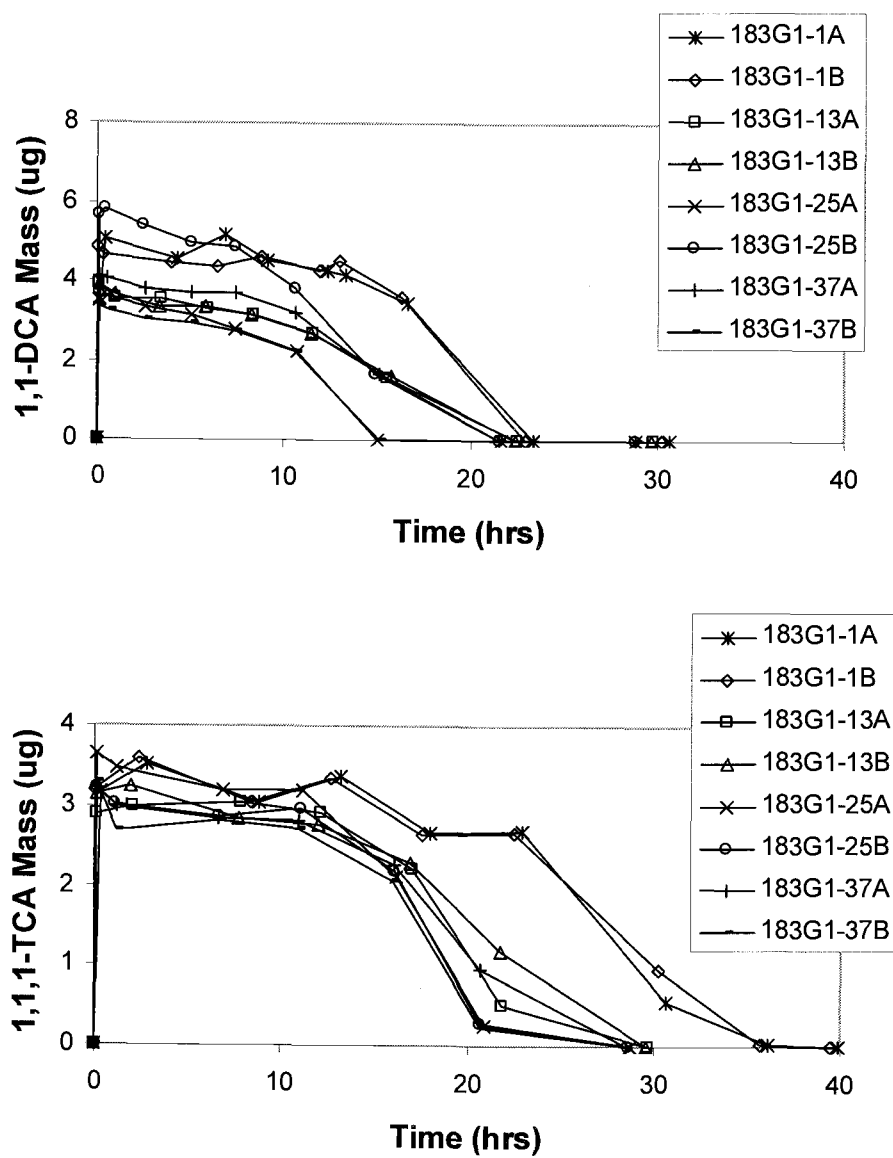


Figure 4.2, Continued Biotransformation activity in media reactors.



The Stella model presented in Appendix B (Kim et al., *in press*) was used to simulate biotransformation observed in the media reactors. Since Kim's culture was a parent to our culture, the kinetic parameters defined by Kim were assumed as starting values for our model simulations (Table 4.1). Some values (the decay constant "b", the transformation capacity of 1,1,1-TCA " $T_{cTCA}$ ", and the constant for noncompetitive inhibition of 1,1-DCA by butane " $K_{ibUTDCA}$ ") were adjusted to achieve a better fit of the experimental data. The adaptations are reasonable due to variations in our culture verses that used by Kim. The initial cell concentration was based on dry weight analysis ( $X_0 = 85$  mg/L).

Results of model simulations for Kim's input values and the adjusted values are presented in Figures 4.3a and 4.3b. The good match between model output and test data for butane, 1,1-DCE and 1,1,1-TCA is shown in Figure 4.3a. The figure also shows that the model overestimated transformation of 1,1-DCA. This was corrected by increasing the noncompetitive inhibition of 1,1-DCA by butane, as shown in Figure 4.3.b. For this latter simulation ( $K_{ibUTDCA} = 0.4$   $\mu\text{mol/L}$ ) there is a good match between model output and test data for all four compounds.

Figure 4.3.b shows that 1,1-DCE is rapidly transformed, while 1,1-DCA and 1,1,1-TCA transformation are deterred by butane inhibition and their own slower kinetic rates. The relatively high  $k_{\text{max}}$  value for 1,1-DCE (2.8  $\mu\text{mol/mg/hr}$ ) influences fast transformation of this compound as opposed to the lower  $k_{\text{max}}$  values for 1,1-DCA, 1,1,1-TCA (0.49 and 0.205  $\mu\text{mol/mg/hr}$ , respectively). Butane as a growth substrate is present at a much higher mass than the three CAHs. Its rapid transformation also results from its high  $k_{\text{max}}$  value (2.5  $\mu\text{mol/mg/hr}$ ). The lower noncompetitive inhibition constants of butane on 1,1-DCA and 1,1,1-TCA (0.4 and 0.5  $\mu\text{mol/L}$ ) result in the inhibition of their transformation. As butane is consumed and concentrations lower, transformation of 1,1-DCA and 1,1,1-TCA increase. All these trends produced by the model simulation closely matched that achieved in the reactors.

**Table 4.1: Input parameters for modeling biotransformation in media.**

Parameter	Units	Value	Parameter	Units	Value
K <sub>ic</sub> DCABUT	μmol /L	39.87*	X <sub>0</sub>	mg/L	85
K <sub>ic</sub> DCADCE	μmol /L	18*	Y	mg/μmol	0.046*
K <sub>ic</sub> DCATCA	μmol /L	16*	b	hr-1	.0016*
					.0035**
K <sub>ic</sub> DCEBUT	μmol /L	8.7*	V <sub>L</sub>	L	.017
K <sub>ic</sub> DCEDCA	μmol /L	3.6*	V <sub>G</sub>	L	.010
K <sub>ic</sub> DCETCA	μmol /L	1.1*			
K <sub>ic</sub> TCABUT	μmol /L	313*	kmaxBUT	μmol /mg/hr	2.5*
K <sub>ic</sub> TCADCA	μmol /L	9.8*	kmaxDCA	μmol /mg/hr	0.49*
K <sub>ic</sub> TCADCE	μmol /L	17*	kmaxDCE	μmol /mg/hr	2.8*
			kmaxTCA	μmol /mg/hr	0.20*
K <sub>iu</sub> BUTDCA	μmol /L	3.5*			
		0.4**	KsBUT	μmol /L	19.2*
K <sub>iu</sub> BUTDCE	μmol /L	6.9*	KsDCA	μmol /L	19.2*
K <sub>iu</sub> BUTTCA	μmol /L	0.5*	KsDCE	μmol /L	1.48*
			KsTCA	μmol /L	12.2*
K <sub>ic</sub> BUTDCE	μmol /L	403	TcDCA	μmol /mg	1.99*
Hcc <sub>DCA</sub>	-	0.18	TcDCE	μmol /mg	0.52*
Hcc <sub>DCE</sub>	-	0.86			0.175**
Hcc <sub>TCA</sub>	-	0.55	TcTCA	μmol /mg	0.52*
Hcc <sub>BUT</sub>	-	38			0.82**

*Nomenclature provided in Appendix C*

*\*Input value per Kim et al. (in press)*

*\*\*Input value adjusted to better fit media reactor data*

Overall, these reactors provided good indication of the culture's biodegradation ability. The simulations suggested that the model performs well in predicting the

culture's behavior. The input values defined in the media experiments were therefore used to simulate the microcosm experiments.

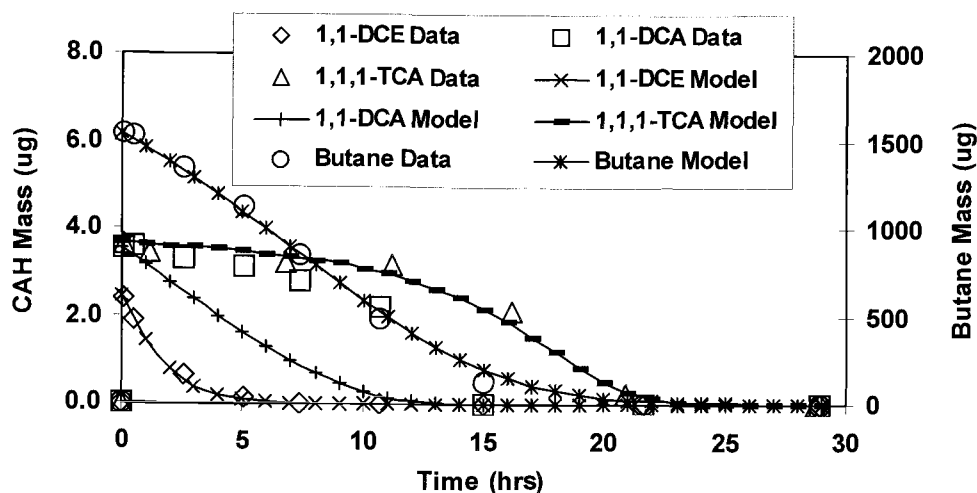


**Figure 4.3a Media experiment data and model output using Kim's (*in press*) data.**  
*Data points depict actual laboratory data. Lines depict model output.*

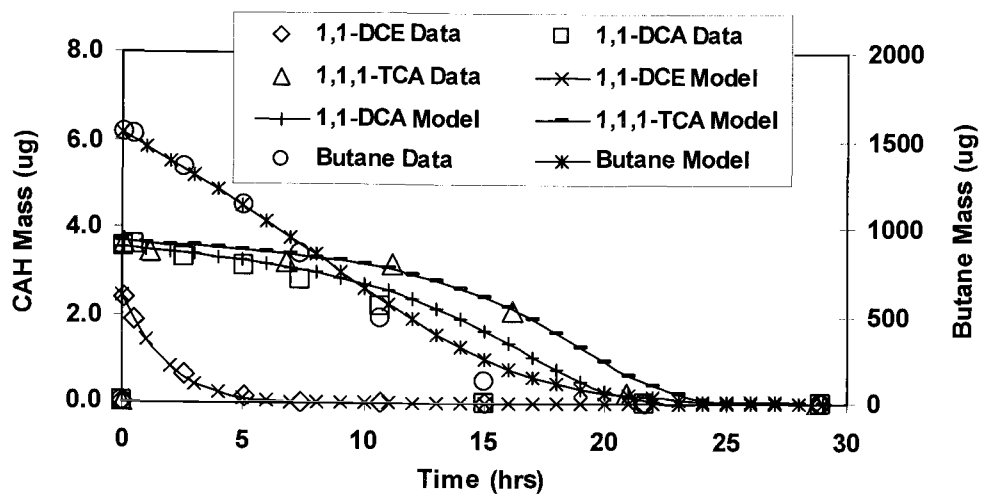


**Figure 4.3b Media data and model output using adjusted input values.**  
*Data points depict actual laboratory data. Lines depict model output.*

## 4.2 COMPARISON OF LABORATORY DATA AND MODEL SIMULATION FROM MICROCOSM EXPERIMENTS

Soil and groundwater microcosm reactors were also used to measure biotransformation of butane and the CAH mixture by the culture. Behavior within the microcosms was simulated using the Stella model (Appendix B). This section presents the results of all microcosm experiments and the model simulations. For a review of the microcosm descriptions, refer to Figure 3.2 (Chapter 3).

### 4.2.1 Results from Microcosms with Indigenous Microorganisms (M1) and Mercury Killed Controls (M4)

To serve as controls, the culture indigenous to Moffett Field (microcosm group M1) and the bioaugmented culture killed with mercury (microcosm group M4) were studied for biotransformation activity. Data for M1 and M4 are presented in Figures 4.4 and 4.5, respectively. The total mass of each compound within triplicate reactors over time is shown. Due to mass transfer limitations (Section 3.4.3), butane is represented as mass in the gaseous phase, while the CAHs are represented by total mass within the reactors. Microcosms M1 showed that for a period of 100 days, the indigenous organisms did not utilize butane or transform any of the CAHs. The mercury killed control microcosms (M4) showed negligible losses over time. Note the reproducibility of the data. These results indicated that transformation of the compounds seen in the other microcosms (M2, M3, and M5) were primarily due to the behavior of the bioaugmented culture - not transformation by the indigenous organisms or seepage losses from the reactors.

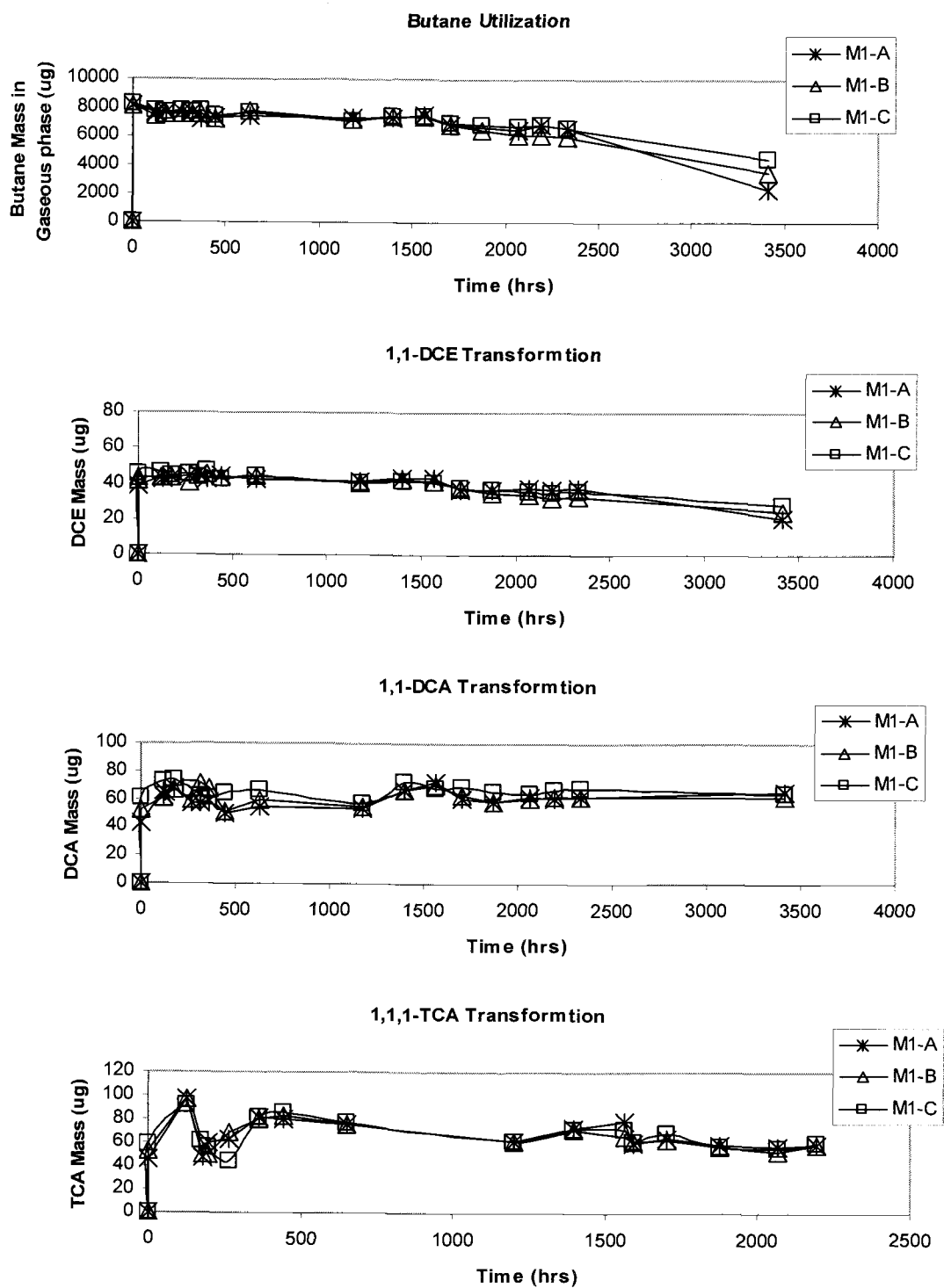


Figure 4.4: Laboratory Data for M1 (indigenous culture).

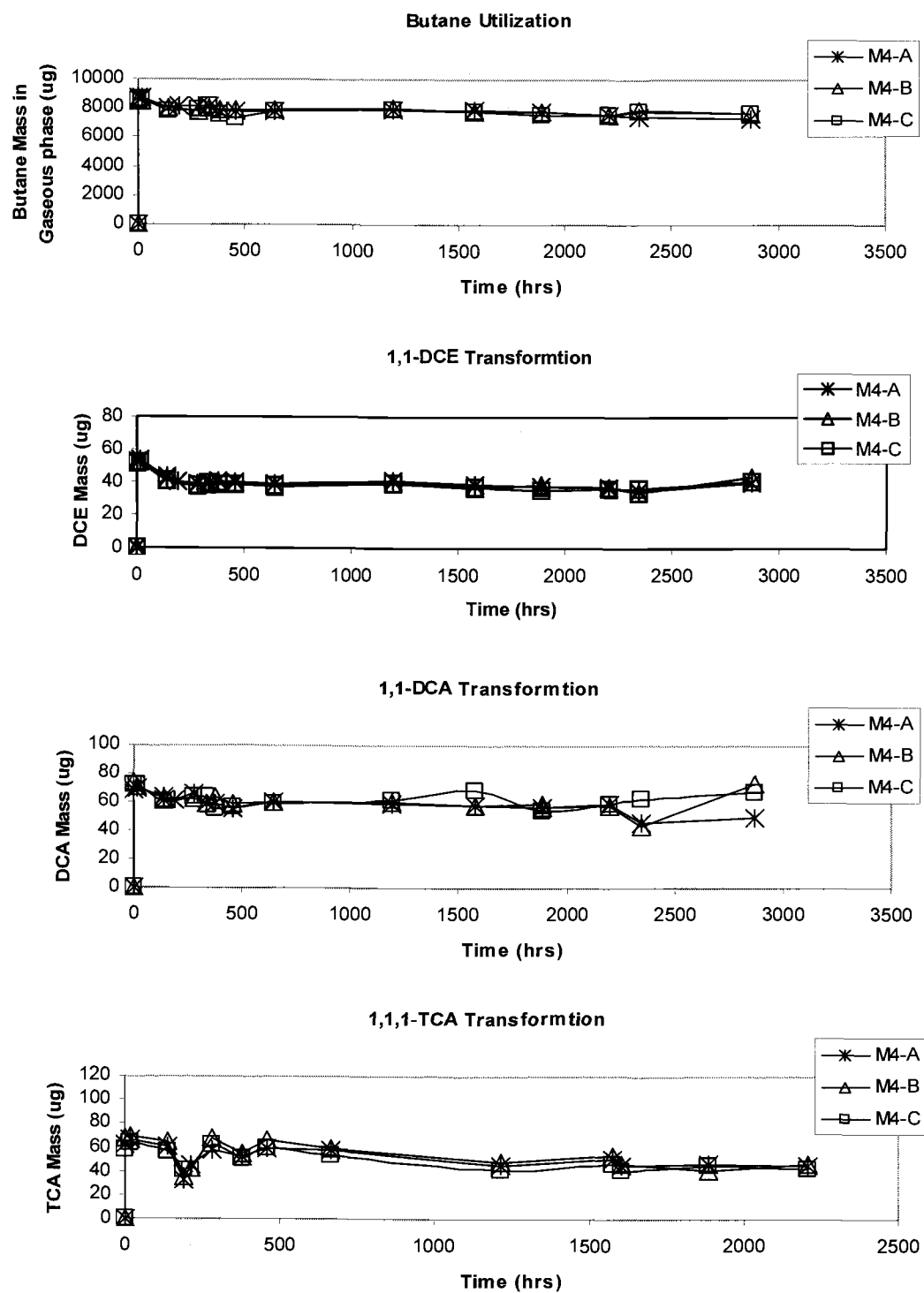


Figure 4.5: Laboratory data for M4 (mercury killed control).

#### 4.2.2 Laboratory Data from Bioaugmented Culture Exposed to Butane and CAHs (M2, M3)

Biodegradation of butane and the CAH mixture by the bioaugmented culture was studied in microcosms M2 and M3. The two groups differed in that the CAHs were added to the M3 group approximately 12 hours after butane, while butane and the CAHs were added simultaneously to the M2 group. This was done to study the effect of the butane pre-exposure on the thawed cells. All microcosms were exposed to 5 repeat additions of the compounds. Transformation over time was measured for each reactor using headspace analysis (Section 3.5).

These microcosm experiments indicated that the bioaugmented culture was capable of butane utilization and biotransformation of the CAH mixture. Data from these microcosms and the control microcosms (M1 and M4), in which no butane utilization or CAH transformation was observed, supported this conclusion. The total mass remaining in each microcosm over time was determined based on equilibrium partitioning between phases. Results for one test reactor (M2B) are presented in Figure 4.6. Due to mass transfer limitations between the gaseous and aqueous phases within the microcosms (Section 3.4.3), butane is reported as mass in the gaseous phase. As seen in the media experiments, microcosm data showed that 1,1-DCE is quickly degraded. Butane strongly inhibited the transformation of 1,1-DCA and 1,1,1-TCA. The decreased time for complete removal of all compounds as seen throughout repeat compound additions is indicative of the growing cell population. Reactors M2A, M2C, M3A, M3B, and M3C showed similar data, despite the time lag (Section 3.4.3) of CAH injection to the M3 set.

A comparison of mass profiles for all reactors is presented in Figure 4.7. Note that there is good reproducibility of trends. For example, in microcosm M3A, slower CAH transformation occurred with a lag in butane. This trend is repeated in later additions as well, and may be attributed to a lower cell mass within this reactor. During bioaugmentation of the fifth substrate addition, transformation and utilization in

microcosm M2C was lost. This was most likely due to nutrient limitations within the reactor.

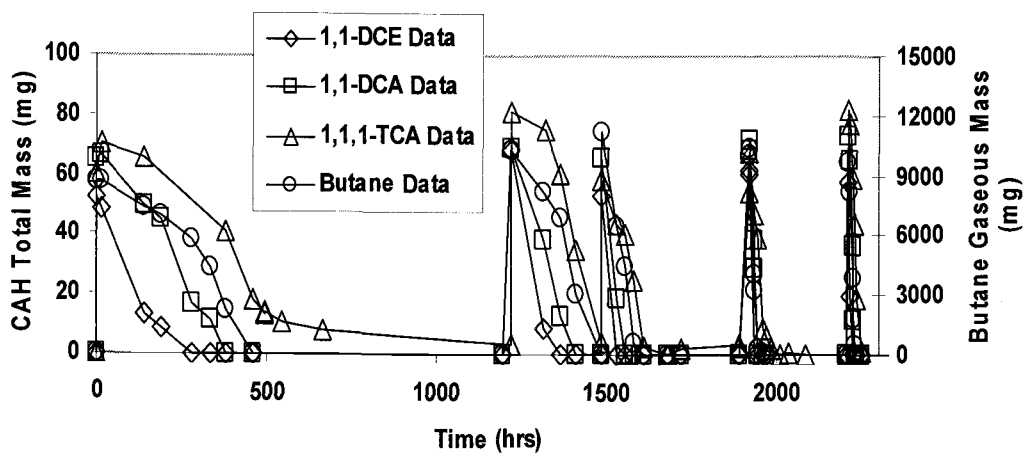
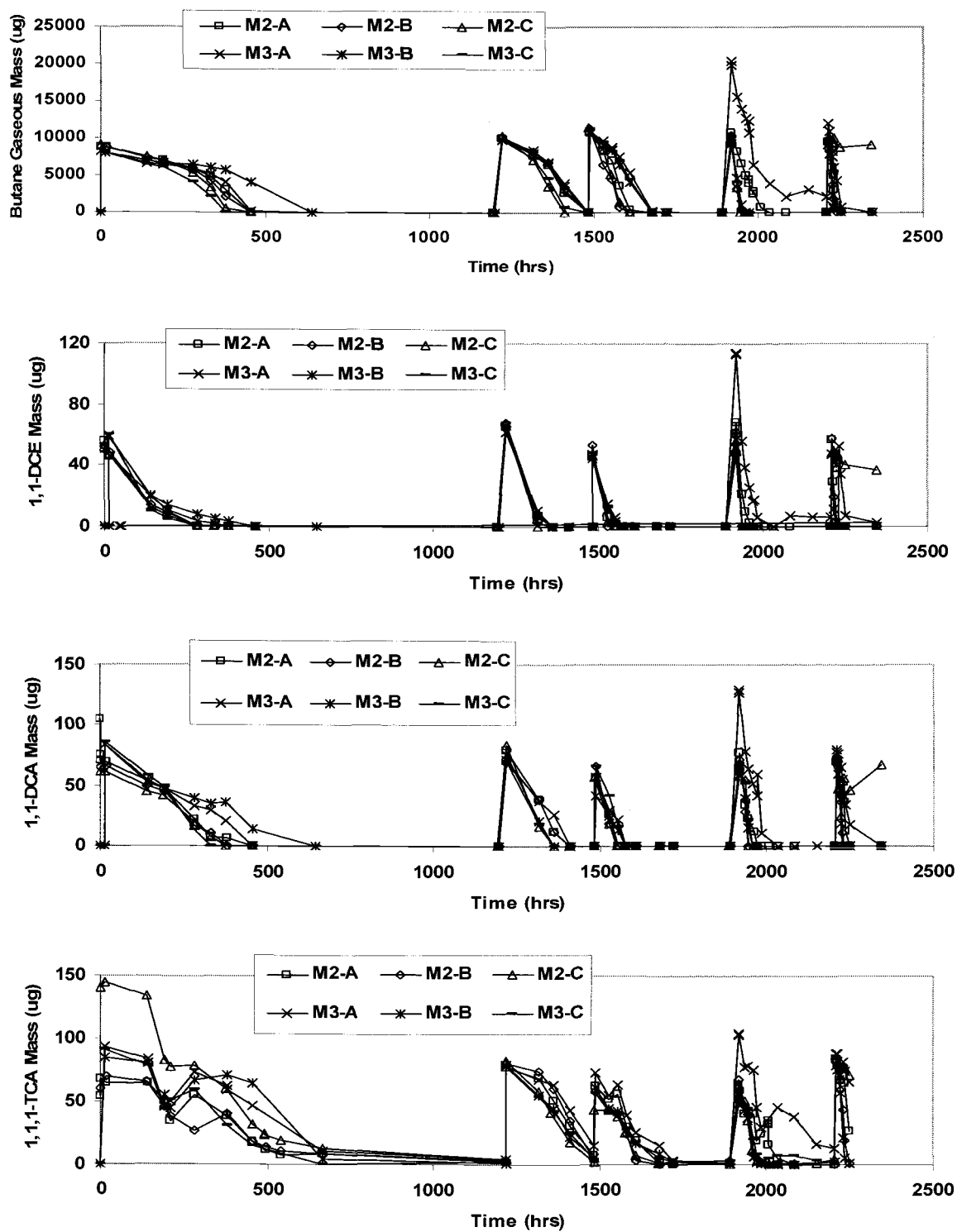


Figure 4.6: Microcosm M2B experimental data.





**Figure 4.7** Results of biotransformation experiments for microcosms M2 and M3. Butane is reported as mass in the gaseous phase.

#### 4.2.3 1,1-DCE Transformation Capacity Experiments in Microcosm

After five additions of butane and the CAH mixture had been degraded and transformed, preliminary model simulations indicated that the product toxicity of 1,1-DCE (Section 1.4.1) for our culture was much greater than that reported by Kim et al. (2000). Kim reported a 1,1-DCE transformation capacity ( $T_{cDCE}$ ) value of 0.52  $\mu\text{mol}$  DCE/mg cells (0.05 mg/mg), while our simulations showed that a value of 0.175  $\mu\text{mol}$  DCE/mg cells (0.017 mg/mg) more adequately fit our laboratory data.

A new set of laboratory experiments was run on four of the bioaugmented microcosms (M2A, M2B, M3A, and M3B) to measure the actual transformation capacity of 1,1-DCE of the culture. This was done by determining the approximate cell mass present in the reactors based on butane utilization simulations, assuming a  $T_{cDCE}$  value of 0.52  $\mu\text{mol}/\text{mg}$ , and calculating an approximate mass of 1,1-DCE required to eradicate all the cells.

To determine the required 1,1-DCE amount, repeat additions of butane were injected into the microcosms to stimulate the cells (which had been resting for several weeks) and develop utilization profiles (Section 3.4.4). These profiles were simulated using the Stella model (Appendix B) to determine approximate cell mass within the reactors. Laboratory data and model output for the latter two butane additions prior to product toxicity experiments are shown in Figure 4.8. The models represent butane utilization for various initial cell concentrations. Microcosm M2A was treated as an outlier and eliminated from further toxicity experiments. It is important to note, however, that the model provides a good fit of data from all four reactors.

Based on the three other microcosms (M2B, M3A, and M3B), 123 mg/L was assumed for the cell concentration at the start of the 1,1-DCE product toxicity tests, which corresponded to a cell mass of 41.2 mg within the reactors (aqueous volume = 0.40 L).

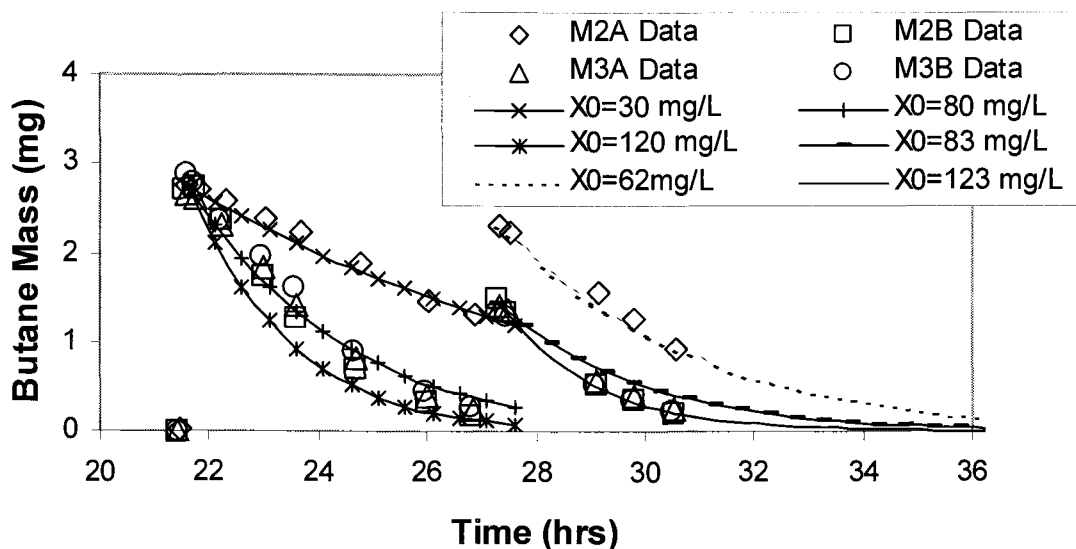


**Figure 4.8 Simulation of butane utilization prior to 1,1-DCE transformation capacity experiments.**

*Model fits to the microcosm data were used to estimate cell mass.*

Previous simulations of the CAH mixture's transformation in microcosms indicated that a  $T_{cDCE}$  value of  $0.175 \mu\text{mol DCE/mg cells}$  ( $0.017 \text{ mg/mg}$ ) better fits transformation data from our culture. Assuming  $T_{cDCE} = 0.017 \text{ mg DCE/mg cells}$ , the required amount of 1,1-DCE to kill 41.2 mg cells is  $717 \mu\text{g 1,1-DCE}$ :

$$M_{DCE} = T_{cDCE} * X = 0.02 * 41.2 = 717 \mu\text{g of 1,1-DCE}$$

where:  $M_{DCE}$  = total mass of 1,1-DCE within the microcosm ( $\mu\text{g}$ )

$T_{cDCE}$  = transformation capacity of 1,1-DCE ( $\mu\text{g DCE/mg cells}$ )

$X$  = cell mass ( $\text{mg/L}$ )

The three microcosms (M2B, M3A, and M3B) were then exposed to this elevated 1,1-DCE mass and transformation over time was measured. Approximately

1200  $\mu\text{g}$  1,1-DCE and 110  $\mu\text{g}$  1,1,1-TCA were added to the microcosm, which were then incubated at 150 rpm so that no mass transfer limitations would occur.

Figure 4.9 displays the laboratory data for the reactors and model output from simulations, including both  $T_{\text{cDCE}}$  values. Input values for the simulations are provided in Table 4.2. The plots show the mass of 1,1,1-TCA and 1,1-DCE remaining in the microcosms during the transformation test. The data are very reproducible. 1,1-DCE was rapidly transformed during the first 5 to 6 hours of these experiments, after which transformation ceased. 1,1,1-TCA transformation was never observed. This may be due to the time lag for 1,1,1-TCA transformation as opposed to 1,1-DCE. 1,1-DCE effectively eradicated all cells, preventing 1,1,1-TCA from ever being transformed. This, along with the model output, indicates that a lower  $T_{\text{cDCE}}$  value ( $0.175 \mu\text{mol}/\text{mg} = 0.017 \text{ mg}/\text{mg}$ ) better describes product toxicity for our culture. This lower  $T_{\text{cDCE}}$  value was therefore used in future model simulations. Note that at the lower  $T_{\text{cDCE}}$  value, the model also predicted that no 1,1,1-TCA transformation would occur.

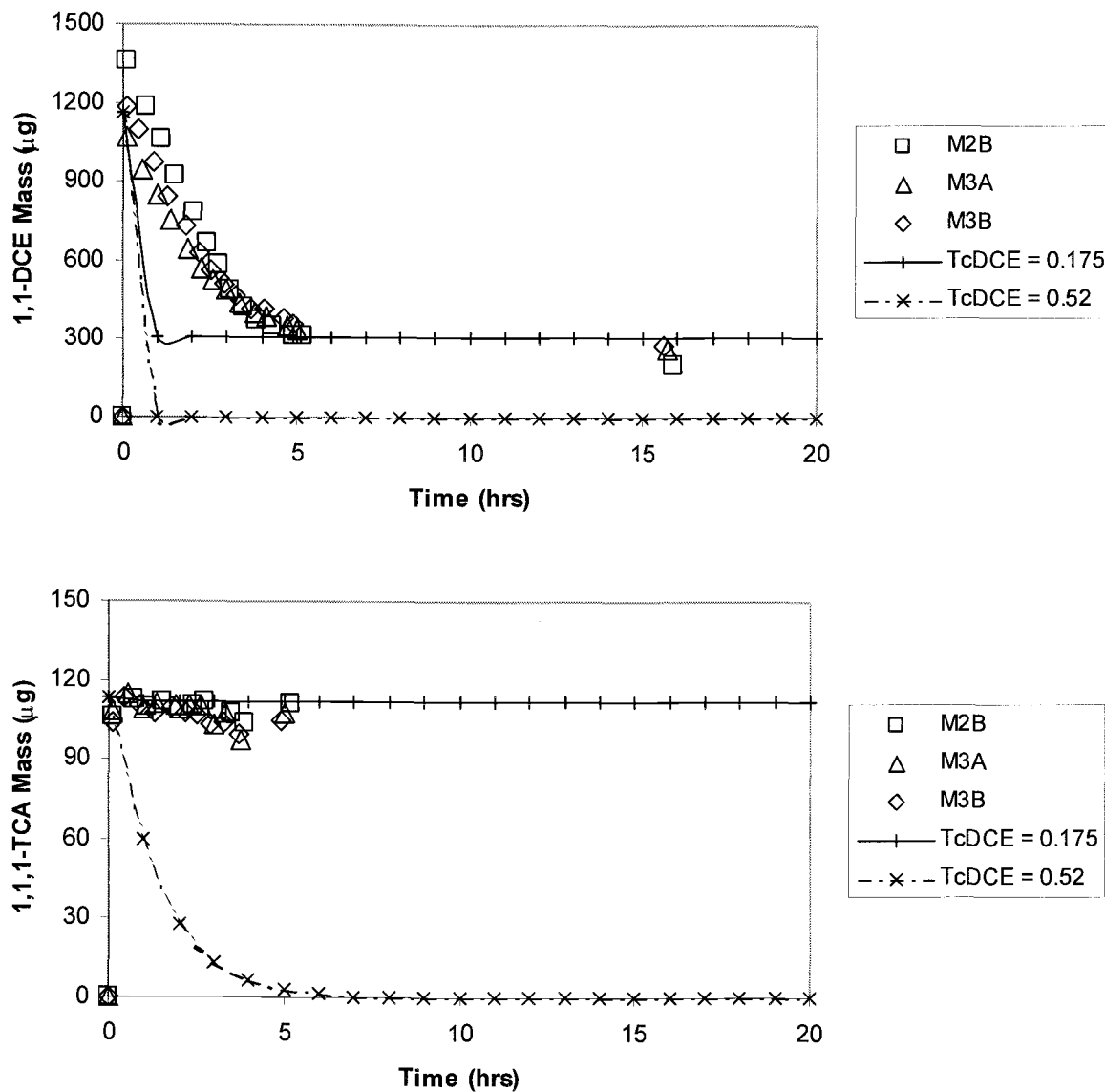


Figure 4.9 Results of transformation capacity experiments of 1,1-DCE.

**Table 4.2 Input parameters for modeling 1,1-DCE product toxicity.**

Parameter	Units	Value	Parameter	Units	Value
$K_{ic}DCABUT$	$\mu\text{mol/L}$	403	$X_0$	mg/L	123*
$K_{ic}DCADCE$	$\mu\text{mol/L}$	18	$Y$	mg/ $\mu\text{mol}$	.046
$K_{ic}DCATCA$	$\mu\text{mol/L}$	16	$b$	$\text{hr}^{-1}$	0.0035
$K_{ic}DCEBUT$	$\mu\text{mol/L}$	8.7	$V_L$	L	.400
$K_{ic}DCEdCA$	$\mu\text{mol/L}$	3.6	$V_G$	L	.267
$K_{ic}DCEtCA$	$\mu\text{mol/L}$	1.1	$k_{max}BUT$	$\mu\text{mol/mg/hr}$	2.5
$K_{ic}TCABUT$	$\mu\text{mol/L}$	313	$k_{max}DCA$	$\mu\text{mol/mg/hr}$	0.49
$K_{ic}TCADCA$	$\mu\text{mol/L}$	9.8	$k_{max}DCE$	$\mu\text{mol/mg/hr}$	2.8
$K_{ic}TCADCE$	$\mu\text{mol/L}$	17	$k_{max}TCA$	$\mu\text{mol/mg/hr}$	0.2
$K_{iu}BUTDCA$	$\mu\text{mol/L}$	4.0	$K_{sBUT}$	$\mu\text{mol/L}$	19.2
$K_{iu}BUTDCE$	$\mu\text{mol/L}$	6.9	$K_{sDCA}$	$\mu\text{mol/L}$	19.2
$K_{iu}BUTTCA$	$\mu\text{mol/L}$	0.5	$K_{sDCE}$	$\mu\text{mol/L}$	1.48
$K_{ic}BUTDCE$	$\mu\text{mol/L}$	0.33	$K_{sTCA}$	$\mu\text{mol/L}$	12.2
$H_{ccDCA}$	-	0.18	$T_{cDCA}$	$\mu\text{mol/mg}$	1.99
$H_{ccDCE}$	-	0.86	$T_{cDCE}$	$\mu\text{mol/mg}$	0.52
$H_{ccTCA}$	-	0.55			0.175
$H_{ccBUT}$	-	38	$T_{cTCA}$	$\mu\text{mol/mg}$	0.82

*Nomenclature provided in Appendix C*

*\*Initial cell concentration for 1,1-DCE toxicity experiments only. Initial cell concentrations for butane utilization models prior to toxicity experiment as noted in the legend of Figure 4.8.*

As seen in Figure 4.9, the model predicts that 1,1-DCE transformation should have occurred much faster than that shown by actual data. This indicated that the 1,1-DCE maximum transformation rate was less than that used as an input value in the model ( $k_{mDCE} = 2.8 \mu\text{mol/mg/hr}$ ). Therefore, simulations were run at lower  $k_{mDCE}$  values (0.28 and 0.10  $\mu\text{mol/mg/hr}$ ) in attempt to better fit this observation. Figure 4.10 shows 1,1-DCE and 1,1,1-TCA transformation simulated with various  $k_{mDCE}$  values and compares the output to the actual data measured in the reactors. All other input values followed those listed in Table 4.2.

Comparison of the model outputs indicated that a  $k_{mDCE}$  value an order of magnitude less than that defined by Kim et al. (*in press*) more accurately describes the laboratory data. Note that even at varying utilization rates, the effect of product toxicity remains constant; there is no degradation after 5 hours. It is difficult to determine what factors result in the possible lower  $k_{mDCE}$  needed to match the laboratory data. It may have been that enzyme activity was lower than in resting cell tests of  $k_{mDCE}$  (Section 4.2.2), or the culture actually has lower  $k_{mDCE}$  values than Kim's culture. Later microcosm tests evaluated the sensitivity to the  $k_{mDCE}$  value (Section 4.2.6).

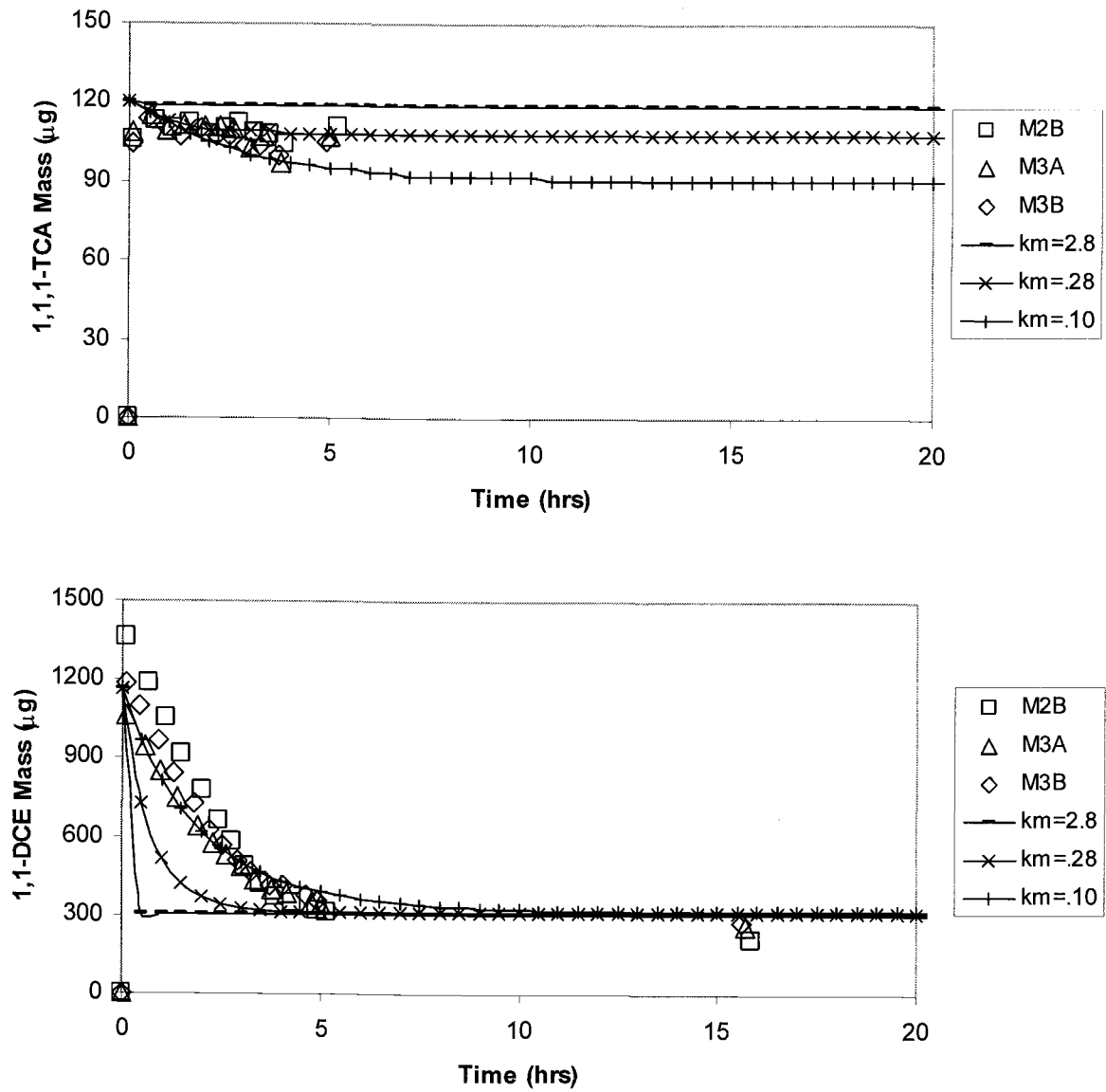


Figure 4.10 Simulations for various  $k_{mDCE}$  values compared to laboratory data.



#### 4.2.4 Results of the Mass Transfer Limitation Studies

Substrate utilization and transformation may be hindered by mass transfer limitations (MTL) due to incomplete partitioning between the reactor's aqueous and gaseous volumes (Section 3.4.3). Because slow transformation was observed during transformation of the first three compound additions in our microcosm tests, we suspected MTL had occurred. Also, because the size of the microcosms was quite large (400 mL groundwater and 267 mL headspace), MTL would have had a significant effect on transformation. If that was the case, non-equilibrium partitioning would need to be incorporated into the model simulations. A laboratory experiment was therefore performed to determine if MTL were likely occurring.

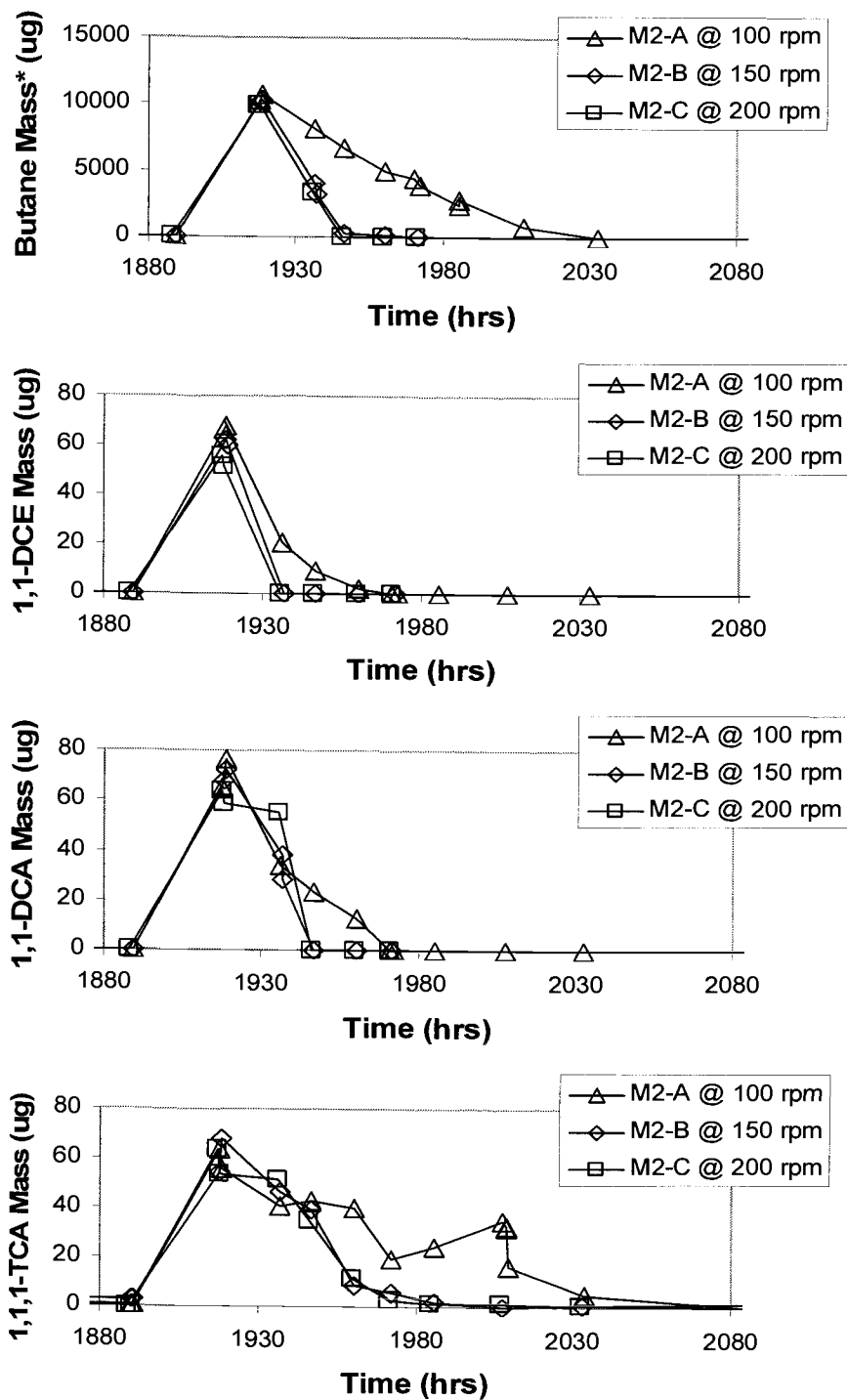
The active microcosms containing the bioaugmented culture (M2 and M3) were separated into three groups after injecting a fourth addition of compounds. M2A and M3B maintained incubation at the shaking speed of the previous three transformation tests (100 rpm). M2B and M3B were set at a shaker speed of 150 rpm, while M2C and M3C were shaken at 200 rpm. Headspace analysis (Section 3.5) was used to create transformation profiles over time.

Figure 4.11 illustrates the influence of MTL on our data by comparing biodegradation in the M2 microcosms at the various shaker speeds. Transformation and utilization in microcosms set at the lower speed (100 rpm) were hindered in contrast to those shaken at higher speeds (150, and 200 rpm). M3 microcosms showed similar behavior, and the data are presented in Appendix F. These results indicated that, when shaken at the slower speed, MTL were occurring in the reactors.

Note that butane mass is reported as mass in the gaseous phase within the reactors. This was done because, while headspace analysis allowed mass measurement of the gaseous phase, MTL restricted the calculation of total mass within the reactor. Since the Henry's coefficient of butane (38) is two orders of magnitude greater than those of the CAHs (1,1-DCE, 0.86; 1,1-DCA 0.86; 1,1,1-TCA 0.55), it would have had the greatest MTL of the compounds tested.

Kim et al. (2000) acknowledged the influence such limitations may have had on their transformation studies and therefore ran experiments with 1,1-DCE to determine mass transfer rate coefficients ( $K_{La}$  and  $K_{Ga}$ ). The equations provided in Appendix G were derived to define each value.

The Stella biotransformation model (Appendix B) was run including the MTL mathematics described in Appendix G to simulate the microcosms and define a  $K_{Ga}$  value. To do this,  $K_{Ga}$  was varied while keeping all other input values constant. Microcosms M5 were chosen to simplify the  $K_{Ga}$  determination because they contained only butane and had been exposed to the same incubating conditions as the first three biotransformation experiments for the M2 and M3 reactors. Results of the MTL simulations for M5 and the  $K_{Ga}$  value are presented in Section 4.2.5.



**Figure 4.11** Mass transfer limitation study results for microcosm M2

*\*Butane Mass is reported as mass in the gaseous phase.*

#### 4.2.5 Results and Modeling of Butane in the Absence of CAHs (M5)

For the M5 microcosms, butane utilization was studied in the absence of CAHs. Butane mass remaining in the gaseous phase within the reactors was measured using headspace analysis (Section 3.5). The mass in the gas phase is presented since it can be computed based on the headspace analysis even if mass transfer limitations (MTL) were occurring (Section 4.2.4). MTL were suspected for the first 3 butane additions in the M5 microcosms, because these reactors were the same size and incubated at the same speed as the M2 and M3 microcosms (Table 3.4), for which MTL had been tested and confirmed (Section 4.2.3). The slow shaking speed (100 rpm) and the reactors' large sizes would have caused significant MTL. Figure 4.12 displays the headspace butane mass after each of four butane spikes. Note that there is good reproducibility.

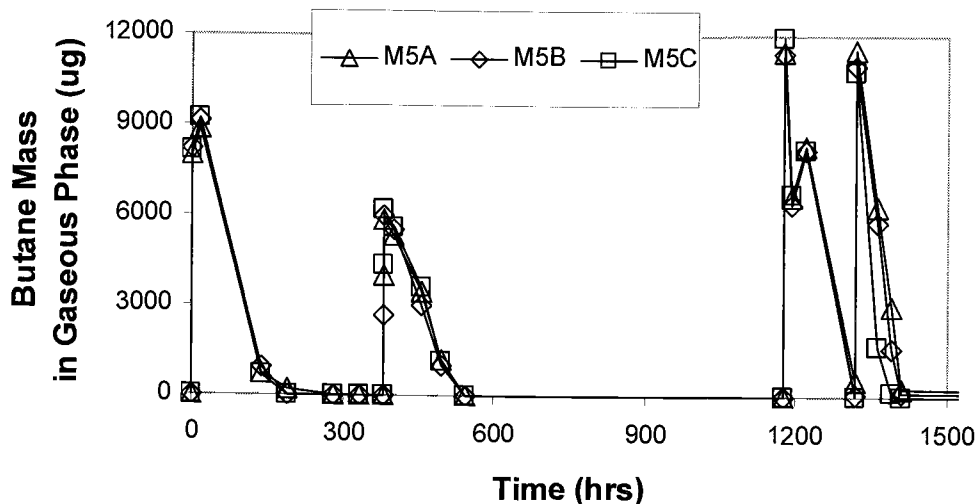


**Figure 4.12 Butane utilization within microcosms M5.**

During transformation of the first three additions of compounds, all the reactors had been shaken too slowly (100 rpm) to create equilibrium partitioning between the

reactor's gaseous and aqueous phases (Section 3.4.3). Results of MTL experiments performed on microcosms M2 and M3 for various shaking speeds (100, 150, and 200 rpm) confirmed this (Section 4.2.4). Using the Stella biotransformation model (Appendix B) combined with mathematics accounting for MTL (Appendix G), simulations were performed on the M5 microcosm data to define a mass transfer rate coefficient,  $K_{Ga}$ .

The simulation input values are provided in Table 4.3, with the exception of initial cell concentration ( $X_0$ ) and  $K_{Ga}$ .  $X_0$  and  $K_{Ga}$  values for each MTL simulation of M5A are listed in Table 4.4.  $K_{Ga}$  values were varied to determine the best fits to the MTL experimental data. For simulating utilization of the first butane addition,  $X_0$  was assigned a value of 3.8 mg/L. This value compares to the estimated initial cell mass of 1.5 mg/L (Section 3.4.1). This first simulation was allowed to run until the time of the second addition of butane (about 380 hours). The model predicted a cell concentration at this time that was used as the initial cell concentration for simulation of butane utilization of the second addition. The same procedure was used for the remaining simulations.

**Table 4.3: Input Values for Simulating MTL during Different Spikes**

Parameter	Units	Value	Parameter	Units	Value
$K_{ic}DCABUT$	$\mu\text{mol/L}$	403	$X_0$	mg/L	varies*
$K_{ic}DCADCE$	$\mu\text{mol/L}$	18	$Y$	mg/ $\mu\text{mol}$	.046
$K_{ic}DCATCA$	$\mu\text{mol/L}$	16	$b$	$\text{hr}^{-1}$	0.0035
$K_{ic}DCEBUT$	$\mu\text{mol/L}$	8.7	$K_{Ga}$	$\text{hr}^{-1}$	varies*
$K_{ic}DCEDCA$	$\mu\text{mol/L}$	3.6	$V_L$	L	.400
$K_{ic}DCETCA$	$\mu\text{mol/L}$	1.1	$V_G$	L	.267
$K_{ic}TCABUT$	$\mu\text{mol/L}$	313	$k_{max}BUT$	$\mu\text{mol/mg/hr}$	2.5
$K_{ic}TCADCA$	$\mu\text{mol/L}$	9.8	$k_{max}DCA$	$\mu\text{mol/mg/hr}$	0.49
$K_{ic}TCADCE$	$\mu\text{mol/L}$	17	$k_{max}DCE$	$\mu\text{mol/mg/hr}$	2.8
$K_{iu}BUTDCA$	$\mu\text{mol/L}$	4.0	$k_{max}TCA$	$\mu\text{mol/mg/hr}$	0.2
$K_{iu}BUTDCE$	$\mu\text{mol/L}$	6.9	$K_{s}BUT$	$\mu\text{mol/L}$	19.2
$K_{iu}BUTTCA$	$\mu\text{mol/L}$	0.5	$K_{s}DCA$	$\mu\text{mol/L}$	19.2
$K_{ic}BUTDCE$	$\mu\text{mol/L}$	0.33	$K_{s}DCE$	$\mu\text{mol/L}$	1.48
			$K_{s}TCA$	$\mu\text{mol/L}$	12.2
$H_{cc}DCA$	-	0.18	$TcDCA$	$\mu\text{mol/mg}$	1.99
$H_{cc}DCE$	-	0.86	$TcDCE$	$\mu\text{mol/mg}$	0.175
$H_{cc}TCA$	-	0.55	$TcTCA$	$\mu\text{mol/mg}$	0.82
$H_{cc}BUT$	-	38			

*Nomenclature provided in Appendix C*

*\*Initial cell concentration and  $K_{Ga}$  varied for each simulation. See Table 4.4*

**Table 4.4: Initial cell concentration and  $K_{Ga}$  used in simulating MTL.**

Spike #	Approx Time since Last Spike (hrs)	$X_0$ (mg/L) <sup>a</sup>			
		MTL <sup>b</sup>			No MTL <sup>c</sup>
		$K_{Ga} = 0.10$	$K_{Ga} = 0.03$	$K_{Ga} = 0.01$	
S1	0	3.8	3.8	3.8	3.8
S2	380	6.3	6.8	7.6	6.1
S3	790	1.2	1.3	1.7	1.2
S4	142.3	17.3	16.4	12.4	17.1

a.  $X_0$  = Initial Cell Concentration at beginning of each simulation

b. MTL = Simulations including mass transfer limitations

c. no MTL = Simulations not including mass transfer limitations

Figure 4.13 displays a comparison of the M5A data (shown in Figure 4.12) and model output with and without MTL. MTL simulations include those for  $K_{Ga}$  values of 0.01, 0.03, and 0.10  $\text{hr}^{-1}$ . Mass from the gaseous phase was recorded instead of total mass due to MTL occurring between fluid phases. Cell concentrations are also presented to show differences between growth and decay according to utilization. Note that during the growth stage, for greater MTL (higher  $K_{Ga}$  values), there is slower butane utilization in conjunction with less cell growth. However, because more butane is available, there is less cell decay during the later period of utilization.

The MTL model with a  $K_{Ga}$  value of 0.03  $\text{hr}^{-1}$  most closely fit the butane utilization data for all repeat additions. This value was therefore used in modeling transformation of the first three compound additions for M2, M3, and M5 microcosms (and the fourth for M2A and M3A).

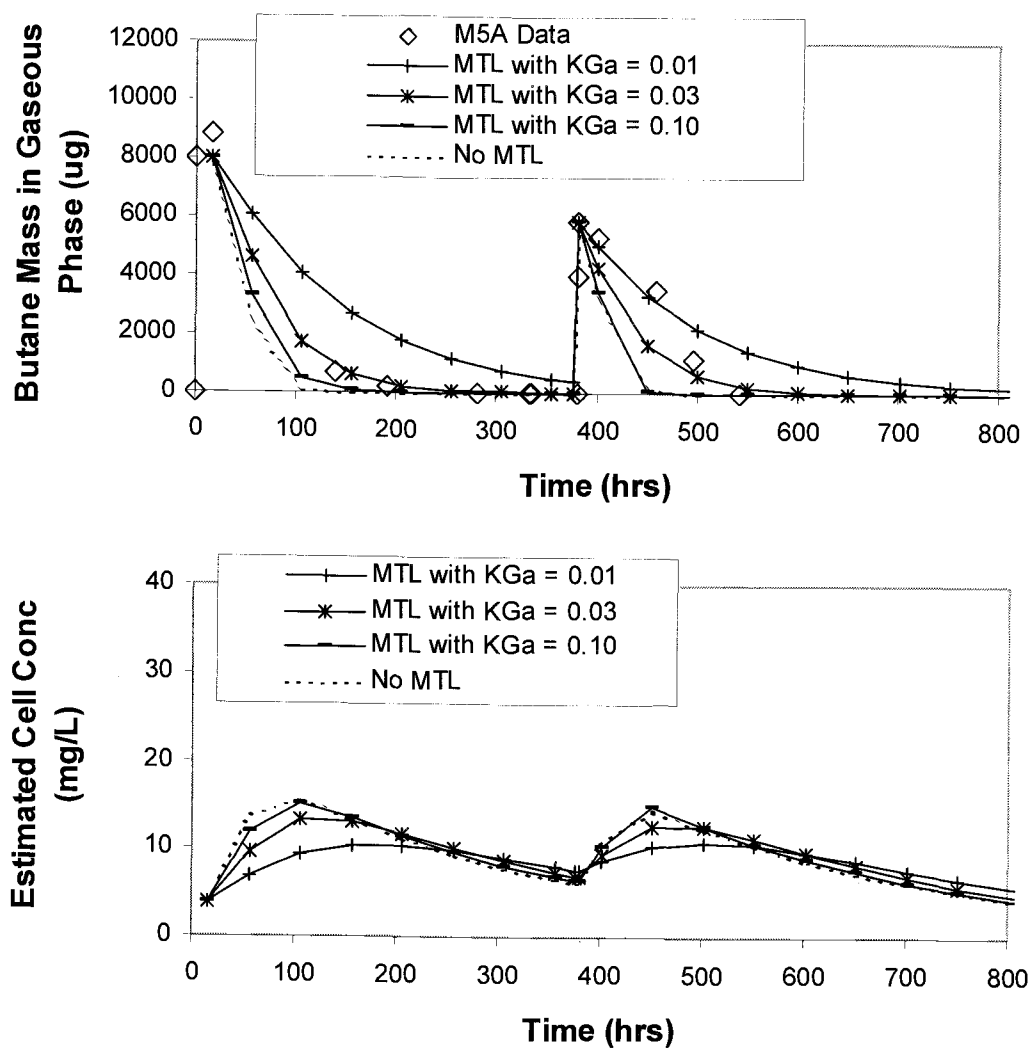


Figure 4.13a Mass transfer limitation model for microcosm M5A, 0 to 800 hrs.



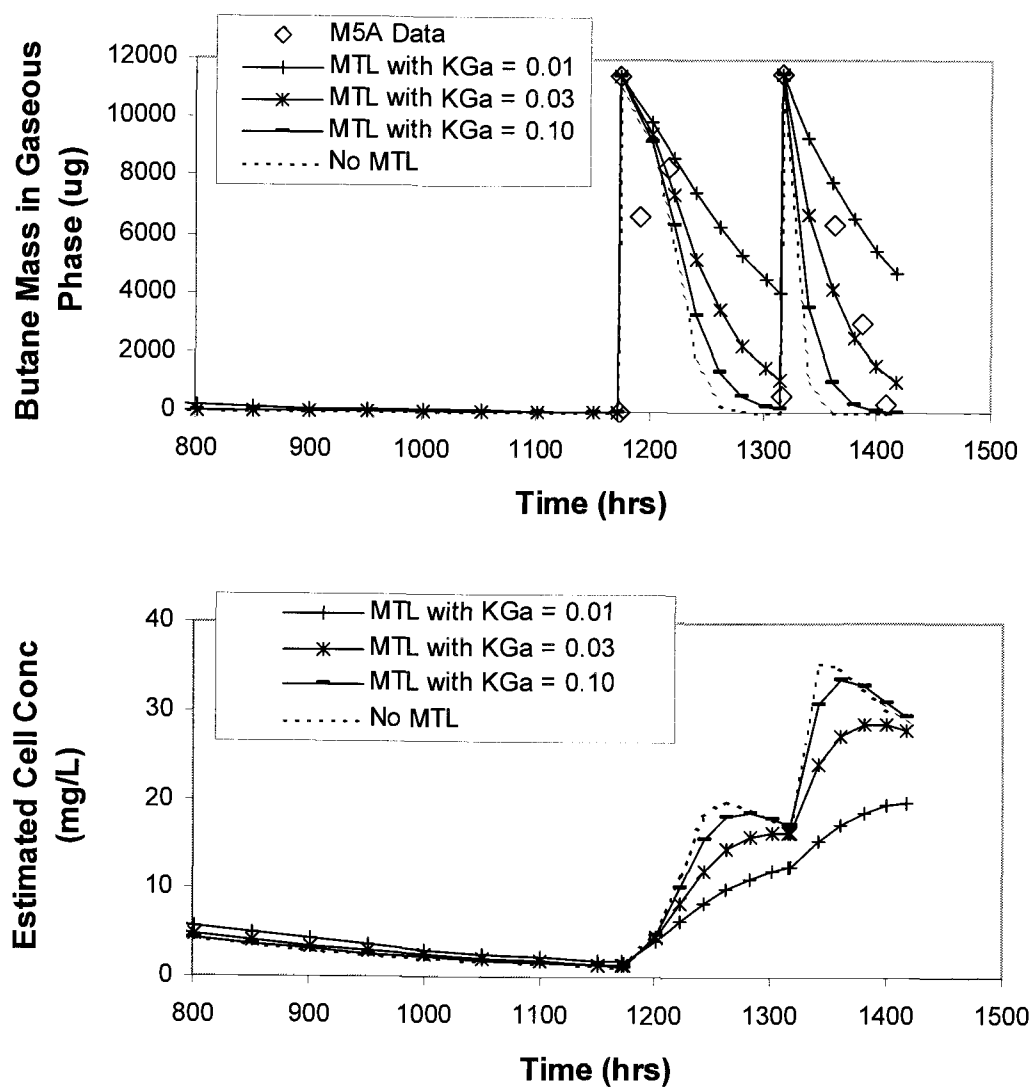


Figure 4.13b Mass transfer limitation model for microcosm M5A, 800 to 1500 hrs.

#### 4.2.6 Model Simulations for Biotransformation in Microcosm M2B

The Stella biotransformation model presented in Appendix B was used to simulate the laboratory data of microcosm M2B. The input values for the model are listed in Table 4.5, and were based on those defined by Kim et al. (*in press*), with the exception of those noted previously in this chapter ( $T_{cTCA}$ ,  $T_{cDCE}$ ,  $K_{Ga}$ ).

Initial cell masses for simulating biotransformation of each compound addition are listed in Table 4.6. For simulating utilization of the first butane addition,  $X_0$  was assigned a value of 4.1 mg/L. This value compares to the estimated initial cell mass of 1.5 mg/L (Section 3.4.1). The first simulation (S1) was allowed to run until the time of the second addition of butane (about 1200 hours). The cell concentration remaining when butane was completely utilized (approximately 500 hrs) was input as the initial cell concentration for simulation of utilization of the second butane addition (S2). This pattern was followed for the remaining simulations. Initial cell concentrations were assigned this way because it was assumed that the decay term for the model is not appropriate for long periods when the cells are not exposed to the primary growth substrate. This lower cell decay is still hard to explain unless product toxicities were actually less than those assumed.

As experiments indicated (Section 4.2.4), non-equilibrium partitioning between the gaseous and aqueous phases occurred in the reactors during biotransformation of the first three compound additions (S1 through S3). Therefore, mass transfer limitations (MTL) were included in these model simulations as done with the simulations of microcosms M5 (Section 4.2.5). A mass transfer coefficient ( $K_{Ga} = 0.03 \text{ hr}^{-1}$ ) determined in Section 4.2.5 was used.

**Table 4.5. Input values for simulating biotransformation in M2 and M3.**

Parameter	Units	Value	Parameter	Units	Value
$K_{ic}DCABUT$	$\mu\text{mol/L}$	403	$X_0$	mg/L	varies*
$K_{ic}DCADCE$	$\mu\text{mol/L}$	18	$Y$	mg/ $\mu\text{mol}$	.046
$K_{ic}DCATCA$	$\mu\text{mol/L}$	16	$b$	$\text{hr}^{-1}$	0.0035**
$K_{ic}DCEBUT$	$\mu\text{mol/L}$	8.7	$K_{Ga}$	$\text{hr}^{-1}$	0.03***
$K_{ic}DCEDCA$	$\mu\text{mol/L}$	3.6	$V_L$	L	.400
$K_{ic}DCETCA$	$\mu\text{mol/L}$	1.1	$V_G$	L	.267
$K_{ic}TCABUT$	$\mu\text{mol/L}$	313	$k_{max}BUT$	$\mu\text{mol/mg/hr}$	2.5
$K_{ic}TCADCA$	$\mu\text{mol/L}$	9.8	$k_{max}DCA$	$\mu\text{mol/mg/hr}$	0.49
$K_{ic}TCADCE$	$\mu\text{mol/L}$	17	$k_{max}DCE$	$\mu\text{mol/mg/hr}$	2.8
$K_{iu}BUTDCA$	$\mu\text{mol/L}$	4.0**	$k_{max}TCA$	$\mu\text{mol/mg/hr}$	0.2
$K_{iu}BUTDCE$	$\mu\text{mol/L}$	6.9	$K_sBUT$	$\mu\text{mol/L}$	19.2
$K_{iu}BUTTCA$	$\mu\text{mol/L}$	0.5	$K_sDCA$	$\mu\text{mol/L}$	19.2
$K_{ic}BUTDCE$	$\mu\text{mol/L}$	0.33	$K_sDCE$	$\mu\text{mol/L}$	1.48
$H_{ccDCA}$	-	0.18	$K_sTCA$	$\mu\text{mol/L}$	12.2
$H_{ccDCE}$	-	0.86	$TcDCA$	$\mu\text{mol/mg}$	1.99
$H_{ccTCA}$	-	0.55	$TcDCE$	$\mu\text{mol/mg}$	0.175**
$H_{ccBUT}$	-	38	$TcTCA$	$\mu\text{mol/mg}$	0.82**

*Nomenclature provided in Appendix C*

*\*Initial cell concentration varied for each simulation. See Table 4.6*

*\*\*Values adjusted to better fit microcosm data.*

*\*\*\*Mass Transfer Limitation was assumed for simulations S1, S2, and S3 only.*

**Table 4.6 Initial cell concentration for simulating biotransformation in M2 and M3.**

<i>Spike #</i>	<i>Approx Time since Last Spike (hrs)</i>	<i>MTL included in Simulation?</i>	<i>X<sub>0</sub> (mg/L)</i>
S1	-	Y	4.1
S2	1200	Y	7.0
S3	270	Y	9.2
S4	430	N	12.7
S5	92	N	17.7

Figure 4.14 displays the modeling and microcosms results, showing the total mass within the microcosm over time for five additions of butane and the CAHs. Butane mass from the gaseous phase was recorded instead of total mass due to MTL occurring between fluid phases (Section 4.2.4). Of interest here is the model's ability to mimic transformation orders and inhibition influences of each compound. Note that as the laboratory studies showed, the model predicted 1,1-DCE to be quickly degraded, followed by 1,1-DCA and 1,1,1-TCA transformation. Butane showed very strong inhibitory affects on 1,1-DCA and 1,1,1-TCA, with faster transformation of these CAHs occurring after butane concentrations were decreased by greater than 50%. The decrease in time for complete biotransformation of all compounds for consecutive substrate additions was indicative of the growing cell mass within the reactors, as seen in Figure 4.14c.

The sharp peaks at hours 1220, 1485, 1920, and 2210 represented the adjusted cell concentrations input into the model to best fit the data. (See first paragraph of this Section.) The sharp decline after each of these peaks resulted from the extreme product toxicity of 1,1-DCE.

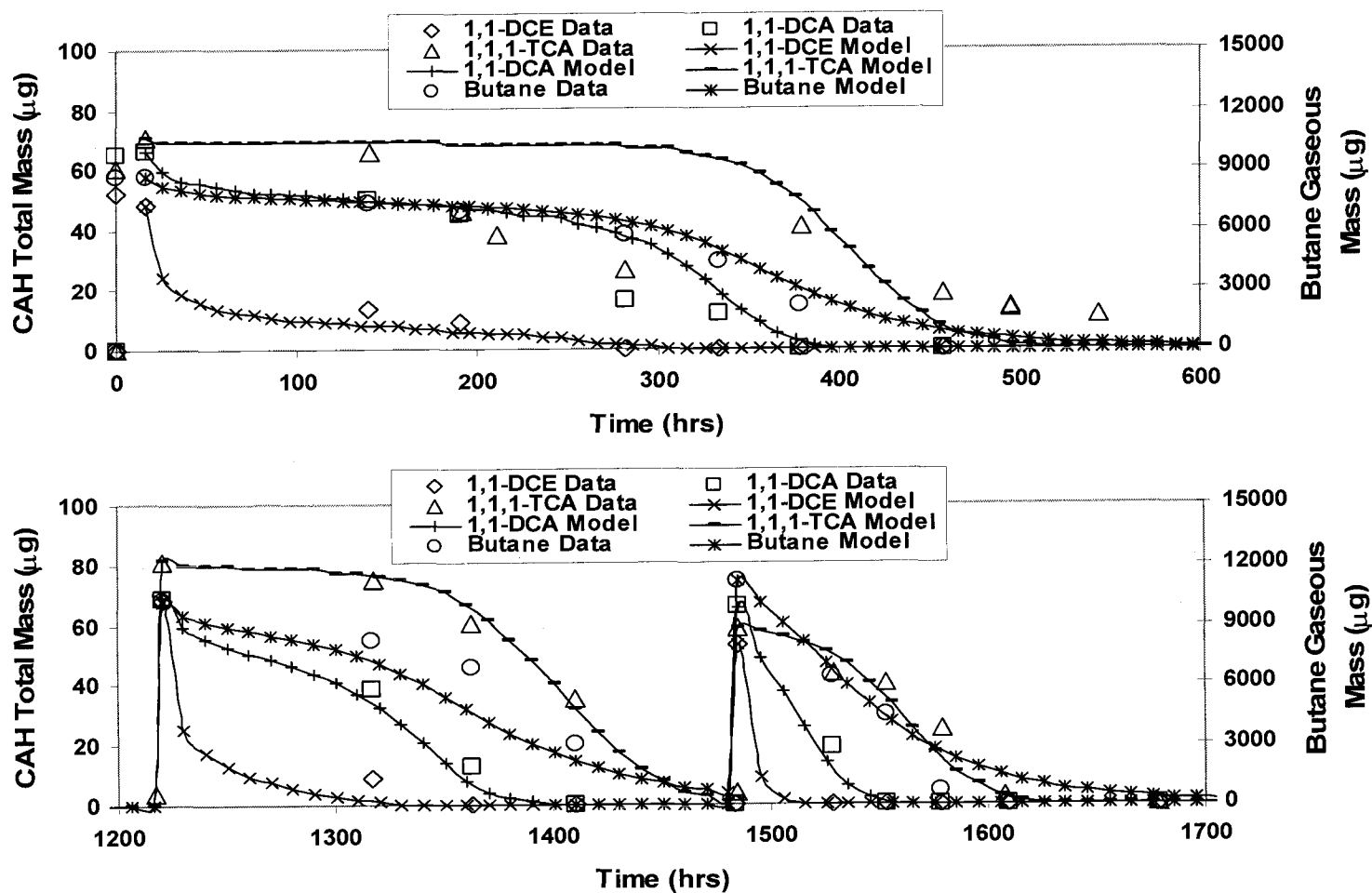


Figure 4.14a Comparison of laboratory data verses model output for M2B, 0 to 1700 hrs.

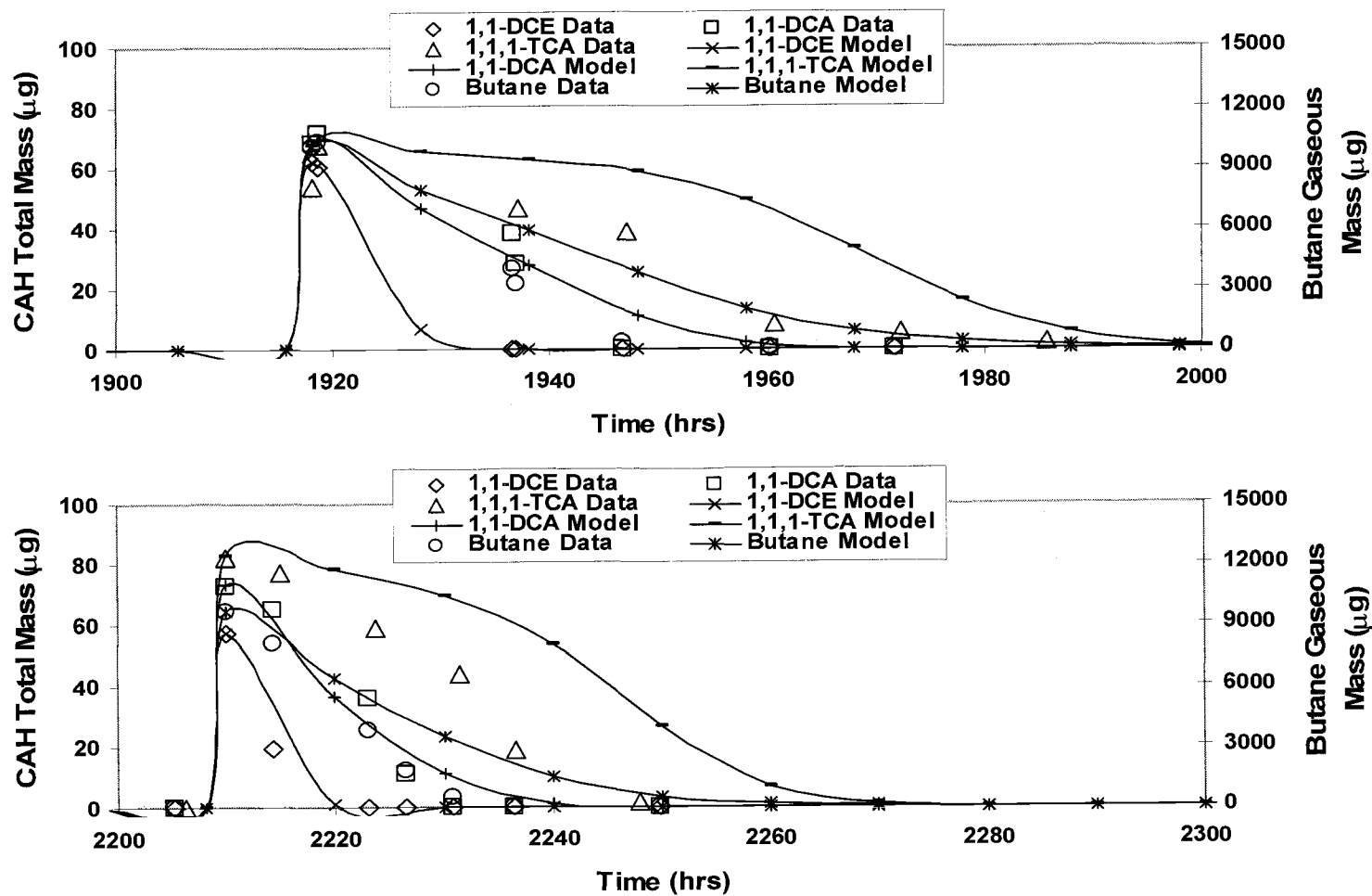


Figure 4.14b Comparison of laboratory data verses model output for M2B, 1900 to 2300 hrs.

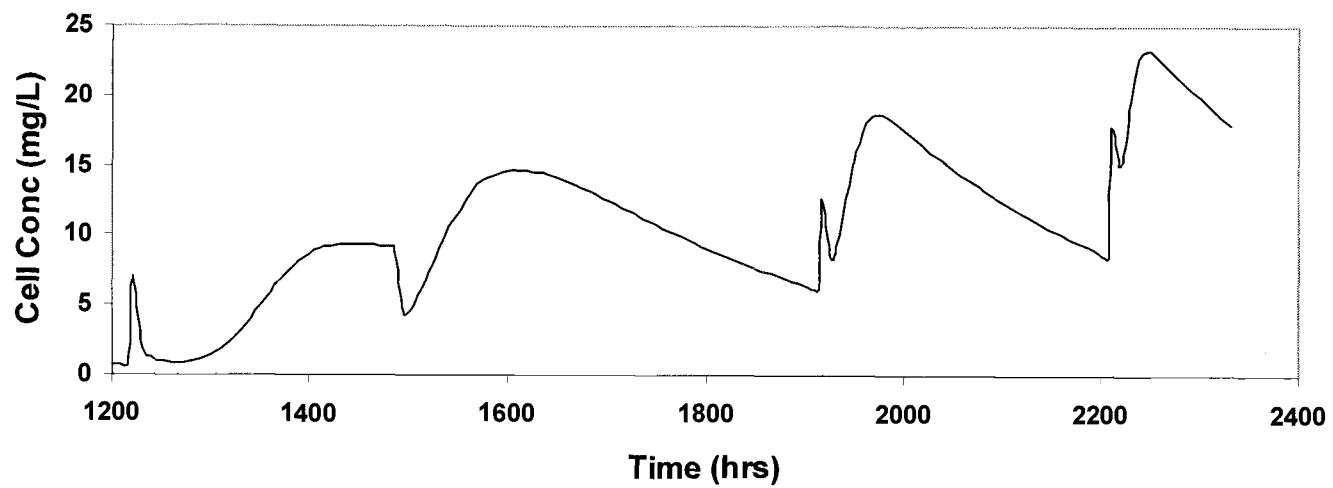
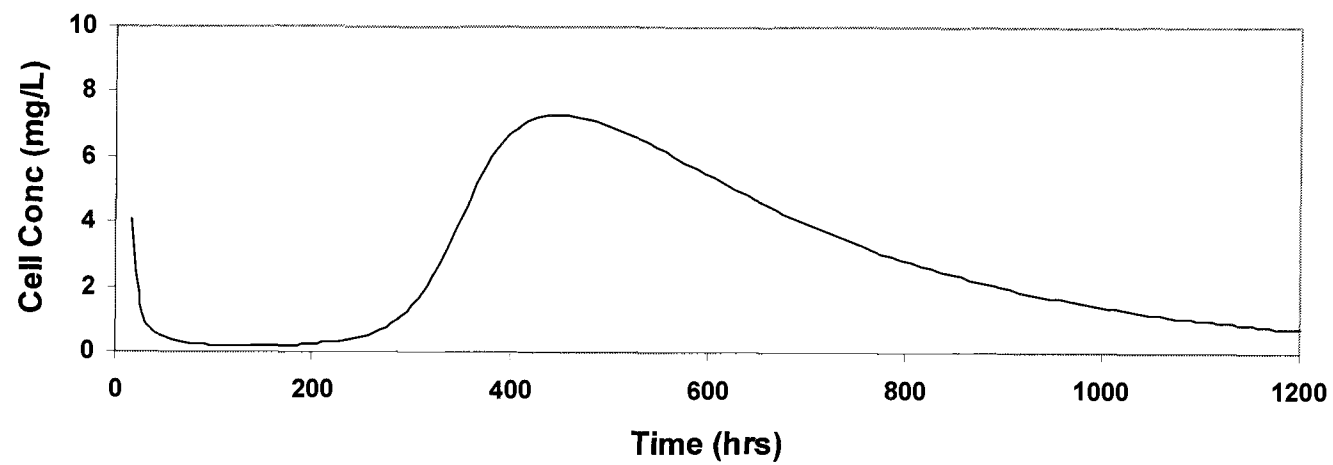


Figure 4.14c Cell concentrations calculated by the Stella model for M2B biotransformation.

Biotransformation simulations were also run for M2B at the lower 1,1-DCE transformation rate ( $k_{mDCE} = 0.1 \mu\text{mol/mg/hr}$ ), which more closely fit the product toxicity experimental data (Section 4.2.3). This value was an order of magnitude lower than the  $k_{mDCE}$  value ( $2.8 \mu\text{mol/mg.day}$ ) defined by Kim et al. (in press). Initial cell concentration was adjusted to most appropriately fit the 1,1-DCE transformation data. The model results are compared to the laboratory data for the first two substrate additions in Figure 4.15. Other parameter values were the same as those presented in Table 4.5 with the exception of  $k_{mDCE}$  and the noncompetitive inhibition constant of butane on 1,1-DCA ( $K_{luBUTDCA}$ ). This latter parameter was assigned a value of  $0.4 \mu\text{mol/mg}$  which was used to fit transformation data from the media experiments (Section 4.1). This value was required for the model to simulate the order of CAH transformation observed: 1,1-DCE transformed first, followed by 1,1-DCA and 1,1,1-TCA. (Using the value from previous M2B simulations,  $K_{luBUTDCA} = 4.0 \mu\text{mol/mg}$ , the model resulted in 1,1-DCA transformation occurring before that of 1,1-DCE.)

In observing Figure 4.15, even though the transformation orders are correct, using the lower  $k_{mDCE}$  value resulted in more rapid butane utilization and 1,1-DCE and 1,1,1-TCA transformation. Varying initial cell concentrations did not improve the model fit. Higher initial cell concentrations resulted in butane consumption occurring even faster than 1,1-DCE transformation. Lower initial cell concentrations did not improve the fit of the data; running the model with an initial cell concentration of  $0.02 \text{ mg/L}$ , an unreasonably small amount, resulted in overestimation of the transformation times (results not shown).

These contrasts illustrate the complexity of the system and the sensitivity and limitations of the model. It is reasonable to suspect that because the culture used in this study was different from that used by Kim et al. (2002, *in press*), other parameter values may also be different from those assumed from Kim. What would have been more useful for modeling these simulations is to have had previously defined values specific for this study's culture.



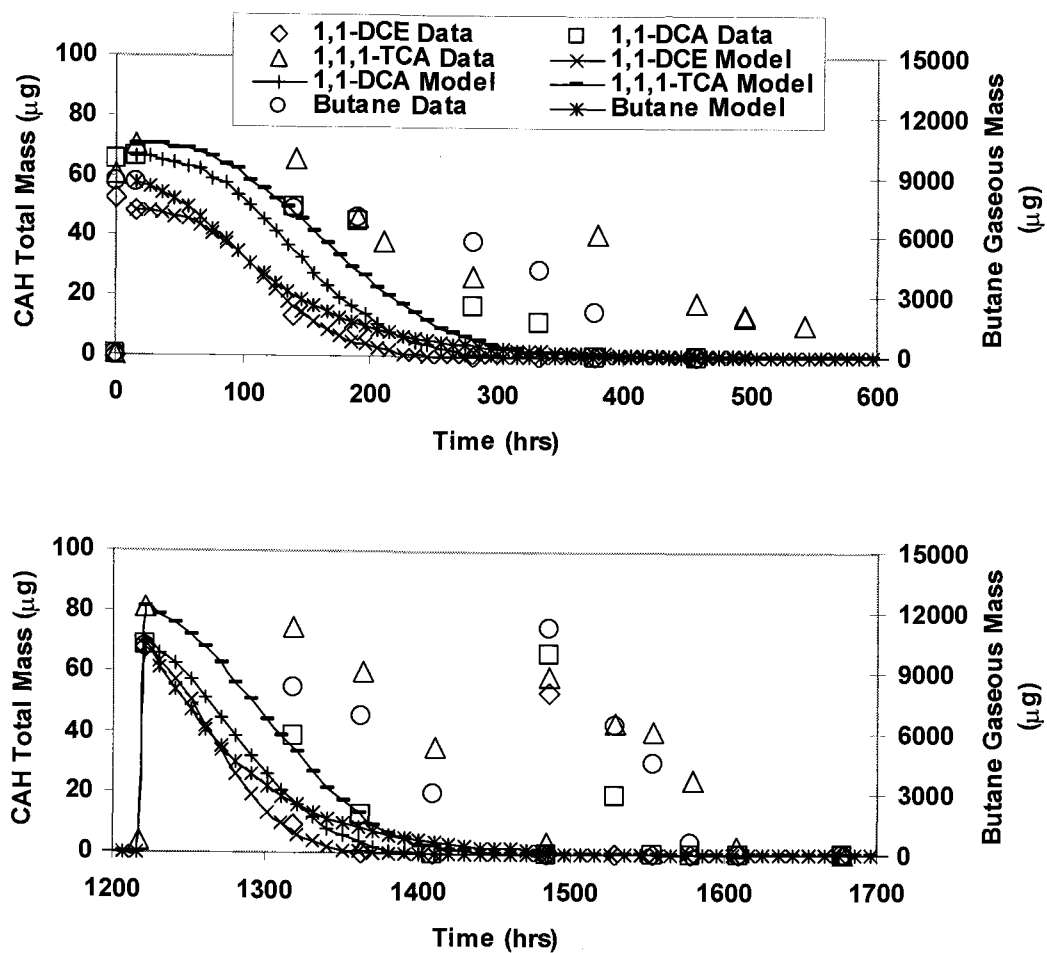


Figure 4.15 Comparison plot of M2B data and model output assuming low  $k_{mDCE}$  ( $0.1 \mu\text{mol/mg/hr}$ ).

#### 4.3 SUMMARY OF LABORATORY EXPERIMENTS AND SIMULATIONS

Laboratory experiments in both growth media and microcosms showed that the culture is capable of cometabolic biotransformation of 1,1-DCE, 1,1-DCA, and 1,1,1-TCA with butane as the primary growth substrate (electron donor). The media reactors and the bioaugmented microcosms (M2 and M3) showed rapid transformation of 1,1-DCE, followed by slower transformation of 1,1-DCA and 1,1,1-TCA. This slower transformation is attributed to butane inhibition. These trends are very reproducible as noted by the similarity within all the reactors. The lack of biotransformation in the control microcosms (M1 and M4) confirmed that transformation is due to cometabolic reactions by this culture; transformation is not due to seepage losses from the reactors or to any species indigenous to Moffett Field.

Modeling of the activity seen in the media reactors indicated that Kim et al.'s (*in press*) parameter values proved to be good initial estimates for the kinetics of our culture. It was only necessary to adjust the noncompetitive inhibition constant of butane on 1,1-DCA ( $K_{\text{IBUTDCA}}$ ), the transformation capacities of 1,1-DCE and 1,1,1-TCA ( $T_{\text{cDCE}}$ ,  $T_{\text{cTCA}}$ ), and the decay constant ( $b$ ) to better fit the transformation data.

Laboratory tests that were run to better define the  $T_{\text{cDCE}}$  value specific to our culture indicated that 1,1-DCE product toxicity was greater than that reported by Kim et al. (*in press*). Simulations of butane utilization in the absence of the CAHs and prior to the product toxicity tests showed a good fit to the laboratory data. This verified that the Stella model's input values for butane utilization values were adequate. The product toxicity simulations showed that a  $T_{\text{cDCE}}$  value of 0.175  $\mu\text{mol DCE/mg cells}$  more appropriately described our culture's product toxicity. However, comparison of the model output to the data suggested that the transformation rate of 1,1-DCE ( $k_{\text{mDCE}}$ ) was much slower than that initially assumed (2.8  $\mu\text{mol/mg/hr}$ ). A  $k_{\text{mDCE}}$  value one order of magnitude lower more closely described the data (0.1  $\mu\text{mol/mg/hr}$ ), although it is difficult to know what caused the requirement of a lower  $k_{\text{mDCE}}$ .

Laboratory experiments confirmed that mass transfer limitations (MTL) were occurring during transformation of the first three substrate additions. Incorporating a

mass transfer coefficient ( $K_{Ga}$ ) for butane into the Stella model allowed an improved match between model output and laboratory data for both butane utilization in microcosms M5 and butane utilization and CAH transformation in microcosms M2 and M3. A  $K_{Ga}$  value of  $0.03 \text{ hr}^{-1}$  was required.

Using the kinetic, inhibition, and product toxicity values defined by Kim et al. (2000, *in press*) and the adjusted values noted above, model simulations showed a fairly good match for the trends of biotransformation observed in microcosms M2 and M3. The similarities included the order of transformation (1,1-DCE transformed first, followed by 1,1-DCA and then 1,1,1-TCA), the strong inhibition of butane on 1,1-DCA and 1,1,1-TCA (resulting in the delayed transformation), and the extreme product toxicity of 1,1-DCE (seen by a sharp decline in cell concentration after 1,1-DCE transformation).

The overall importance of these laboratory experiments and the model simulations was demonstrating the model's ability to mimic such trends using laboratory values defined from independent experiments. The values were then carried over to simulate field experiments (Chapter 5).

## CHAPTER 5

### RESULTS OF MODELING FIELD DATA

---

The overall goal of the biotransformation/transport model presented in Chapter 2 was to simulate cometabolic biotransformation by a specific culture in an actual aquifer environment. This chapter presents the modeling results of field scale experiments conducted at Moffett Field Test Facility in California.

The culture grown in the laboratory (Section 3.2) was inoculated in a confined aquifer and exposed to alternating pulses of butane and oxygen and constant sources of 1,1-DCE, 1,1,-DCA, and 1,1,1-TCA. Monitoring wells spaced at various distances from the injection well allowed substrate concentrations to be measured over time.

The biotransformation/transport code was used to simulate the biostimulation of the butane culture and the transformation of the CAH mixture from the field experiment. Specific values for utilization rates, saturation constants, inhibition constants, transformation capacities, etc. defined from laboratory experiments (Chapter 4) were used as input values for the biotransformation kinetics of the combined model. Tracer tests prior to bioaugmentation allowed determination of aquifer characteristics and the model's advection, dispersion, and sorption parameter values.

This chapter discusses the simulations and output for determining transport parameters via tracer tests and for evaluating the model's ability to simulate cometabolic transformation, inhibition, and product toxicity by comparing model output to actual field observations.

#### 5.1 FIELD EXPERIMENT

Field experiments took place in a shallow aquifer at Moffett Field Test Facility in California. The test zone was confined to a 1.5 m thickness of alluvial sands and gravels between silty-clay aquitards. Details of the Moffett subsurface have been

previously described by Roberts et al. (1990). Flow gradients were induced by injection and extraction wells spaced 7 meters apart. This also allowed for maintaining hydraulic controls at the site and approximating one dimensional flow (Roberts et al., 1990). Three monitoring wells, S1, S2, and S3, were spaced 1 m, 2.2 m, and 4 m from the injection well, respectively, to provide sampling access. A schematic of the field test zone is presented in Figure 5.1.

Aquifer hydraulic characteristics (Table 5.1) were defined from previous experiments (Semprini and McCarty, 1991,1992) and from model simulations of recent tracer tests (Section 5.2). Since 1-D model simulations were performed, the groundwater velocity and a dispersion coefficient were obtained from bromide tracer tests performed on the test leg.

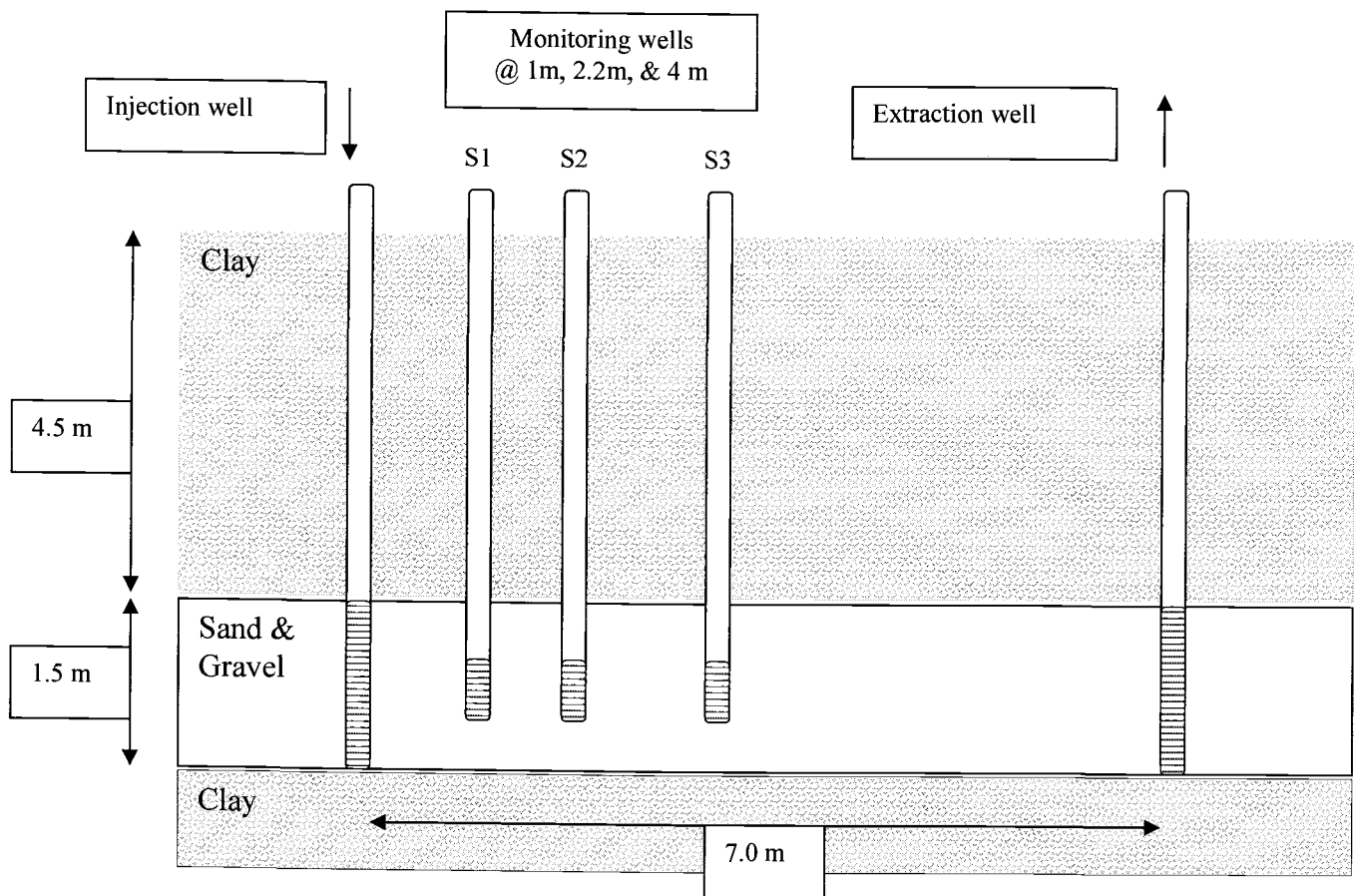


**Figure 5.1 Conceptual model of Moffett Field Test Aquifer. Not to scale.**

**Table 5.1 Aquifer hydraulic characteristics.**

Average flow*, Q (m <sup>3</sup> /day)	Aquifer Thickness, b (m)	Porosity, $\Phi$ (-)	Bulk Density, $\rho_b$ (kg/L)	Dispersion Coeff., $D_h$ (m <sup>2</sup> /day)
1.0-1.5	1.5	0.33	1.6	0.31

\*Defined from Bromide tracer tests (Section 5.2), based on test zone with 1.5 m thickness and 1 m width.

The injection system allowed for alternating, pulsed additions of butane and oxygen and continuous additions of 1,1-DCE, 1,1-DCA, 1,1,1-TCA. During the bioremediation experiment, concentrations and pulsing durations of butane and oxygen were varied periodically in attempt to improve bioremediation. Injection concentrations of the CAHs were held approximately constant. Specific details on injection concentrations and pulsing durations are provided in Section 5.4.

## 5.2 DETERMINATION OF FLOW

Bromide tracer tests were conducted in the test zone before bioaugmentation to determine flow and dispersion characteristics of the test zone. Bromide (150 mg/L) was injected into the site, and breakthrough concentrations were monitored from the monitoring wells S1, S2, and S3. Figure 5.2 presents the monitoring and injection wells' concentration histories. Times to 50% breakthrough of the bromide tracer observed for S1, S2, and S3 were 0.44, 1.12, and 1.42 days, respectively.

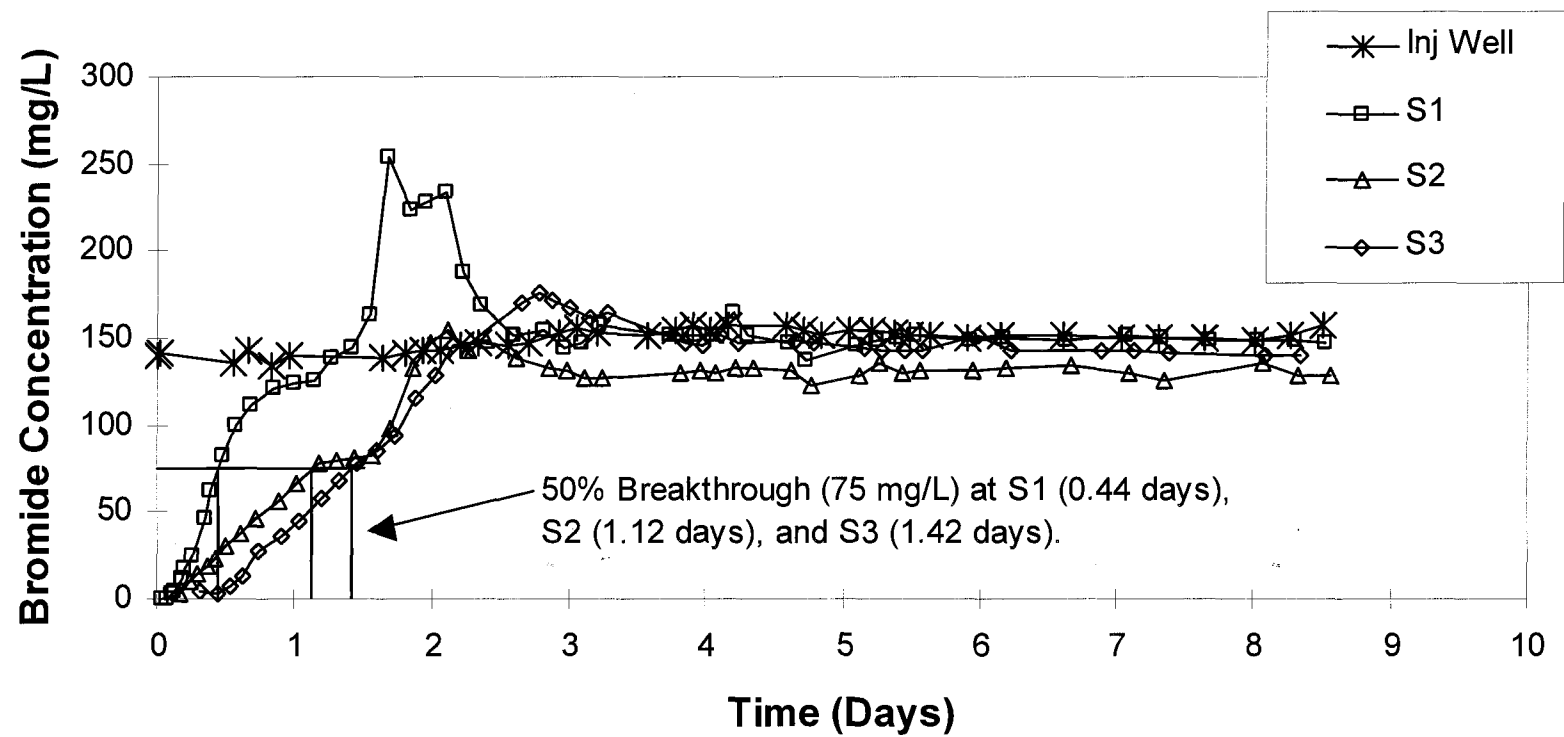
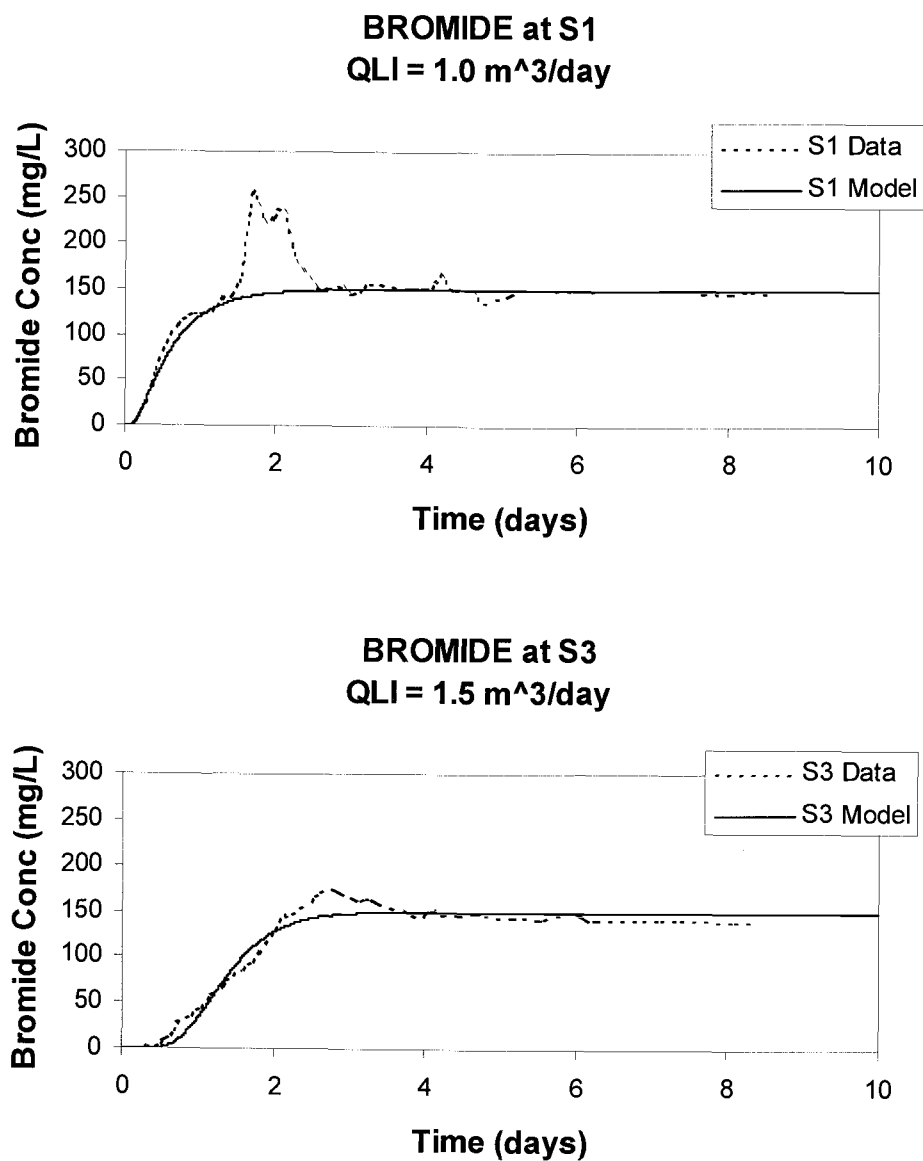


Figure 5.2 Bromide tracer test data at the three monitoring wells S1 (1m); S2 (2.2m); S3 (4m) and the injection well.



The tracer test was simulated using the transport model presented in Chapter 2, with no transformation. This was done by setting utilization rates ( $k_m$ ) to 0. Flow input values were varied and compared to the monitoring data at the first and third sampling wells (S1 @ 1m and S3 @ 4m). Transport values for the simulations are provided in Table 5.1. Specific input for the model are provided in Appendix H.

Comparison plots of the tracer data and model output for a  $1.0 \text{ m}^3/\text{day}$  volumetric flow ( $2.0 \text{ m/day}$  average groundwater velocity) at S1 and  $1.5 \text{ m}^3/\text{day}$  flow ( $3.0 \text{ m/day}$  average groundwater velocity) at S3 are presented in Figure 5.3. Note that there is a good match during the breakthrough period for each well, although different flow inputs were required to achieve this fit. Data from S1 showed some perturbations in bromide injection, resulting in high concentrations (days 1.3 to 2.6). The different flows may be explained by aquifer heterogeneities and the monitoring wells being partially penetrating. Similar observations were made by Semprini and McCarty (1991) for bromide tracer tests conducted on another test leg at the site. The combined model was run to simulate biotransformation seen at monitoring well S1 (1m from the injection well) using the flow rate determined at this location ( $1.0 \text{ m}^3/\text{day}$ ).



**Figure 5.3 Comparison of tracer data to model output.** Distances from the Injection Well: S1 (1m), S3 (4m). Groundwater velocities at S1 and S3 were 2.0 and 3.0 m/day, respectively, with aquifer porosity 0.33 width 1.0 m, and thickness 1.5 m.

### 5.3 DETERMINATION OF SORPTION PARAMETER VALUES

Before bioaugmentation, the three CAHs studied in the laboratory were injected into the aquifer to develop breakthrough curves of each compound. Injection concentrations of 1,1-DCE, 1,1-DCA, and 1,1,1-TCA were approximately 45  $\mu\text{g/L}$ , 130  $\mu\text{g/L}$ , and 140  $\mu\text{g/L}$ , respectively. Background 1,1-DCE in the aquifer was 5  $\mu\text{g/L}$ . Concentrations over time were measured from the three monitoring wells, S1, S2, and S3. Breakthrough curves for the CAHs at the injection well, S1, and S3 are presented in Figure 5.4.

Compared to the bromide tracer data (Figure 5.3), the CAHs showed retarded breakthrough, indicating sorption was taking place. 1,1-DCA was sorbed with 50% breakthrough times (65  $\mu\text{g/L}$ ) at S1 and S3 of 1.5 and 3.1 days, respectively. Half of the 1,1,1-TCA injected concentration (70  $\mu\text{g/L}$ ) appeared at S1 and S3 at 1.5 and 3.2 days, respectively. Finally, 1,1-DCE showed the most sorption characteristics, with 50% of the injection concentrations (22.5  $\mu\text{g/L}$ ) appearing at S1 and S3 at 1.9 and 3.2 days, respectively. Retardation factors based on these breakthrough times are presented in Table 5.2 (discussed below).

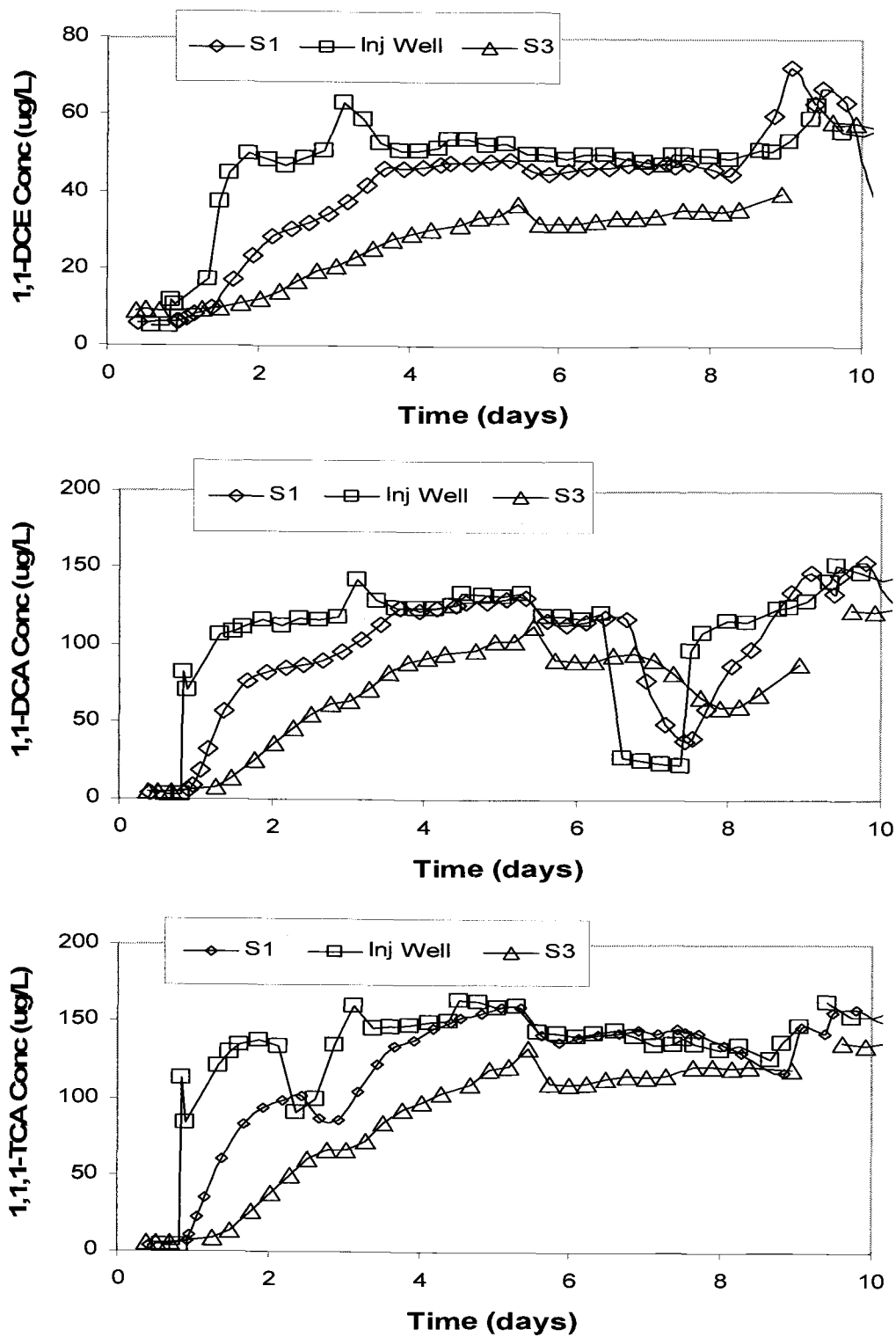


**Figure 5.4 Breakthrough curves of 1,1-DCE, 1,1-DCA, and 1,1,1-TCA.**  
 Distances from injection well: S1 (1m); S2 (2.2m); S3 (4m).

The breakthrough curves were used to determine initial estimates of sediment sorption coefficients ( $K_d$ ) and the first order mass transfer rate coefficients ( $F_k$ ). This was done by calculating a retardation value ( $R$ ) for each CAH. The retardation value was defined as the time to 50% breakthrough of the CAH normalized to the time to 50% breakthrough of bromide.

$$R = T_{CAH} / T_{BR} \quad (5.1)$$

where:  $R$  = retardation factor

$T_{CAH}$  = time for 50% of CAH injection concentration to reach well

$T_{BR}$  = time for 50% of Bromide injection concentration to reach well

Approximate breakthrough times, 50% injection concentrations, and retardation factors at wells S1 and S3 are presented in Table 5.2. Partitioning coefficients ( $K_d$ ) were then calculated by rearranging the relationship between  $R$  and  $K_d$ :

$$R = 1 + \frac{\rho_b k_d}{\phi} \quad (5.2) \quad k_d = \frac{\phi}{\rho_b} (R - 1) \quad (5.3)$$

where:

$k_d$  = solids partitioning coefficient (L/kg)

$\rho_b$  = bulk density (kg/L)

$\phi$  = porosity

Porosity ( $\phi$ ) and bulk density ( $\rho_b$ ) listed in Table 5.1 (0.33 and 1.6 kg/L, respectively) were used with the retardation factors tabulated in Table 5.2 to calculate  $k_d$ . The  $k_d$  values determined from these calculations are also presented in Table 5.2. Note that there are differences between the retardation factors and sorption coefficients for each CAH at the two different wells. Like the variations seen in flow velocities

(Section 5.2), these differences may be attributed to non-homogenous conditions within the aquifer test zone.

**Table 5.2 Retardation factors and solids partition coefficients.**

	<u>Bromide</u>	<u>1,1-DCE</u>	<u>1,1-DCA</u>	<u>1,1,1-TCA</u>
<b>50% Inj. Conc. (<math>\mu\text{g/L}</math>)</b>	75	22.5	65	70
<b>Breakthrough time to S1 (days)</b>	0.44	1.9	1.5	1.5
<b>Breakthrough time to S3 (days)</b>	1.42	3.2	3.1	3.2
<b>Retardation Factor, R @ S1</b>	-	4.3	3.4	3.4
<b>Retardation Factor, R @ S3</b>	-	2.3	2.2	2.3
<b>Partition Coeff. , <math>K_d</math> @ S1 (L/kg)</b>	-	0.69	0.50	0.50
<b>Partition Coeff. , <math>K_d</math> @ S3 (L/kg)</b>	-	0.27	0.25	0.27

Mass transfer rate coefficients ( $F_k$ ) were determined by simulating the CAH breakthrough curves using the flows and sorption coefficients determined above (Section 5.2 and 5.3, respectively). Specific inputs for the model are tabulated in Appendix J. Figure 5.5 presents comparison plots of the S1 breakthrough data and two simulations with  $F_k$  values of 0.2 and 2.0  $\text{day}^{-1}$  representing equilibrium and non-equilibrium cases, respectively. These values were assumed for all three CAHs. Simulations were also run for  $F_k$  values of 20.0 and 200  $\text{day}^{-1}$ , with exactly the same results obtained with the 2.0  $\text{day}^{-1}$  simulations.

With the quality of the data from the field demonstrations, it was difficult to determine if non-equilibrium (lower  $F_k$ ) with higher partitioning (higher  $K_d$ ) was

occurring, or if equilibrium (higher  $F_k$ ) with lower partitioning ( $K_d$ ) was occurring. A value of 2.0 day<sup>-1</sup> was used for all future field modeling for simplification. However, as seen in Figure 5.5, the  $F_k$  value of 0.2 day<sup>-1</sup> gave a general “best fit” to the breakthrough data. Also, the work done by Harmon et al. (1992) would indicate that rate limited sorption was occurring under Moffett Field test zone conditions. Simulations were therefore run to study the sensitivity of equilibrium versus non-equilibrium conditions (Section 5.5.4).

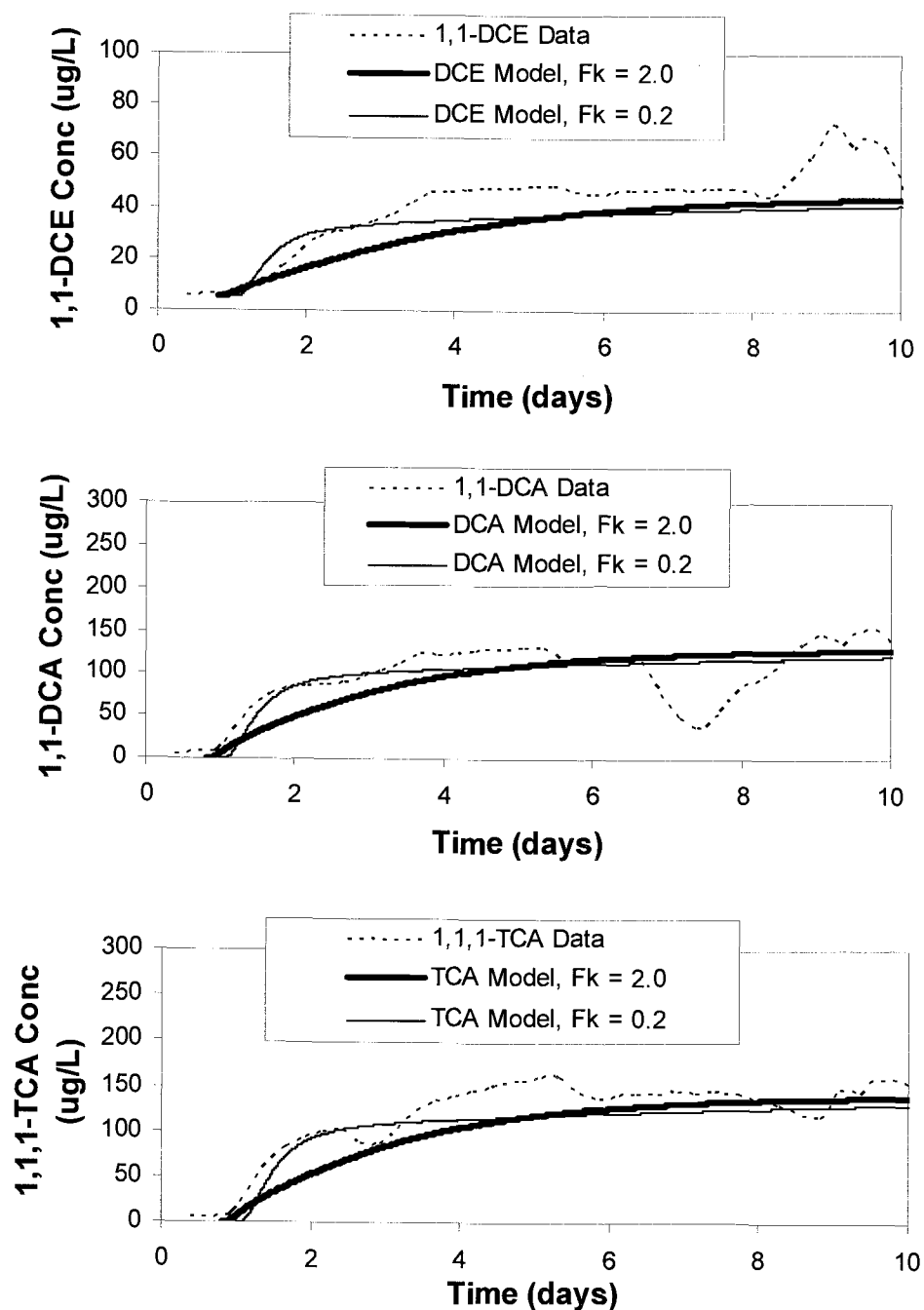


**Figure 5.5 Comparison of CAH breakthrough data with model output for varying mass transfer rate coefficient ( $F_k$ ) at S1 (1m).**



#### 5.4 INTERPRETATION OF BIOTRANSFORMATION/TRANSPORT FIELD DATA

The breakthrough tests discussed in Section 5.3 were carried out for 9 days. The culture (Section 3.2) was then introduced to the aquifer test zone, with continued injection of 1,1-DCE, 1,1-DCA, and 1,1,1-TCA and alternating injections of butane and oxygen. (Introduction of the electron donor and electron acceptor were actually begun 12 hrs prior to bioaugmentation.) The culture was added to the site by diluting 4 g of the harvested cells (Section 3.2) in 25 L of Moffett groundwater and dispensing it via the injection well over a 4-hour period. The injected cell concentration was approximately 12 mg/L and the injection flow was approximately 1.35 L/min. Upon inoculation, it was assumed that the biomass was non-uniformly distributed throughout the test zone, with higher concentrations closest to the injection well.

After bioaugmentation, concentrations of dissolved butane and oxygen and the three CAHs were measured in the injection and monitoring wells. Because of the random sampling times and varied pulse intervals, it was difficult to know specific quantities and pulse durations of the substrate injections being delivered into the aquifer. Estimated concentrations and pulse cycles for butane and oxygen injections are presented in Table 5.3. Table 5.4 lists approximate CAH concentrations continuously delivered to the aquifer during the breakthrough tests (days 0-9) and bioaugmentation (days 9-70).

**Table 5.3 Butane and oxygen injection pulsing durations and concentrations.**

<u>Days 9-20: 15/45 min BUT/O<sub>2</sub></u>	<u>Days 9-20: 35/25 mg/L BUT/O<sub>2</sub></u>
<u>Days 20-30: 2/22 hr BUT/O<sub>2</sub></u>	<u>Days 20-23: 35/25 mg/L BUT/O<sub>2</sub></u>
<u>Days 30-40: 1/23 hr BUT/O<sub>2</sub></u>	<u>Days 23-30: 35/5 mg/L BUT/O<sub>2</sub></u>
<u>Days 40-75: 15/45 min BUT/O<sub>2</sub></u>	<u>Days 30-40: 35/18 mg/L BUT/O<sub>2</sub></u>
	<u>Days 40-75: 20/25 mg/L BUT/O<sub>2</sub></u>

*Pulsing durations are read as from day 9 to day 20, butane was injected for 15 minutes, followed by 45 minutes of oxygen. Pulsing concentrations are read as from day 9 to day 20, butane was injected at 35 mg/L and oxygen was injected at 25 mg/L.*

**Table 5.4 1,1-DCE, 1,1-DCA, & 1,1,1-TCA injection concentrations.**

<u>1,1-DCE Injection</u>	<u>1,1-DCA Injection</u>	<u>1,1,1-TCA Injection</u>
<u>Days 0-9: 45 µg/L</u>	<u>Days 0-9: 130 µg/L</u>	<u>Days 0-9: 140 µg/L</u>
<u>Days 9-75: 65 µg/L</u>	<u>Days 9-20: 200 µg/L</u>	<u>Days 9-30: 140 µg/L</u>
	<u>Days 20-35: 100 µg/L</u>	<u>Days 30-75: 175 µg/L</u>
	<u>Days 35-60: 175 µg/L</u>	
	<u>Days 60-75: 150 µg/L</u>	

*Injections are read as from day 0 to day 9, approximately 45 µg/L 1,1-DCE, 130 µg/L 1,1-DCA, and 140 µg/L 1,1,1-TCA was delivered into the aquifer.*

These injection estimates were based on concentrations read from the injection well, as shown in Figure 5.6 (days 0-20), Figure 5.7 (days 0-40) and Figure 5.8 (days 0-70). The plots also display the measured substrate concentrations from monitoring wells S1 and S3. Note that injections during the breakthrough tests (Section 5.3) are included as days 0 to 9 in the figures.

The oscillations observed in Figures 5.6 through 5.8 result from the alternating, pulsed injections of butane and oxygen. In general, the plots of the field data show that

butane utilization was reduced in conjunction with longer pulsing durations (days 20-40) and limited oxygen availability (days 23-30). Oxygen utilization occurred with butane consumption and when adequate quantities of oxygen were delivered to the test zone. CAH transformation occurred early on (days 9-20), but was lost when butane and oxygen pulsing cycles were elongated (days 20-40). Transformation returned when pulsing was shortened again (days 40-75). Discussion of these observations are provided below.

Immediately after bioaugmentation (days 9 to 17), when adequate quantities of butane and oxygen had been delivered to the test zone, there was good transformation of 1,1-DCE, as seen in Figure 5.6b. 1,1-DCA and 1,1,1-TCA were also transformed during this period, although there was a time lag of approximately 6 days. This lag may be indicative of butane's inhibitory effects on these two CAHs; transformation did not occur until butane was well consumed. These observations are consistent with that seen in laboratory experiments (Chapter 4).

Note from Figure 5.6 that soon after bioaugmentation (days 9-20), peak concentrations of butane at S1 were higher than at S3. This implies that not as much butane was delivered to the farther well. Also, there is better transformation of all three CAHs at S1. These phenomena suggest that the microbial mass was predominately located within the first meter of the injection well.

In an attempt to distribute the microbial mass farther away, the pulsing cycle of butane and oxygen was set to longer durations (Table 5.3). At day 20, the pulse durations were extended from 15 min of butane followed by 45 min of oxygen, to 2 hrs of butane followed by 22 hrs of oxygen. During this period, CAH and butane concentrations gradually increased as measured from S1 and S3 (Figure 5.7). This indicated biotransformation and utilization had ceased, most likely due to the infrequent availability of butane. This would have increased cell decay, resulting in a reduced microbial population.

To restore biotransformation, the system was reset on day 40 to the shorter pulsing cycle (15 min butane followed by 45 min oxygen). Observations at S1 (figure

5.8) showed that at close proximity to the injection well (where most activity was assumed to occur) this change restored the transformation of 1,1-DCE. 1,1-DCA and 1,1,1-TCA transformation were never revived. Loss of degradation may possibly be explained by extreme product toxicity of 1,1-DCE transformation, effectively inactivating cellular function. This was also observed in laboratory experiments (Chapter 4). At day 70 the injection system was shut off.

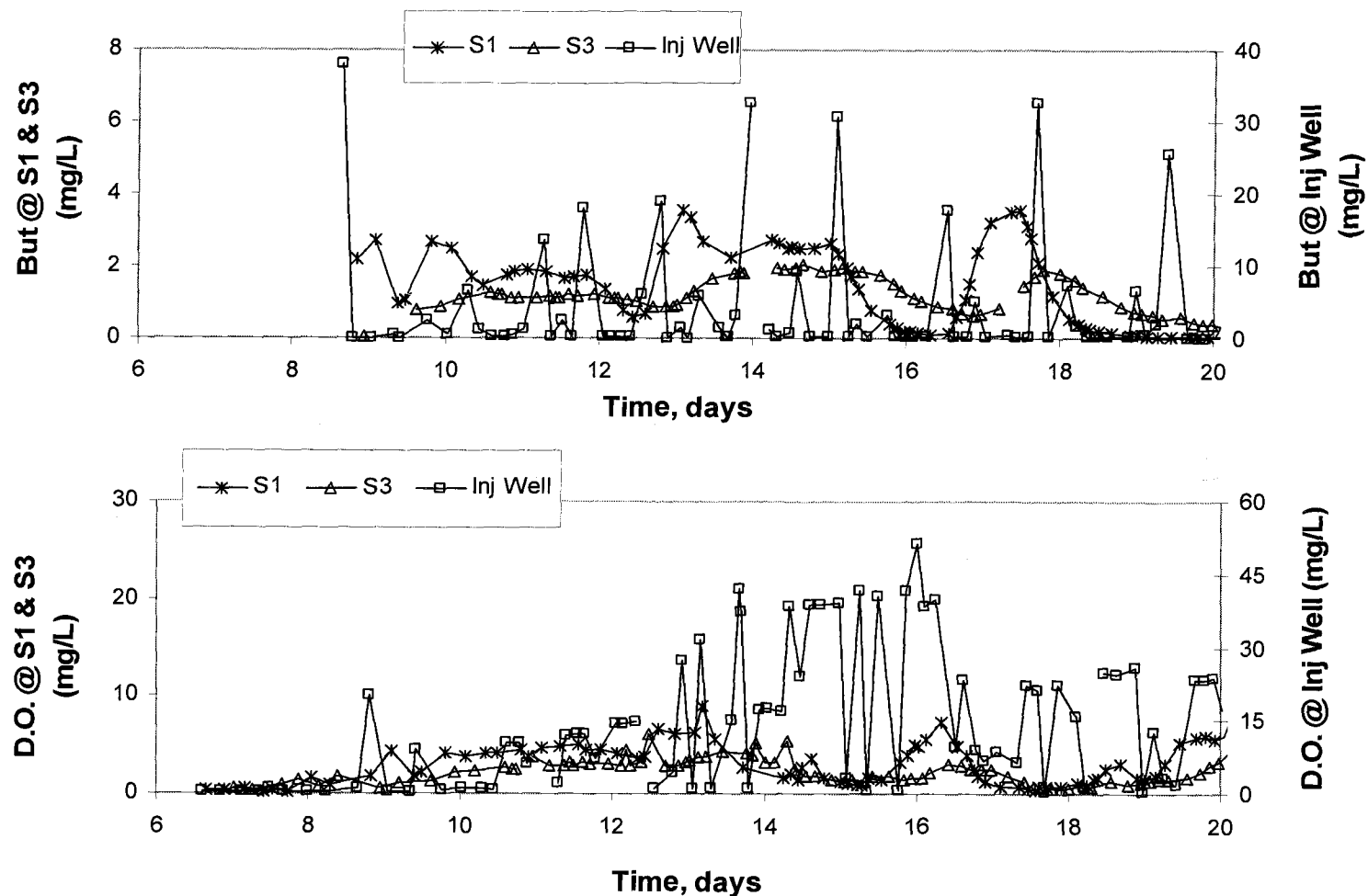
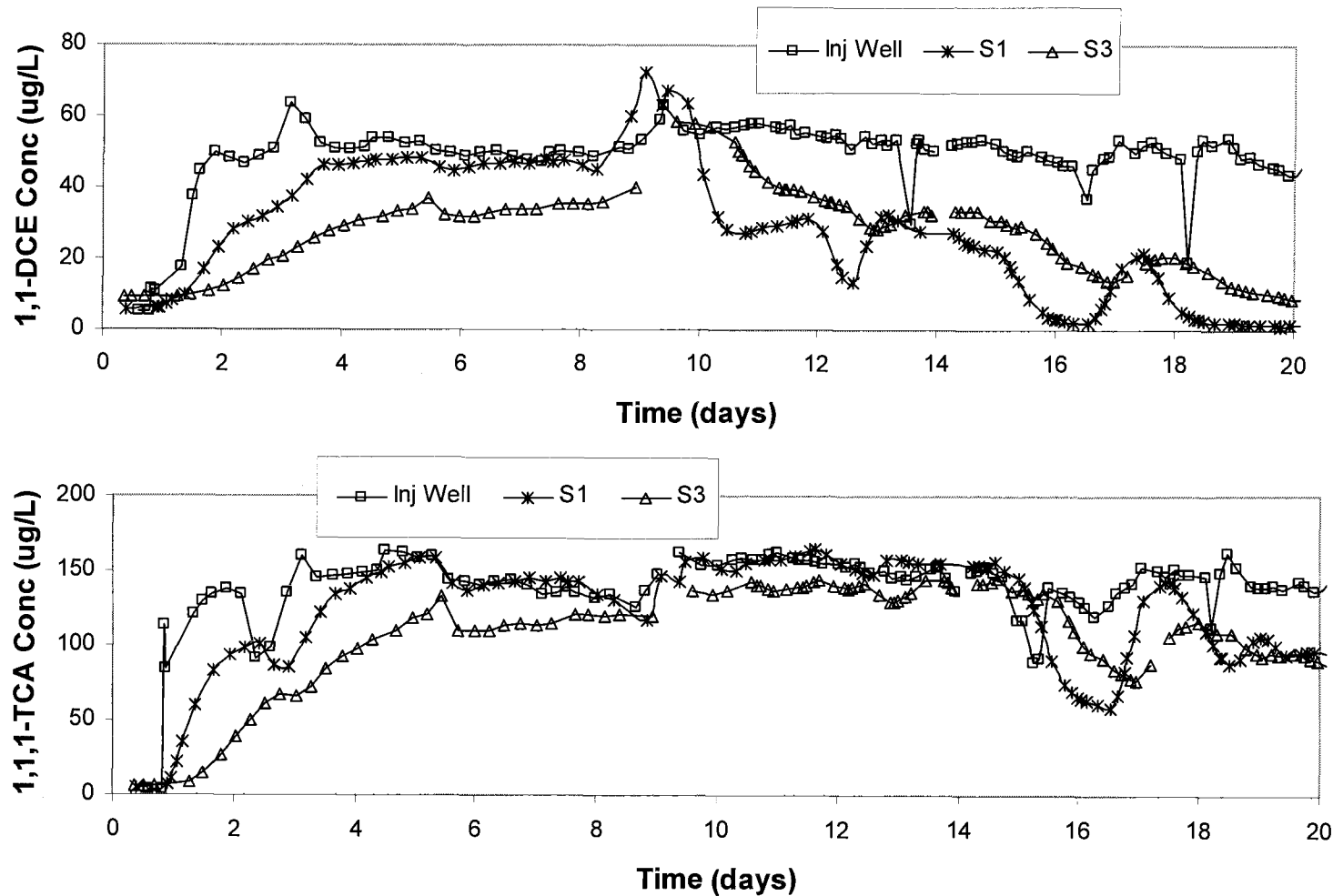
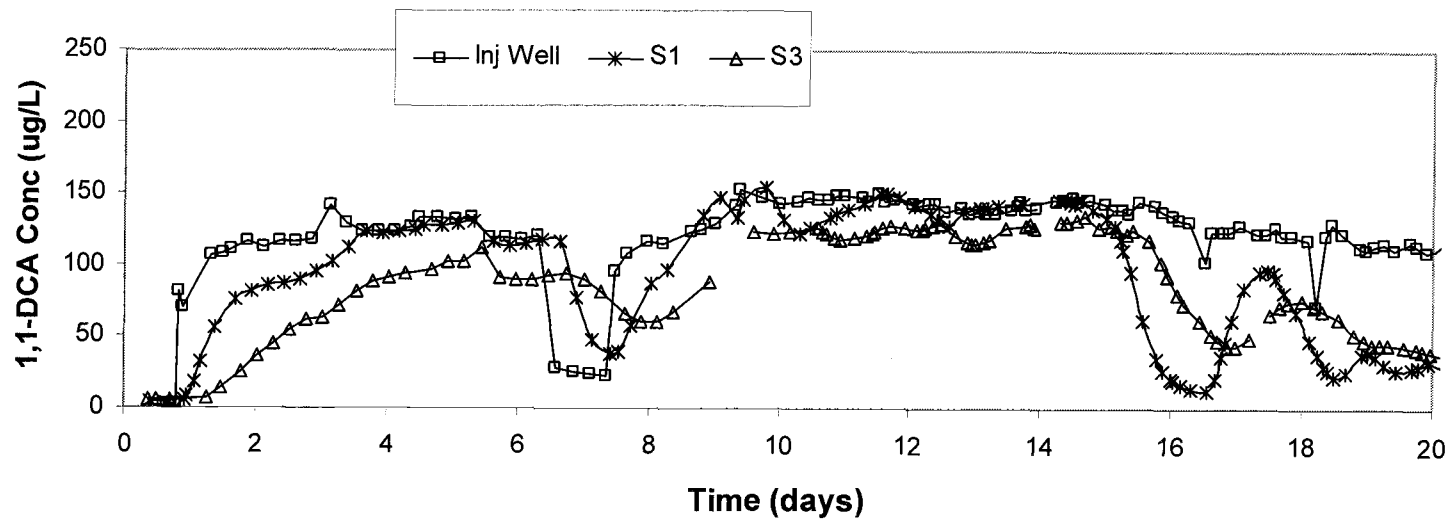


Figure 5.6a Butane and oxygen concentrations measured at S1 (1m), S3 (4m), and injection well during the first twenty days of the field experiments. The bioaugmented culture was introduced on day 9.



**Figure 5.6b** 1,1-DCE and 1,1,1-TCA concentrations measured at S1 (1m), S3 (4m), and the injection well during the first twenty days of the field experiments. The bioaugmented culture was introduced on day 9.



**Figure 5.6c** 1,1-DCA concentrations measured at S1 (1m), S3 (4m), and the injection well during the first twenty days of the field experiments. The bioaugmented culture was introduced on day 9.

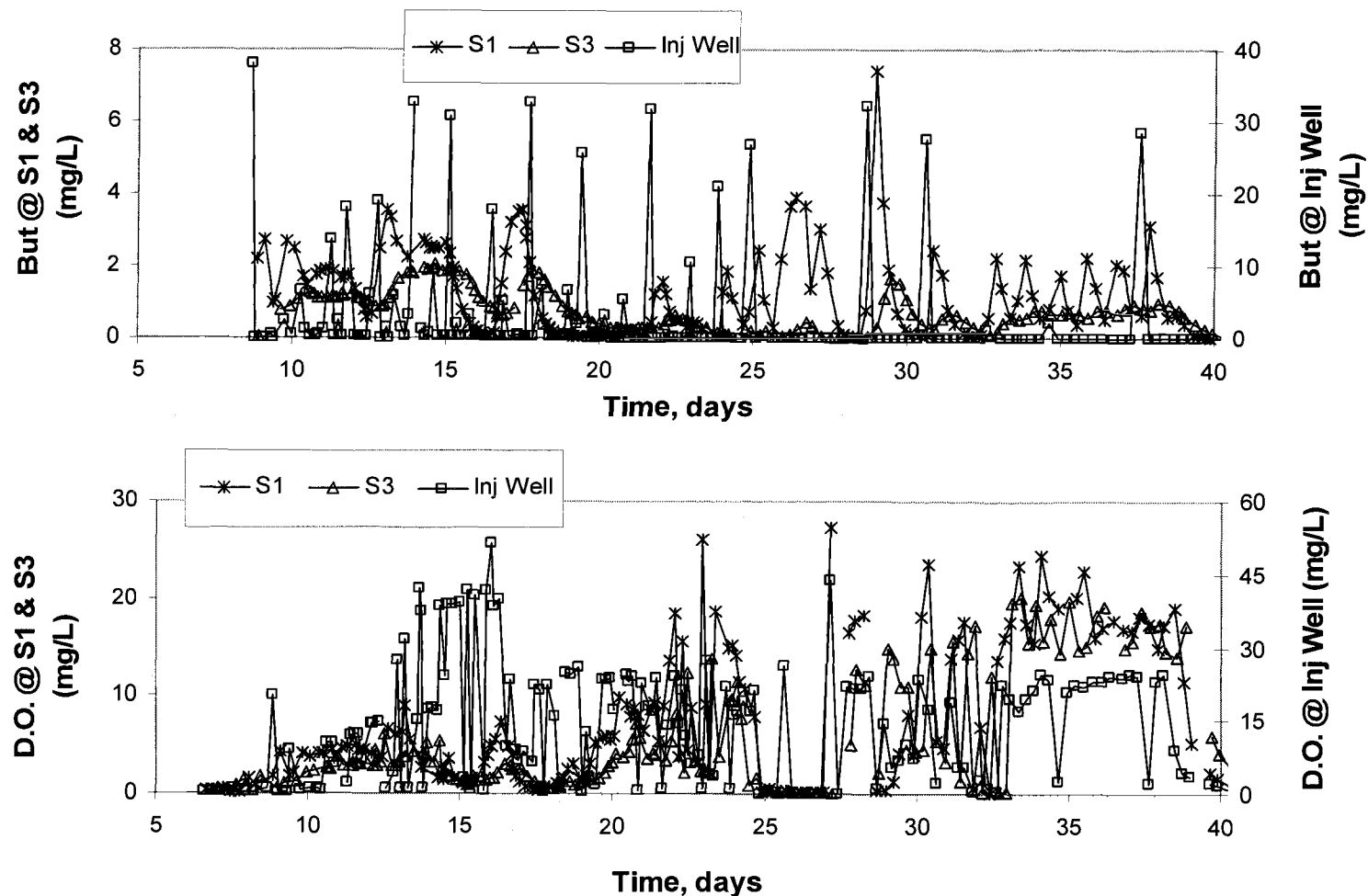


**Figure 5.7a Butane and oxygen concentrations measured at S1 (1m), S3 (4m), and the injection well during the first forty days of the field experiments. The bioaugmented culture was introduced on day 9.**



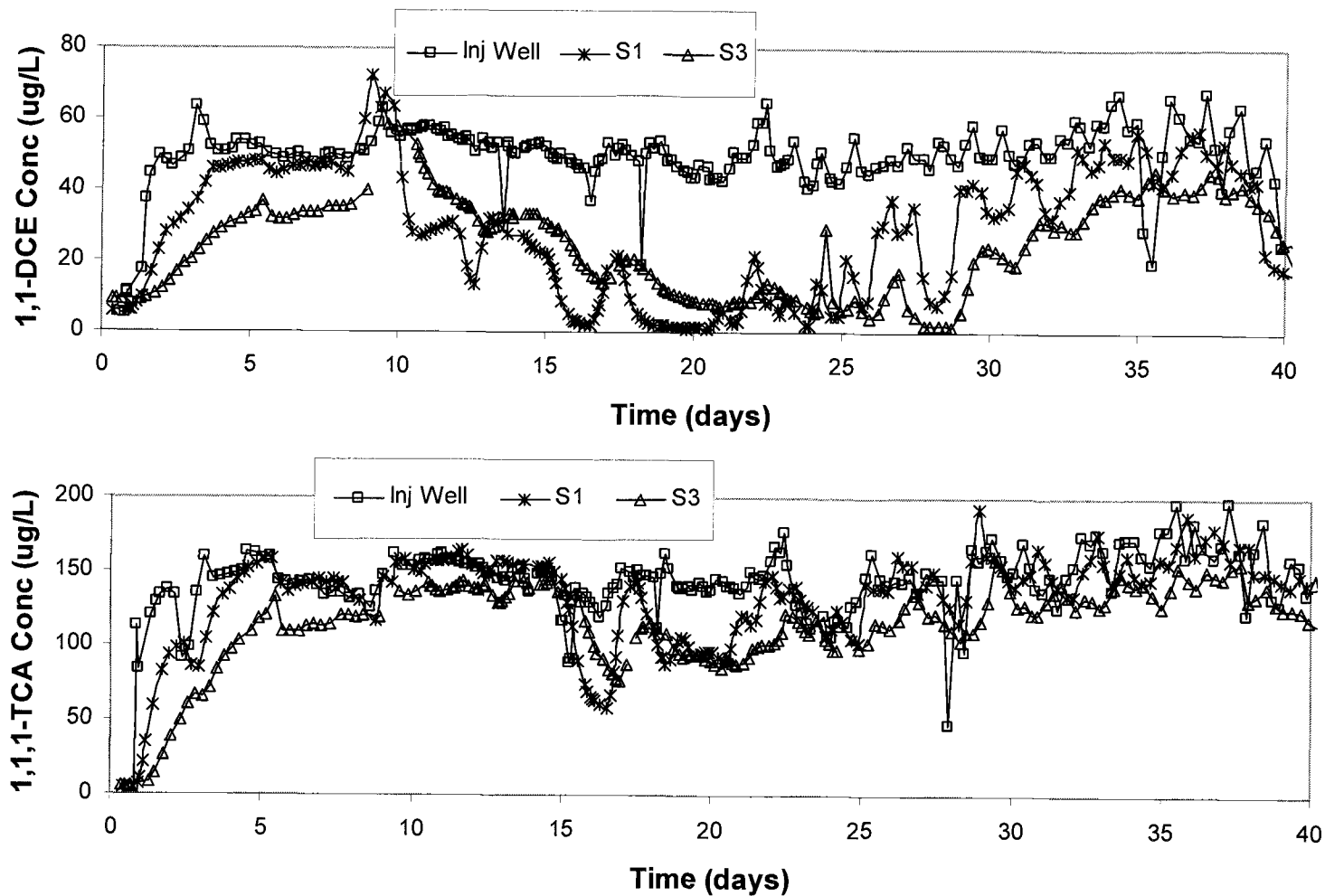


**Figure 5.7b 1,1-DCE and 1,1,1-TCA concentrations measured at S1 (1m), S3 (4m), and the injection well during the first forty days of the field experiments. The bioaugmented Culture was introduced on day 9.**

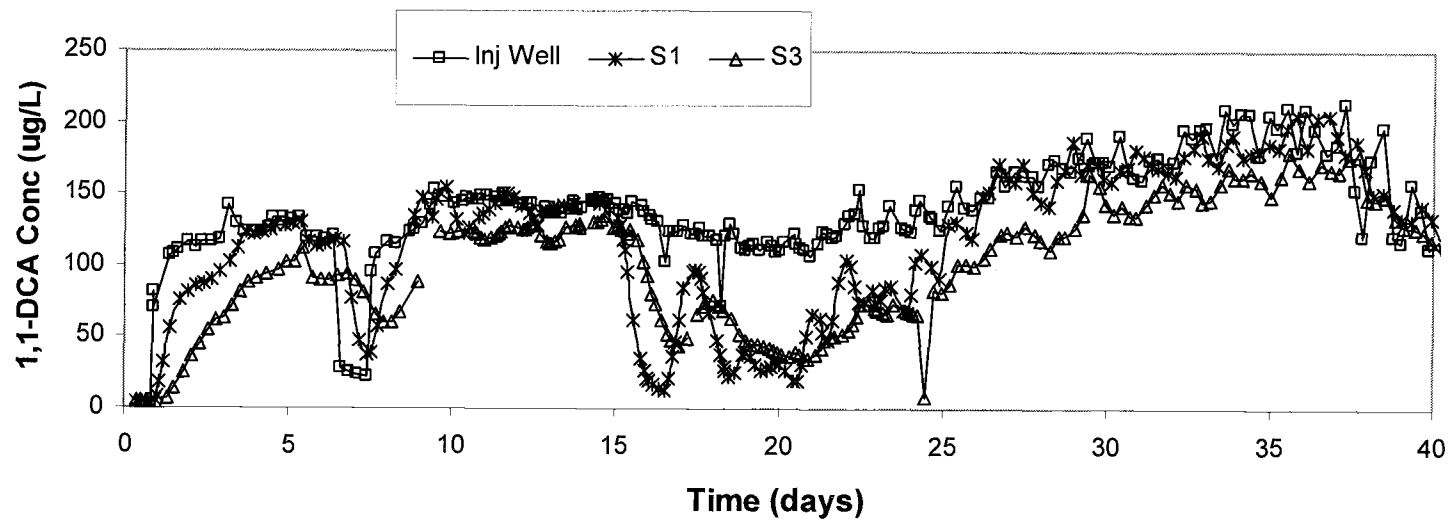


**Figure 5.7c** 1,1-DCA concentrations measured at S1 (1m), S3 (4m), and the injection well during the first forty days of the field experiments. The bioaugmented culture was introduced on day 9.

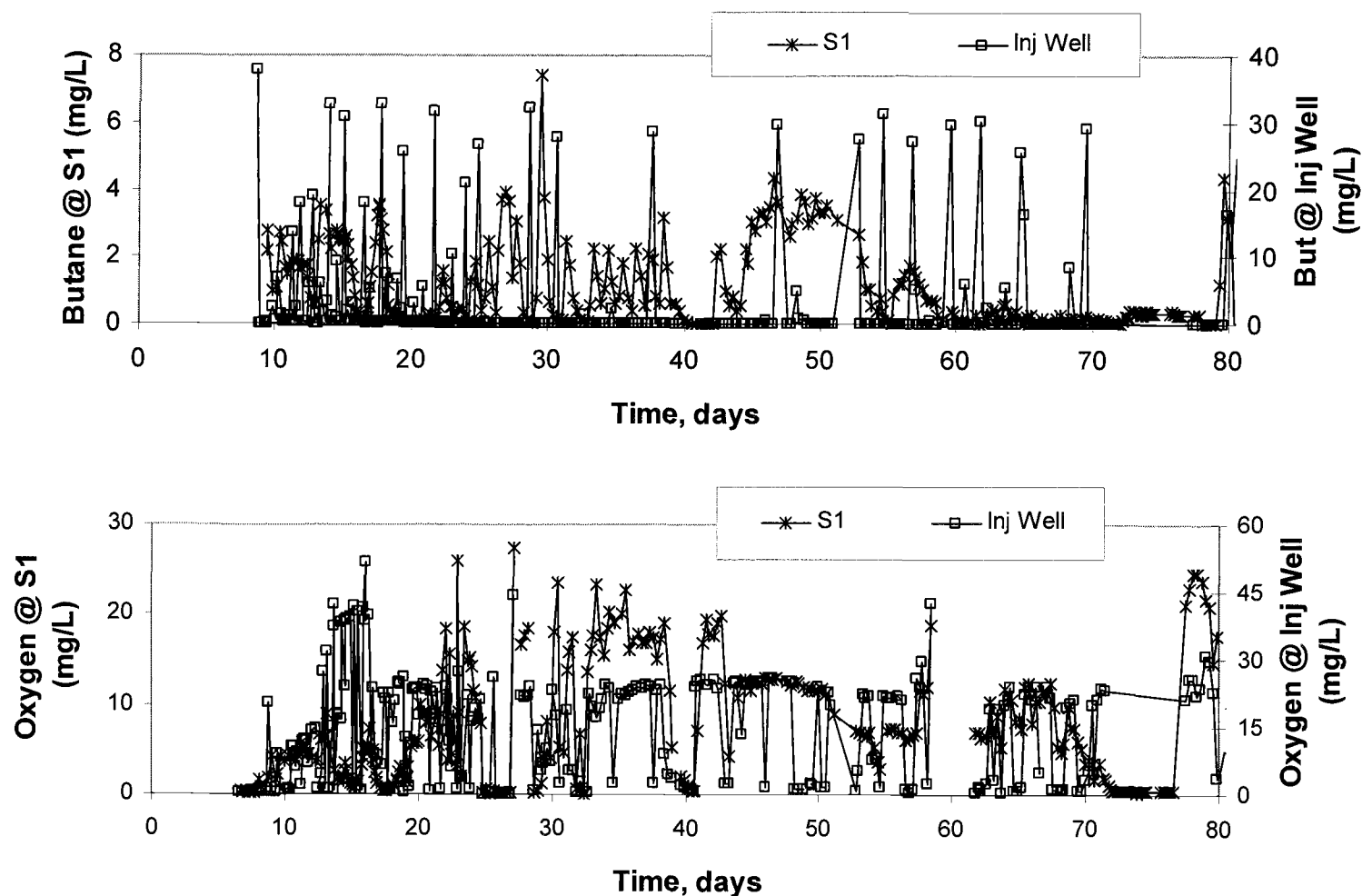


**Figure 5.8a Butane and oxygen concentrations measured at S1 (1m) and the injection well during the field experiments (days 0-75). The bioaugmented culture was introduced on day 9.**

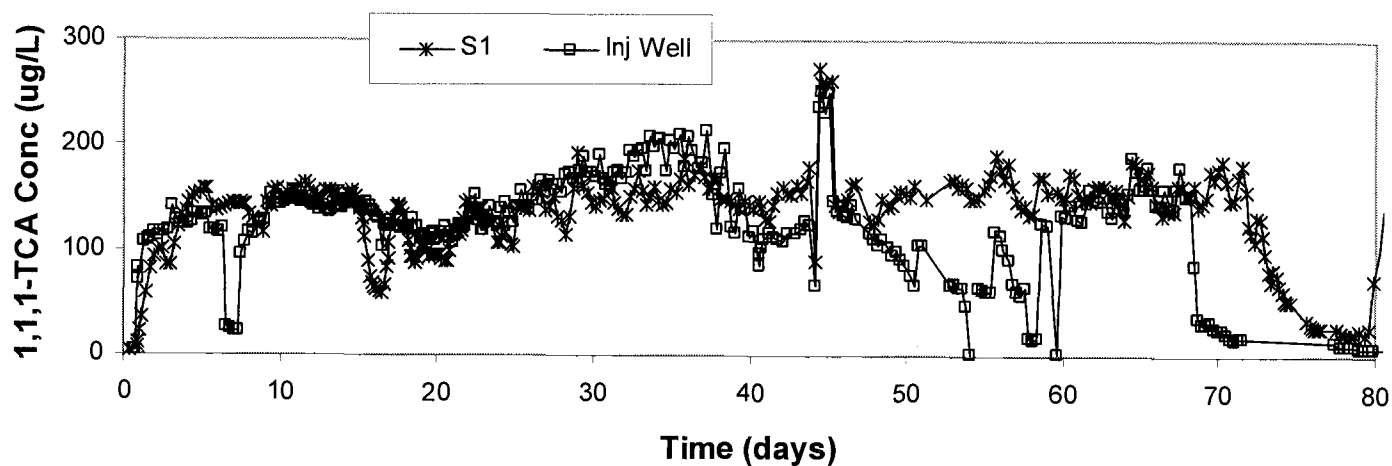
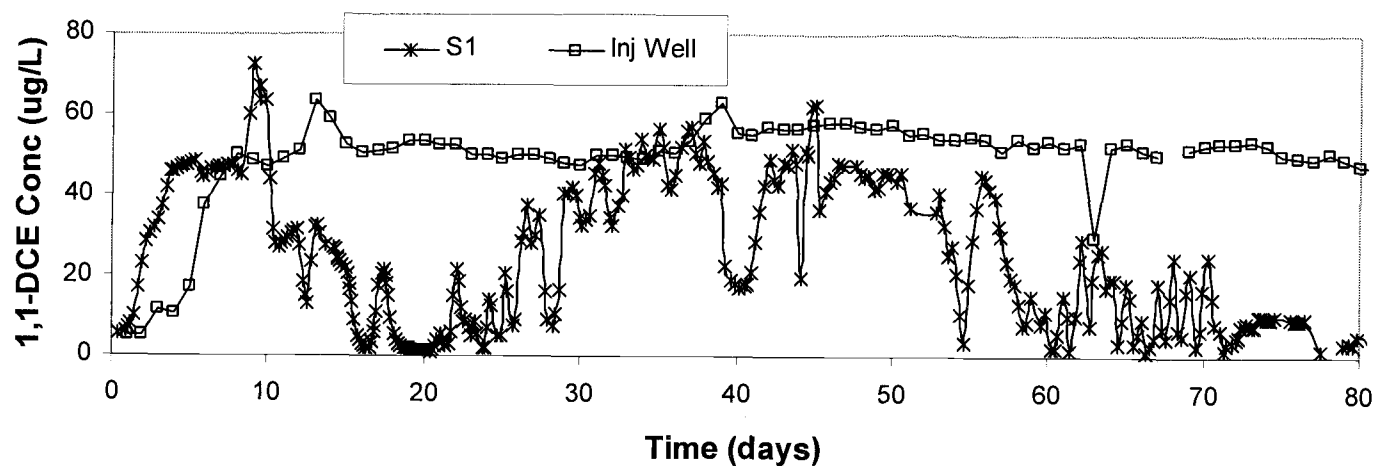


**Figure 5.8b** 1,1-DCE and 1,1,1-TCA concentrations measured at S1 (1m) and the injection well during the field experiments (days 0-75). The bioaugmented culture was introduced on day 9.

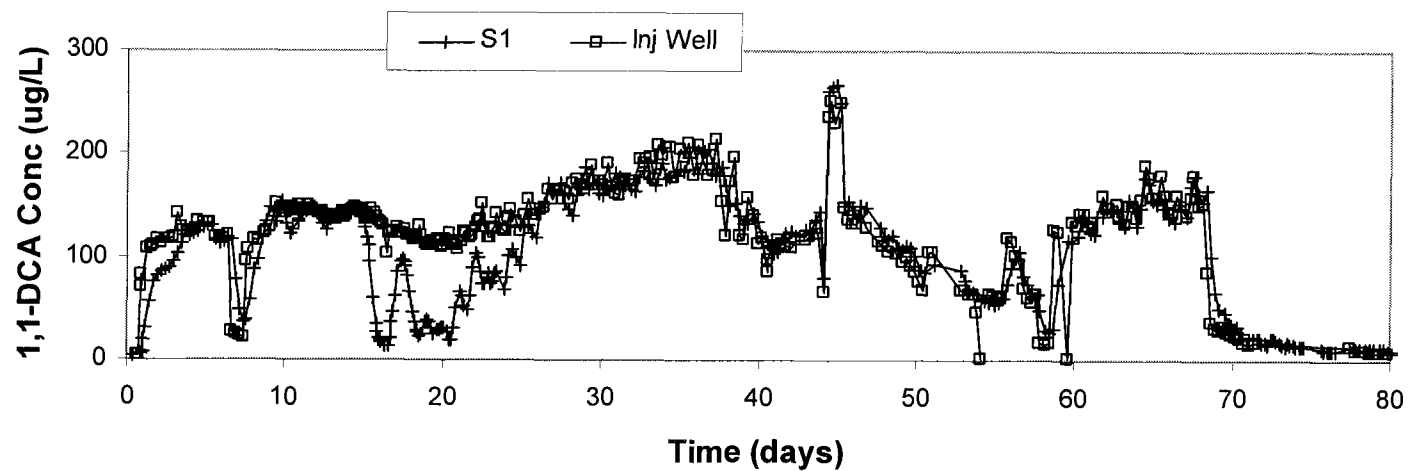


**Figure 5.8c 1,1-DCA concentrations measured at S1 (1m) and the injection well during the field experiments (days 0-75).**

The bioaugmented culture was introduced on day 9.

## 5.5 MODELING OF BIOTRANSFORMATION/TRANSPORT FIELD DATA

Using the biotransformation parameter values determined from the laboratory experiments (Chapter 4) and the aquifer characteristics defined above (Sections 5.1-5.3), the tests (Section 5.4) were simulated with the model presented in Chapter 2. A summary of the biotransformation input values is listed in Table 5.5, while transport input is provided in Table 5.6. Kim et al.'s (2002) inhibition, rate, and half-saturation constant values were used. As with the microcosm experiments, cell decay was increased to a value of  $0.1 \text{ day}^{-1}$  which more accurately describes aerobes (Semprini and McCarty, 1991). Oxygen utilization parameters ( $f_d$ , and  $d_c$ ) were used according to published values (Semprini and McCarty, 1991) and stoichiometry between butane and oxygen. Transformation capacity of 1,1-DCA ( $T_{cDCA}$ ) as defined by Kim was incorporated along with that for 1,1,1-TCA ( $T_{cTCA}$ ) used in modeling microcosm data. The lower transformation capacity of 1,1-DCE ( $T_{cDCE}$ ) defined from laboratory experiments was also used. Microbial mass was assumed to be non-uniformly distributed, with most of the microbes existing within the first meter of the test zone. Injection concentrations and pulsing durations were input as listed in Tables 5.3 and 5.4. Actual data input including microbial distribution, pulsing durations, and model nomenclature are tabulated in Appendices J, K, and L.

**Table 5.5 Biotransformation values for simulating field data.**

Parameter	Units	Value	Parameter	Units	Value
K <sub>ic</sub> DCABUT	mg /L	39.88	X <sub>0</sub>	mg/L	*
K <sub>ic</sub> DCADCE	mg /L	1.78	Y	mg/mg	0.79
K <sub>ic</sub> DCATCA	mg /L	1.58	b	day <sup>-1</sup>	0.1
			Fa	-	0.8
K <sub>ic</sub> DCEBUT	mg /L	0.84	kmaxBUT	mg /mg/day	3.48
K <sub>ic</sub> DCEDCA	mg /L	0.35	kmaxDCA	mg /mg/day	1.16
K <sub>ic</sub> DCETCA	mg /L	0.11	kmaxDCE	mg /mg/day	6.50
			kmaxTCA	mg /mg/day	0.64
K <sub>ic</sub> TCABUT	mg /L	41.79			
K <sub>ic</sub> TCADCA	mg /L	1.31	KsBUT	mg /L	1.11
K <sub>ic</sub> TCADCE	mg /L	2.27	KsDCA	mg /L	1.90
			KsDCE	mg /L	0.14
K <sub>iu</sub> BUTDCA	mg /L	0.23	KsTCA	mg /L	1.63
K <sub>iu</sub> BUTDCE	mg /L	0.40	KsO <sub>2</sub>	mg /L	1
K <sub>iu</sub> BUTTCA	mg /L	0.03			
			TcDCA	mg /mg	0.20
K <sub>ic</sub> BUTDCE	mg /L	0.02	TcDCE	mg /mg	0.017
			TcTCA	mg /mg	0.11
f <sub>d</sub>	mg/mg	4			
d <sub>c</sub>	mg/mg	1.42			

*Nomenclature provided in Appendix A*

*\*Microbial mass was assumed non-uniformly distributed (Appendix L)*

**Figure 5.6 Transport parameter values for simulating field data.**

Average flow*, Q	Aquifer Thickness, thick	Aquifer Width, width	Porosity, $\Phi$	Bulk Density, $\rho_b$	Dispersion Coeff., $D_h$
( <u>m<sup>3</sup>/day</u> )	( <u>m</u> )	( <u>m</u> )	( <u>-</u> )	( <u>kg/L</u> )	( <u>m<sup>2</sup>/day</u> )
1.0	1.5	1.0	0.33	1.6	0.31
Sorption Coefficient**, $k_d$ (L/kg)			Mass Transfer Rate Coefficient**, $F_k$ (day <sup>-1</sup> )		
<u>1,1-DCE</u>	<u>1,1-DCA</u>	<u>1,1,1-TCA</u>	<u>1,1-DCE</u>	<u>1,1-DCA</u>	<u>1,1,1-TCA</u>
0.69	0.50	0.50	2.0	2.0	2.0

\*Defined from Bromide tracer tests (Section 5.2)

\*\*Defined from CAH breakthrough tests (Section 5.3)

Because the model was limited to simulate only two CAHs, double simulations were run to create biotransformation/transport profiles of each of the 3 CAHs. The first simulations included the analysis of 1,1-DCE and 1,1,1-TCA. The second simulations evaluated 1,1-DCE with 1,1-DCA. These combinations were chosen because 1,1-DCE was the most toxic and most quickly transformed. It was therefore assumed that 1,1-DCE had the most influence on the 1,1-DCA and 1,1,1-TCA transformation, while these latter CAHs have minimal influences on one another.

To confirm this assumption, two additional runs were performed using the Stella model to simulate behavior of the laboratory microcosms in the absence of one CAH. One simulation included 1,1-DCE and 1,1,1-TCA in the absence of 1,1-DCA, while, the other included 1,1-DCE and 1,1-DCA in the absence of 1,1,1-TCA (results not shown). Both sets of output showed similar results to those from the laboratory simulations (Section 4.2.6), indicating that the presence/absence of 1,1-DCA or 1,1,1-TCA has minimal influence on CAH transformation and butane utilization.



### 5.5.1 Simulation of Field Bioaugmentation Data

The model was run to simulate the S1 monitoring data described in Section 5.4, using biotransformation values and transport values listed in Tables 5.5 and 5.6. The injection boundary conditions followed pulsing schedules listed in Tables 5.3 and 5.4. Actual model inputs for the simulations are tabulated in Appendix J. Model simulation output is compared to field data in Figure 5.9. Plots of the cell concentration at the end of the simulation (day 75) and the microbial spatial distribution, as calculated from the model are included. As all models have limitations, the focus of this study was to capture trends interpreted from the field data. Overall, these trends were well simulated, particularly during the first 60 days of the experiments. Butane utilization decreased during longer pulsing durations (days 20-40) and limited oxygen availability (days 23-30). Oxygen was consumed with butane and when adequate quantities of oxygen were delivered to the test zone. During initial bioaugmentation (days 9-20) there was good transformation of 1,1-DCE, 1,1-DCA, and 1,1,1-TCA, with the latter two lagging behind until significant butane had been consumed and reduced to low concentrations. This follows the observations from the laboratory experiments, where 1,1-DCE was quickly transformed (due to its high transformation rate) and 1,1-DCA and 1,1,1-TCA were inhibited by butane. Transformation of all three CAHs was lost when butane and oxygen pulsing cycles were elongated (days 20-40). 1,1-DCE transformation returned when pulsing was shortened again (days 40-75). Using equilibrium sorption ( $F_k = 2.0 \text{ day}^{-1}$ ) compared to lower first order mass transfer kinetics ( $F_k = 0.2 \text{ day}^{-1}$ ) likely resulted in a dampening of pulses due to competitive inhibition in the model (Section 5.5.5).

The model predicted significantly more 1,1-DCA transformation for the latter period of the simulations (days 60-75) than was indicated by field data. It also predicted that slightly more 1,1,1-TCA should have been degraded. These contrasts were possibly due to a change in the microbial community within the test zone. It was speculated that an indigenous population was eventually stimulated and the

bioaugmented population diminished. This was supported by data observed from a non-bioaugmented control test leg which had been treated in the same manner as the augmented leg. In the control leg, butane utilization was observed and 1,1-DCE was transformed at a later time, while 1,1,1-TCA and 1,1-DCA were not transformed. Based on this information, the modeling results would suggest that the indigenous microorganisms predominated at the later time.

There were other discrepancies between the model output and field data, indicating a number of possible complications. These may have been attributed to perturbations in field control, such as substrate delivery to the aquifer and fluctuations in hydraulics.

The cell concentration profiles (Figure 5.9d) provide additional understanding and interpretation of the model and field data. The upper plot depicts cell growth and decay during the entire simulation period, while the lower plot provides a blown-up scale for the first 40 days. Biomass peaked at the S1 well location when large amounts of butane were utilized (days 25-30 and 45-52). Cell death occurred after large amounts of 1,1-DCE were transformed and when butane consumption was limited (days 30-35 and 52-65). This is indicative of high 1,1-DCE product toxicity (as seen in the laboratory experiments, Chapter 4) and cell decay in the absence of a primary growth substrate. There was a greater magnitude of cell growth during the latter period. This was due to the greater amount of butane consumed and a lower mass of 1,1-DCE transformed. The lower transformation caused less cell inactivation. The spatial distribution plot for cell concentrations recorded at 20 days and 75 days (Figure 5.9e) both show that most cell mass exists within the first meter of the test zone.

Overall, the field transformation trends were well simulated by the biotransformation/transport model. This indicates the ability to successfully apply laboratory derived parameters to larger scale experiments.

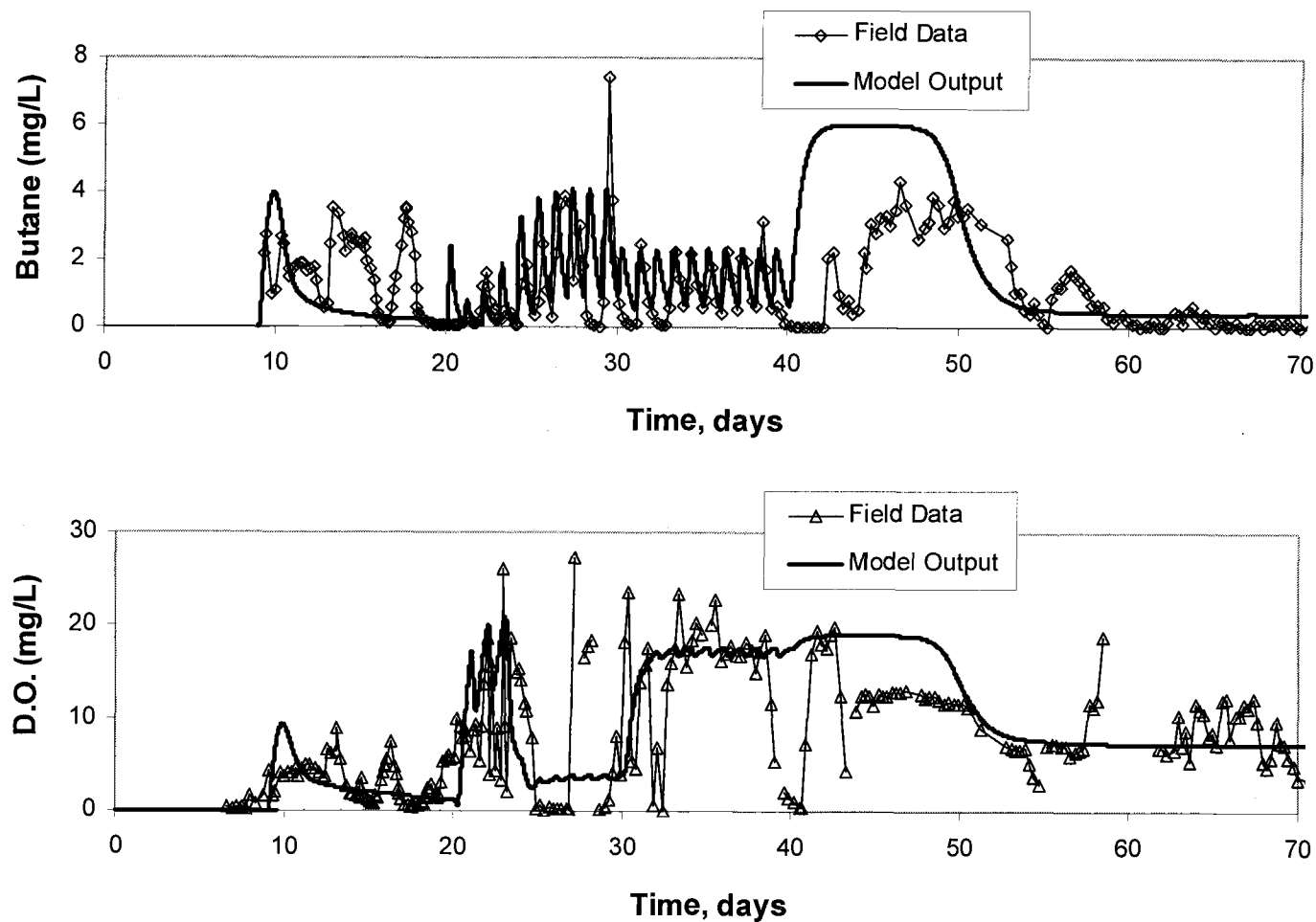


**Figure 5.9a Comparison of butane and oxygen field data and model output at S1 (1m).**  
The bioaugmented culture was introduced on day 9.

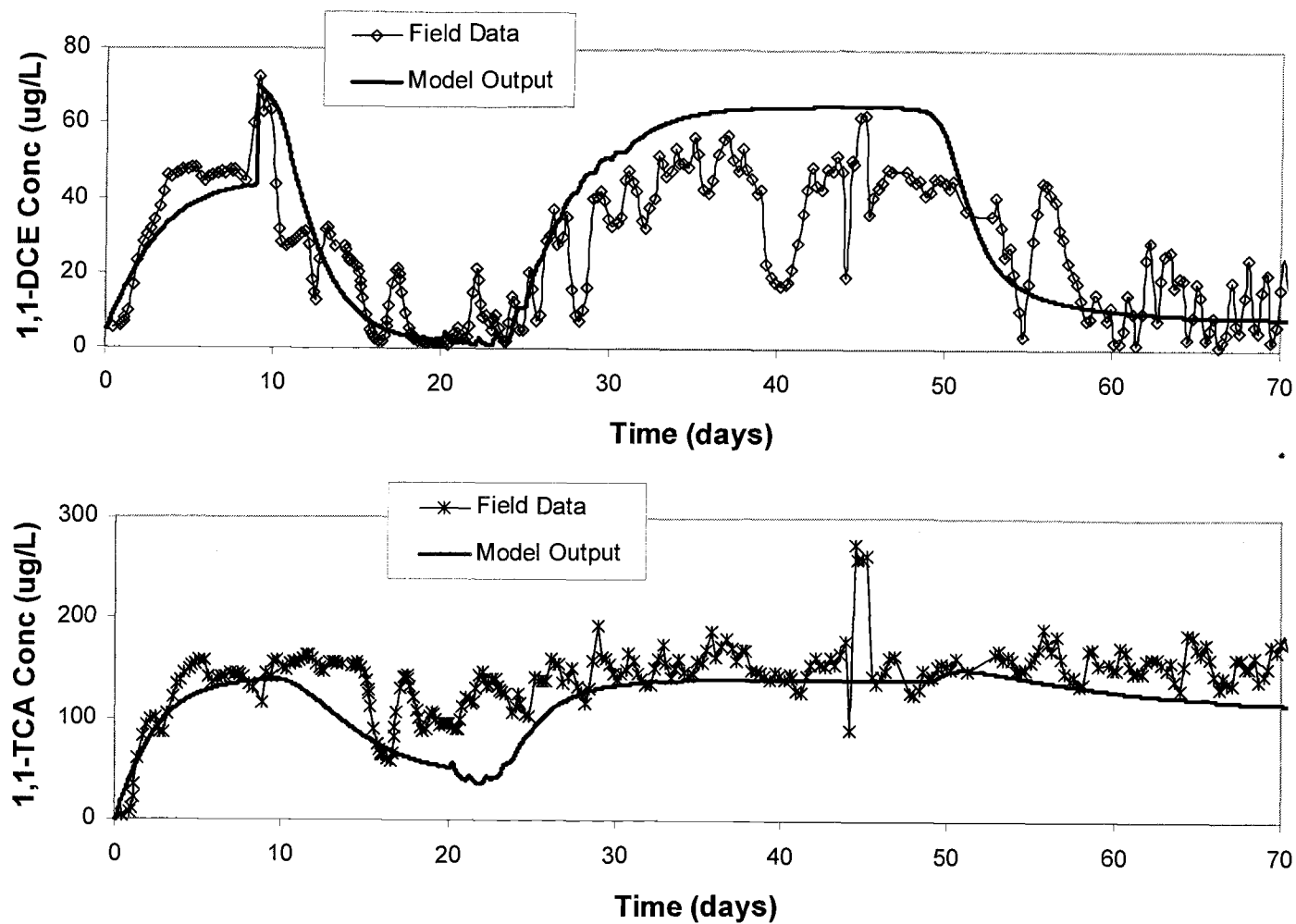


**Figure 5.9b Comparison of 1,1-DCE and 1,1,1-TCA concentrations for the field data and model output at S1 (1m).**  
The bioaugmented culture was introduced on day 9.

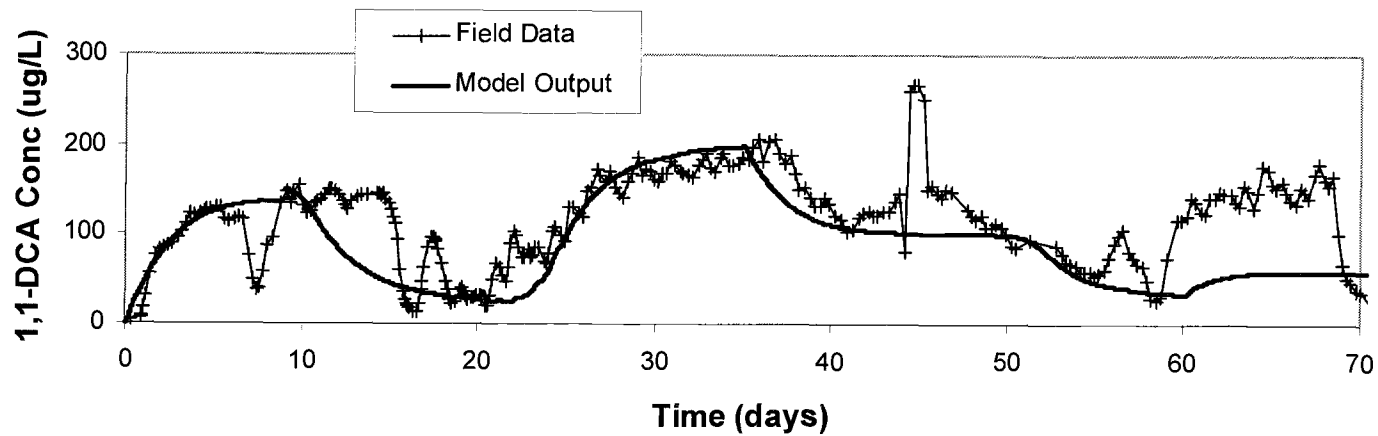


**Figure 5.9c Comparison of 1,1-DCA concentrations for the field data and model output at S1 (1m).** The bioaugmented culture was introduced on day 9. 1,1-DCA injection stopped at day 48.

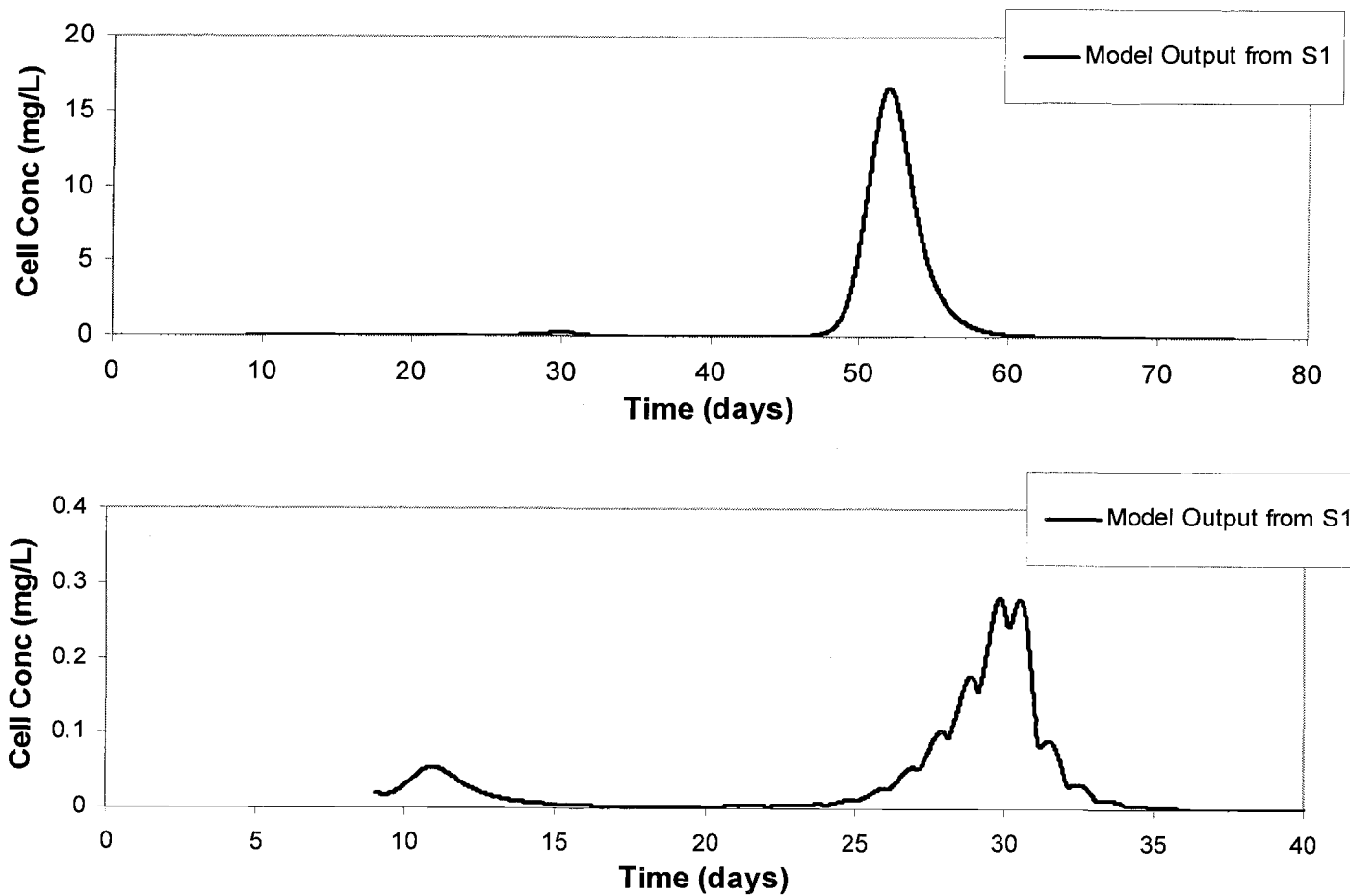


**Figure 5.9d Model output of cell concentration at S1 (1m).** The bioaugmented culture was injected on day 9. The lower figure is a blowup of cell growth, decay, and inactivation during the early part of bioaugmentation.

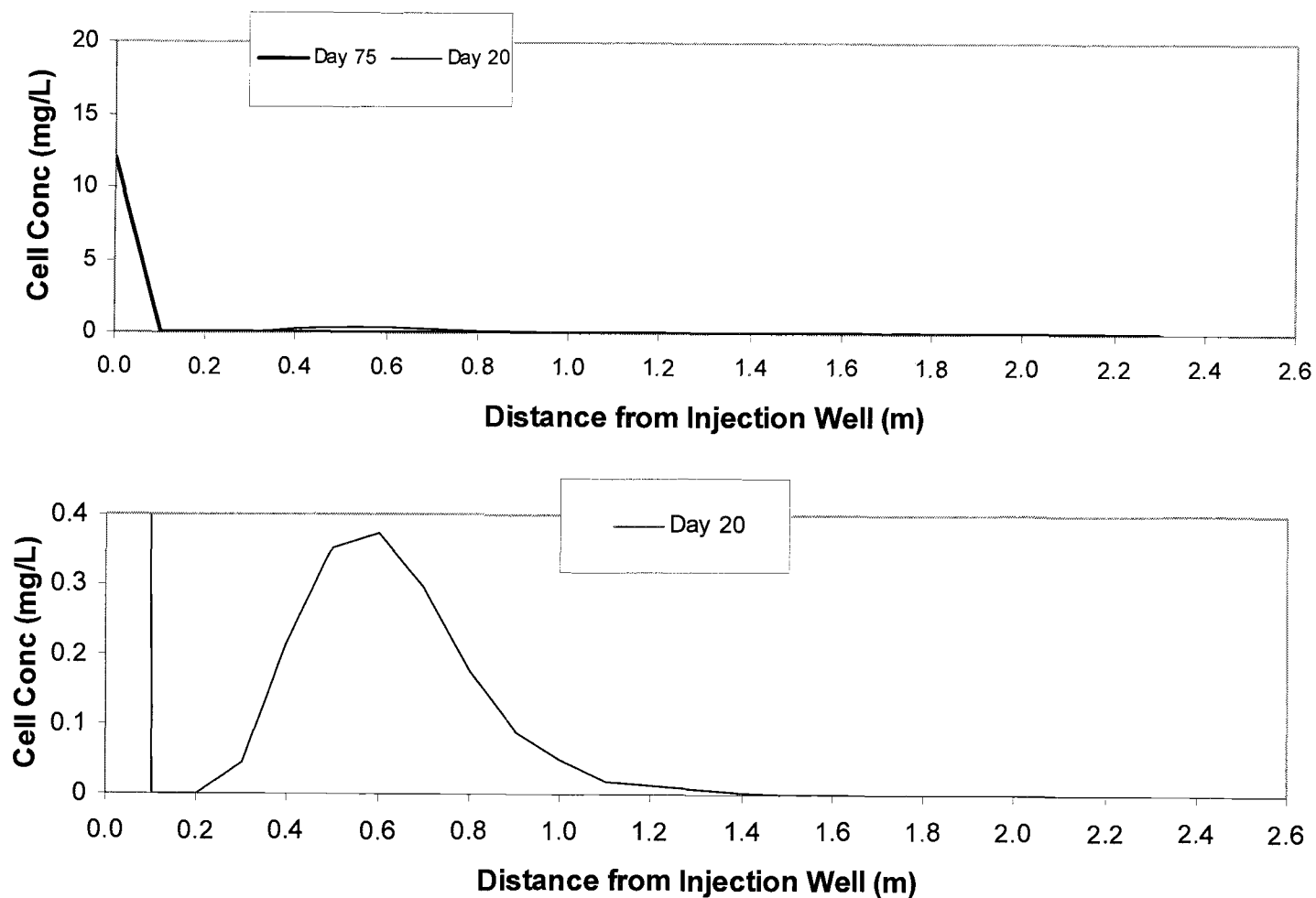


**Figure 5.9e** Model output of cell distribution over the first 2.6 m of the test zone on day 20 and day 75. The bioaugmented culture was injected on day 9. The lower figure is a blowup of cell concentration for day 20

### 5.5.2 Simulations to Predict Activity after Bioaugmentation

Two simulations were run to predict activity within the test zone at S1 (1m from the injection well) after initial bioaugmentation ceased (day 75). This was done by expanding the simulation time to 90 days, with the first 75 days modeled for breakthrough and bioaugmentation seen in the field (Section 5.5.1). After this period (days 75-90), the model was manipulated to simulate delivery of (1) oxygen alone and (2) elevated butane and oxygen concentrations. The simulations were run to observe transformation of only 2 of the 3 CAHs. 1,1-DCE was chosen to study because of its fast transformation ability and highly toxic effects on the culture. 1,1,1-TCA was chosen because it is the most recalcitrant of the three CAHs.

The first simulation included an oxygen injection concentration of 25 mg/L during days 75-90. This was pulsed every hour into the aquifer for 45 min durations. Results of the simulation are presented in Figure 5.10. Utilization and transformation during the first 75 days follow that seen in the simulations discussed in Section 5.5.1. After day 75 there is rapid but short utilization of butane and transformation of 1,1-DCE and 1,1,1-TCA, followed by a rise in butane, oxygen, and CAH concentrations. This indicates that a large quantity of cells were inactivated during biotransformation of the highly toxic 1,1-DCE, leaving a nonviable population. The remaining (if any?) cells were unable to transform the CAHs in the absence of butane.

The second simulation included butane and oxygen injection concentrations of 50 mg/L between days 75 and 90. This would represent much higher values with butane near its solubility limit. These were alternately pulsed into the aquifer, with butane being injected for 15 minutes followed by 45 minutes of oxygen. This shorter cycling time was chosen because the best transformation was observed in the field at this duration. Results of this simulation are presented in Figure 5.11. Utilization and transformation during the first 75 days follow that seen in the simulations from Section 5.5.1. After day 75 there is rapid utilization and transformation, with particularly good degradation of 1,1,1-TCA due to 1,1-DCE having been reduced to low concentrations.



This indicates that there is enough of a viable cell population at day 75 to restore transformation, once 1,1-DCE toxicity was eliminated. The results suggested that the addition of more butane and oxygen (through peroxide injection,  $\text{H}_2\text{O}_2$ ) would be beneficial.

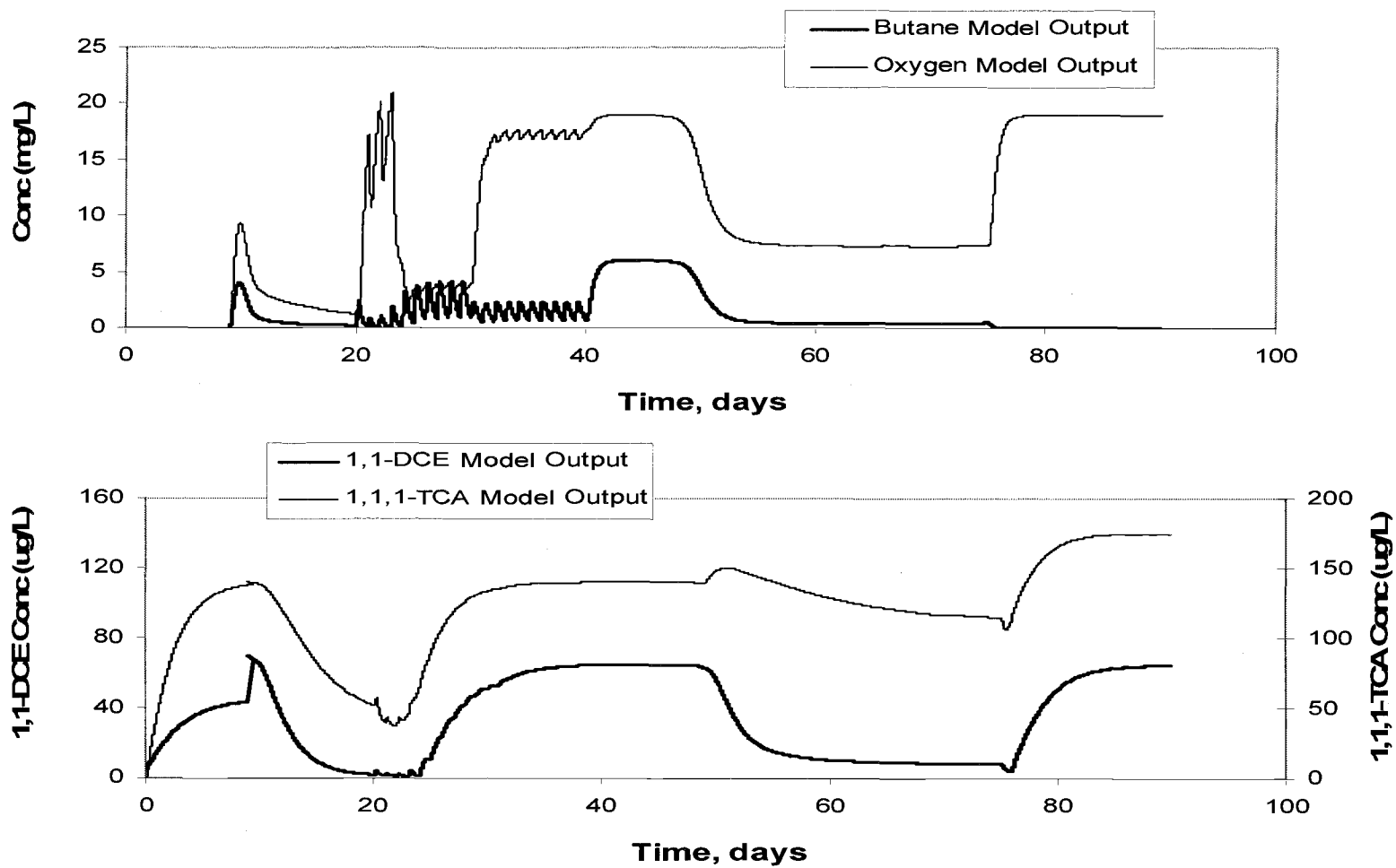


Figure 5.10 Model output for simulating utilization and transformation at S1 (1m) if 25 mg/L oxygen is injected between days 75 and 90.

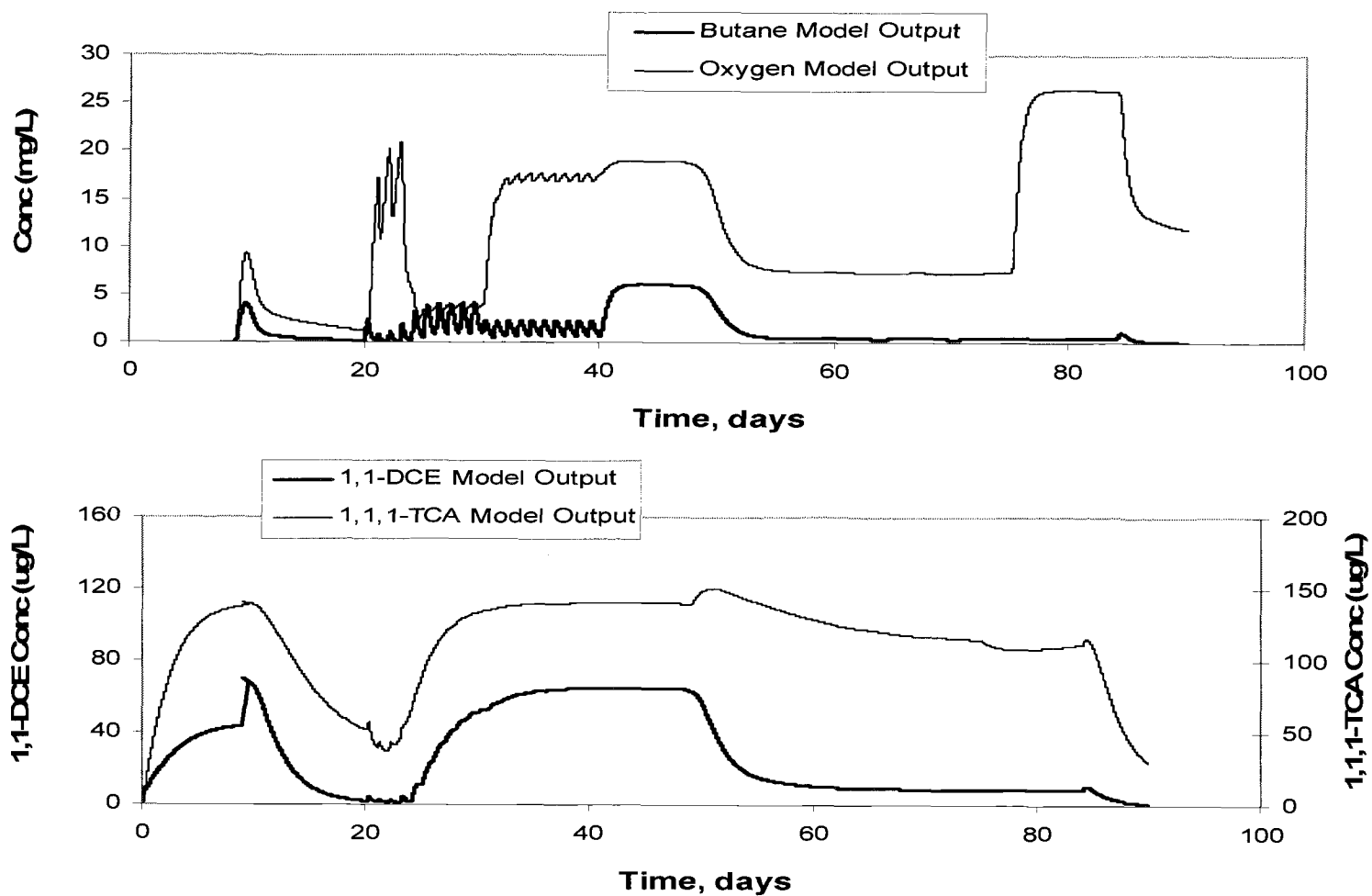
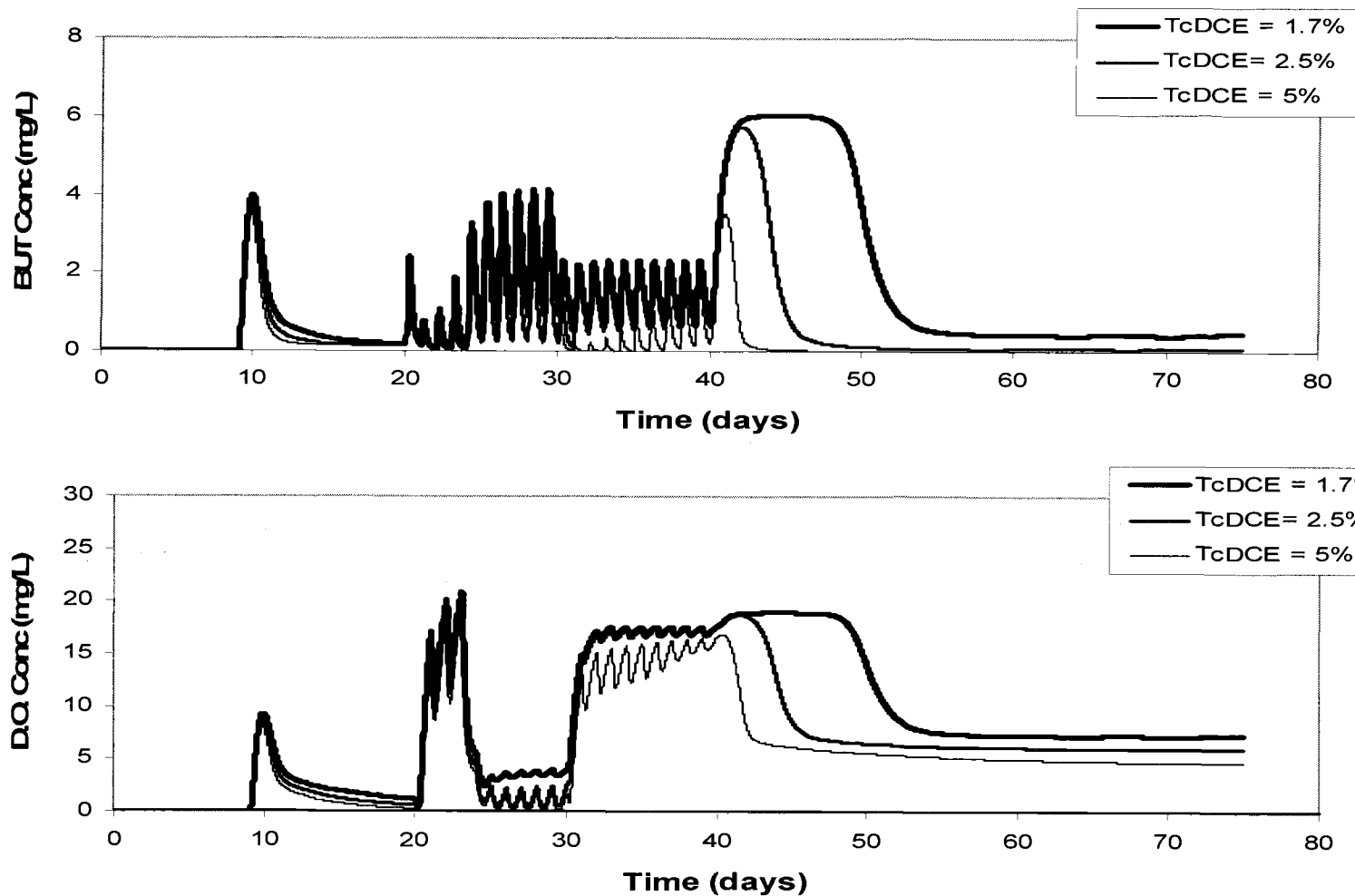


Figure 5.11 Model output for simulating utilization and transformation at S1 (1m) if 50 mg/L butane and 50 mg/L oxygen are injected between days 75 and 90.

### 5.5.3 Sensitivity Analysis of 1,1-DCE Product Toxicity

As done with the laboratory data (Section 4.2.2), the field data were simulated using various 1,1-DCE transformation capacity values ( $T_{cDCE}$ ) to evaluate the effect of product toxicity on the system's activity. Pulsing concentrations and durations (Tables 5.3 and 5.4), and biotransformation and transport values (Tables 5.5 and 5.6) were maintained from the simulation of Section 5.5.1, with the exception of  $T_{cDCE}$ . This parameter was varied to represent three different product toxicities: 0.0167 (1.7%), 0.025 (2.5%), and 0.05 (5%) mg 1,1-DCE/mg cells. Note that the two extremes of this range are those studied in the laboratory modeling (Section 4.2.2). Actual input for these simulations are listed in Appendix J, Table J.1, with additional values of  $T_{cDCE}$  tabulated in Appendix M.

Simulation results recorded at monitoring well S1 (1m from the injection well) are compared in Figure 5.12. The lower product toxicity (greater  $T_{cDCE}$  value, 0.05 mg DCE/mg cells) resulted in the most utilization and transformation. This observation is as expected, as lower product toxicity would inactivate less cells, allowing the microbial population to flourish. This phenomena is depicted in Figure 5.12c., where the distributed biomass from lower product toxicity shows higher concentrations close to the injection well.



**Figure 5.12a Butane and Oxygen Output from Sensitivity Analysis of 1,1-DCE Product Toxicity at S1 (1m).** Transformation capacities for 1,1-DCE ( $T_{cDCE}$ ) values: 0.0167 (1.7%), 0.025 (2.5%), and 0.05 (5%) mg DCE/mg cells.

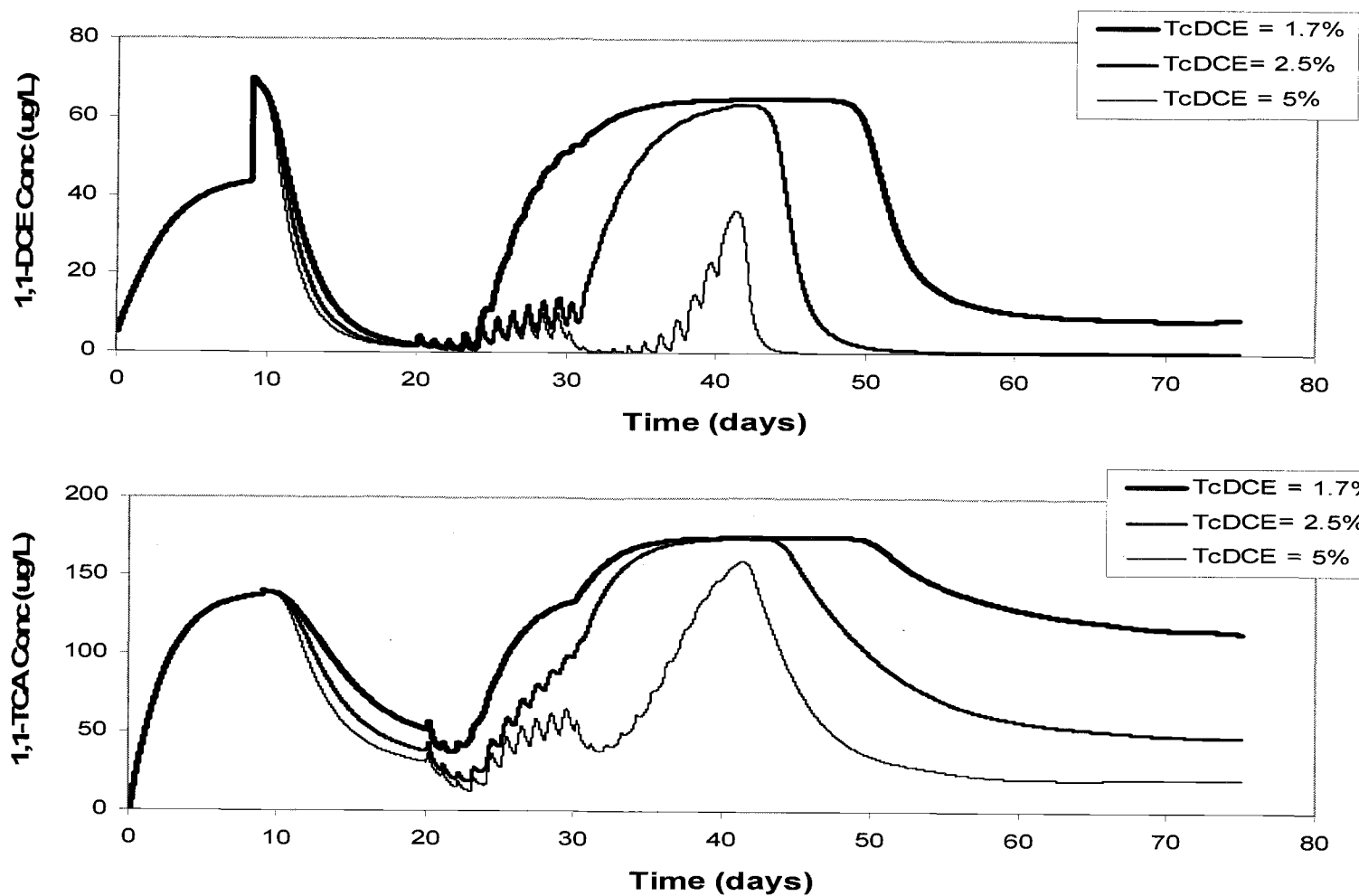
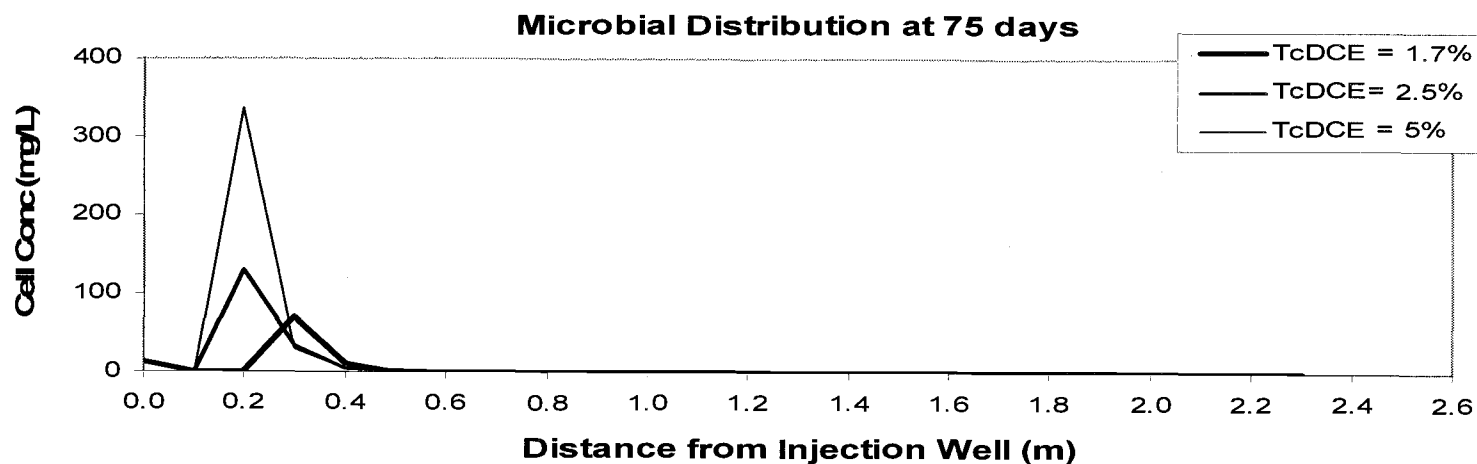
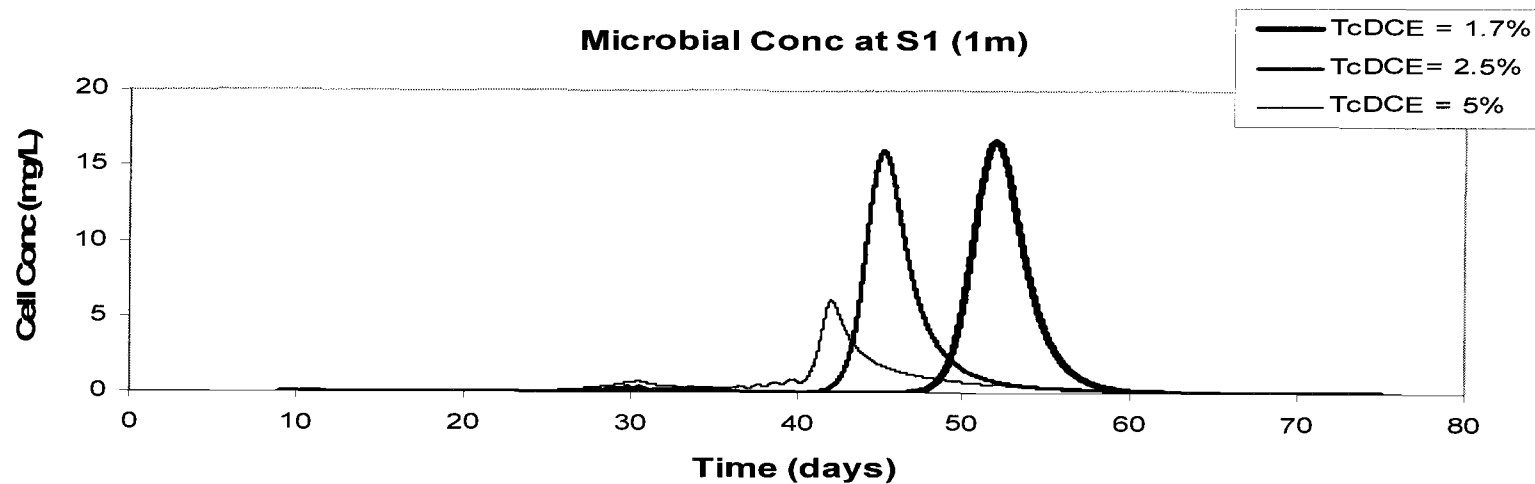


Figure 5.12b 1,1-DCE and 1,1,1-TCA results from sensitivity analysis of 1,1-DCE product toxicity at S1 (1m). Transformation capacities for 1,1-DCE ( $T_{cDCE}$ ) values: 0.0167 (1.7%), 0.025 (2.5%), and 0.05 (5%) mg DCE/mg cells..



**Figure 5.12c Biomass results from sensitivity analysis of 1,1-DCE product toxicity.**

Transformation capacities for 1,1-DCE  $T_{cDCE}$  values: 0.0167 (1.7%), 0.025 (2.5%), and 0.05 (5%) mg DCE/mg cells.

#### 5.5.4 Sensitivity of 1,1-DCE Transformation Rate

Field simulations were also run using the lower 1,1-DCE transformation rate ( $k_{mDCE} = 0.1 \mu\text{mol/mg/hr} = 0.23 \text{ mg/mg/day}$ ) which had more closely fit the product toxicity laboratory data (Section 4.2.3). This value was an order of magnitude lower than the  $k_{mDCE}$  value ( $2.8 \mu\text{mol/mg./hr} = 6.5 \text{ mg/mg/day}$ ) defined by Kim et al. (in press). The model results are compared for both values of  $k_{mDCE}$  in Figure 5.13. Other parameter values were the same as those presented in Tables 5.5 and 5.6.

The model output for transport and biotransformation is consistent with that from the Stella model. At the lower  $k_{mDCE}$  value, butane utilization and 1,1,1-TCA transformation became faster during the short butane and oxygen pulsing cycles (days 9-20). During the later period (after day 20), 1,1-DCE transformation increased using the lower  $k_{mDCE}$  value ( $0.23 \text{ mg/mg/day}$ ). This may have been caused by an increase in the microbial population at this location or inhibition by butane. Also note that the oscillations in CAH concentrations became more apparent. This observation suggested that the pulsing effect on CAH transformation was dampened using the higher  $k_{mDCE}$ .

As with the simulations of the laboratory data for varying  $k_{mDCE}$ , the contrasts illustrate the complexity of the system and the sensitivity and limitations of the model. It is reasonable to suspect that because the culture used in this study was different from that used by Kim et al. (2002, *in press*), other parameter values may also be different. A more useful approach in extrapolating model parameters from laboratory experiments to field experiments would have been to independently define the parameter values specific for our culture.



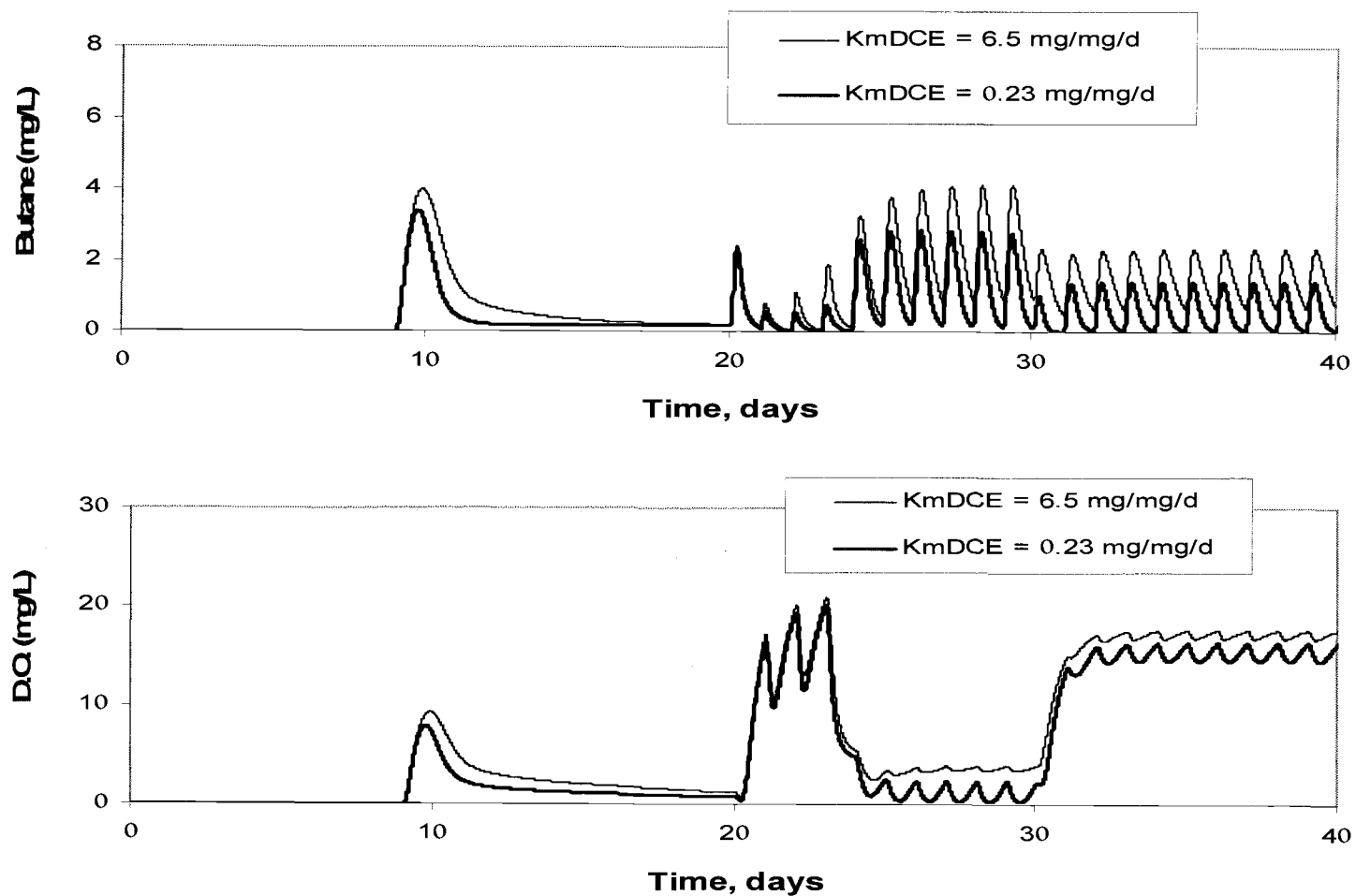


Figure 5.13a Comparison of butane and oxygen utilizations from field biotransformation assuming different 1,1-DCE transformation rates.

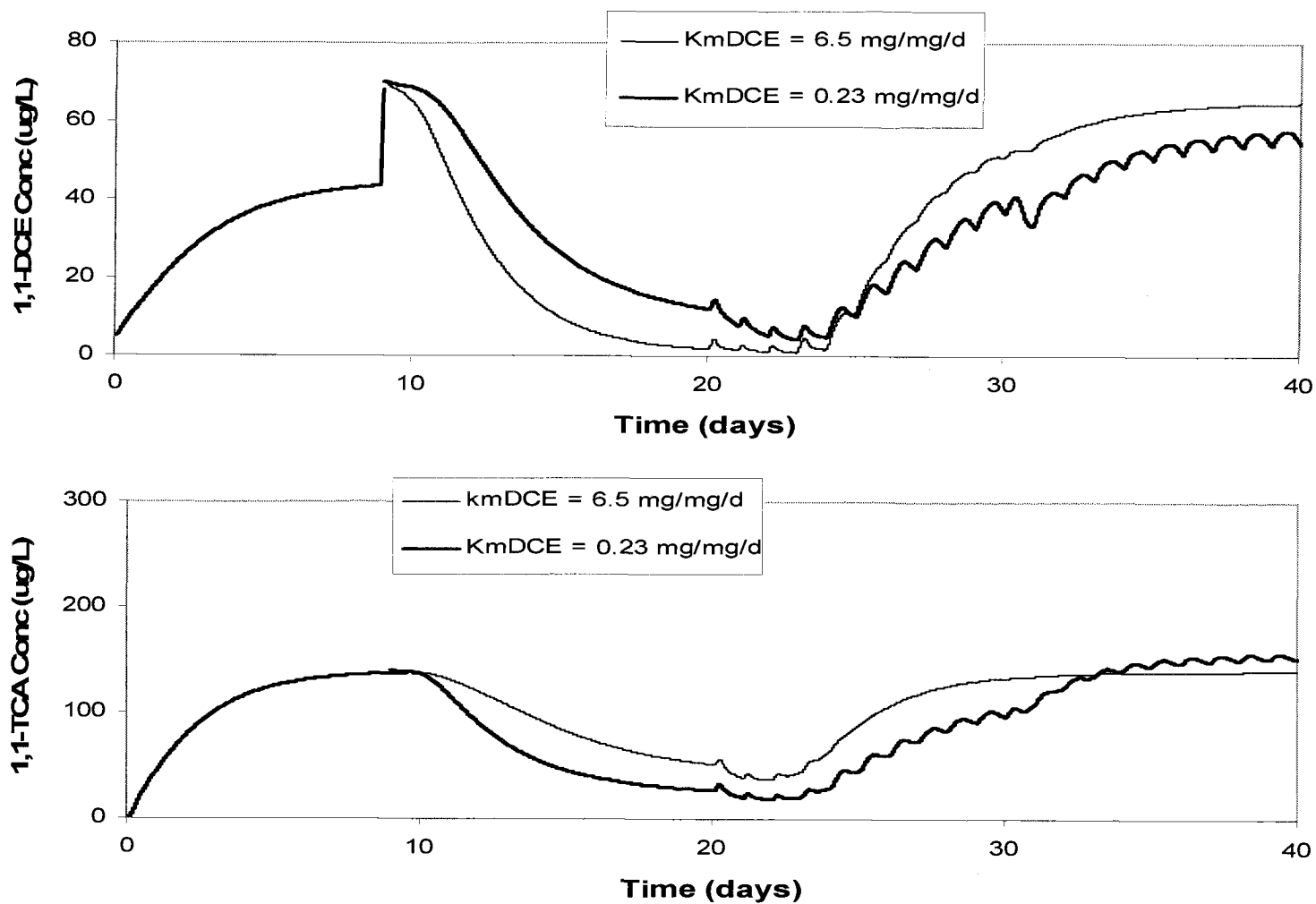


Figure 5.13b Comparison of 1,1-DCE and 1,1,1-TCA transformation from field biotransformation assuming different 1,1-DCE transformation rates.

### 5.5.5 Sensitivity of First Order Mass Transfer Rate and Pulsing Cycles

Since sorption parameters were difficult to ascertain from simulating breakthrough data (Section 5.3), a sensitivity analysis was run for variations in the first order mass transfer rate coefficient ( $F_k$ ). The analysis included a variation in pulse durations, while maintaining the same butane to oxygen ratio. This was done because previous simulations for elongating pulsing durations included a decrease in the ratio of butane to oxygen that was being injected (15 min butane; 45 min oxygen at a 1:3 ratio, followed by 2 hrs butane; 22 hrs oxygen at a 1:10 ratio). It was suspected that, for actual field demonstrations and the previous simulations (Figure 5.9), it was not the longer pulse duration that caused transformation to cease (after day 20), but the reduction in the butane to oxygen delivery ratio, which made butane less available, resulted in transformation ceasing.

Simulations were therefore run to study the differences at monitoring well S1 between equilibrium and non-equilibrium sorption, with butane and oxygen pulsing durations elongated. The  $F_k$  value used in the previous simulations ( $2.0 \text{ day}^{-1}$ ) represented the case of equilibrium partitioning between the solid and liquid phases. A lower  $F_k$  value ( $0.2 \text{ day}^{-1}$ ) was incorporated to create a non-equilibrium case. All other biotransformation and transport parameters were maintained from the original 75 day simulations (Tables 5.5 and 5.6 and Appendix L). For these simulations, butane and oxygen were initially pulsed (days 9-30) at a 1:3 butane to oxygen ratio for short durations (15 min butane; 45 min oxygen). Later in the simulations, the pulse durations were elongated (3 hours butane; 9 hours oxygen), while maintaining the 1:3 butane to oxygen ratio. This allowed the same amount of butane to be delivered for both short and long pulse stages. This simulation included only the study of 1,1-DCE and 1,1,1-TCA transformation. Actual input for the simulation is tabulated in Appendix N.

Figure 5.14 provides comparison plots of butane and oxygen utilization and CAH transformation for the variation in pulsing durations and the two different first order mass transfer rates. There are two main points resulting from these simulations.

The first is the influence of elongating the butane and oxygen pulsing durations (days 30-70). As seen in Figure 5.14a, when the duration was increased (3 hrs butane to 9 hrs oxygen ) while maintaining the same oxygen to butane ratio (1:3) as the shorter cycle (15 min butane to 45 min oxygen), oscillations in the concentrations became more apparent. As oxygen became more available, transformation of 1,1-DCE (Figure 5.14c) and 1,1,1-TCA (Figure 5.14d) was maintained. This contrasted with the previous simulations in which both the butane to oxygen pulse durations and ratios changed (Figure 5.9) after day 40, making less butane available and stopping CAH transformation. From these simulations we can conclude that, had the butane to oxygen ratio been maintained during the field demonstration, CAH transformation may have continued.

The second point of understanding comes from observing the comparison plots of the equilibrium ( $2.0 \text{ day}^{-1}$ ) and non-equilibrium ( $0.2 \text{ day}^{-1}$ ) simulations. As seen in Figures 5.14c and 5.14d, when non-equilibrium was included during the longer pulsing cycles (days 30 to 70), the oscillations in CAH concentrations became more exaggerated. This indicated the effect of equilibrium conditions dampening out the effects of competitive inhibition by butane. As the rate of CAH mass being sorbed onto and off of aquifer solids varied, less mass was exchanged between the liquid and sorbed phases over short time periods, causing greater variations in aqueous concentrations. This indicated that, based on the CAH oscillations observed during the field demonstration (Figure 5.9), non-equilibrium sorption was most likely occurring.

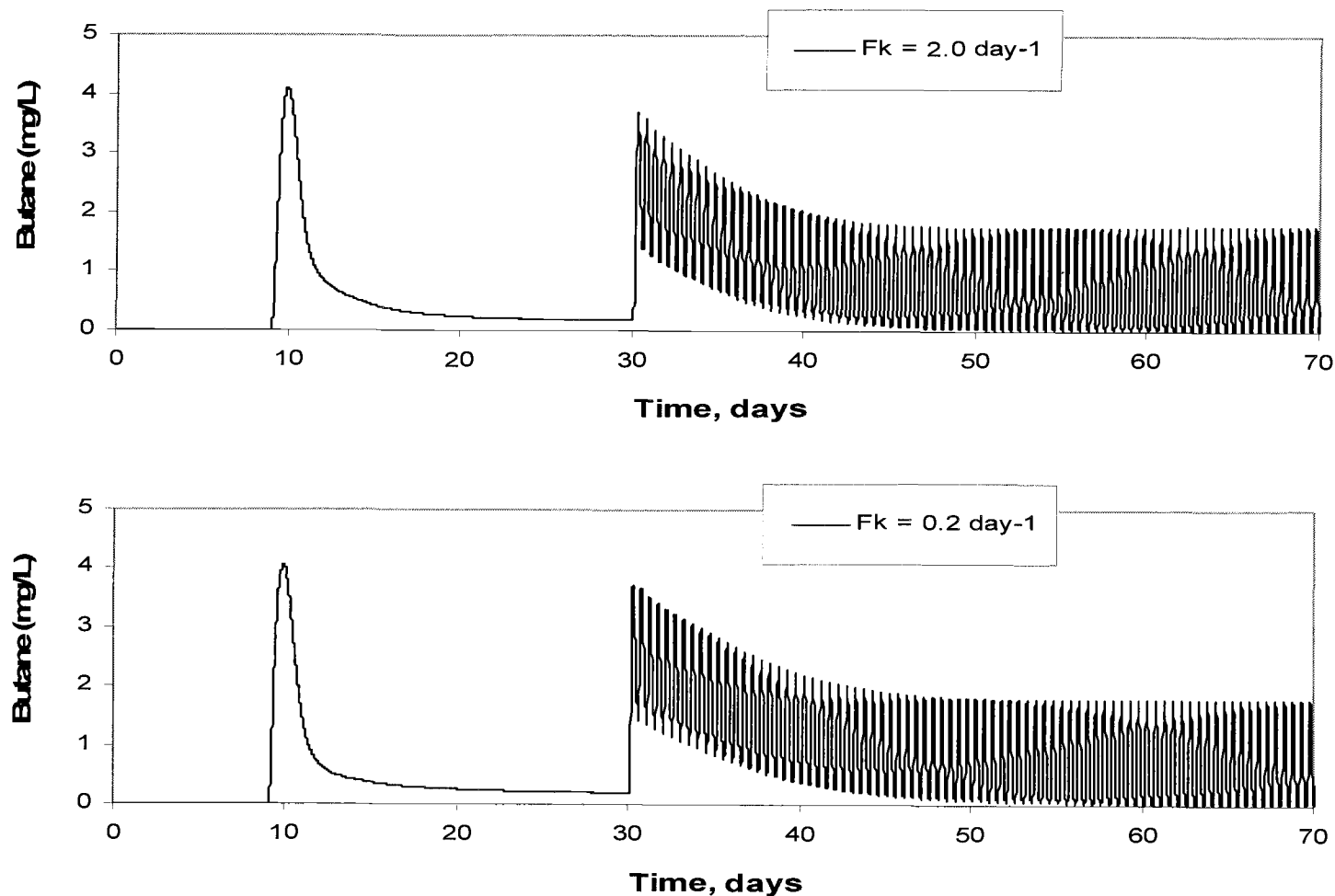
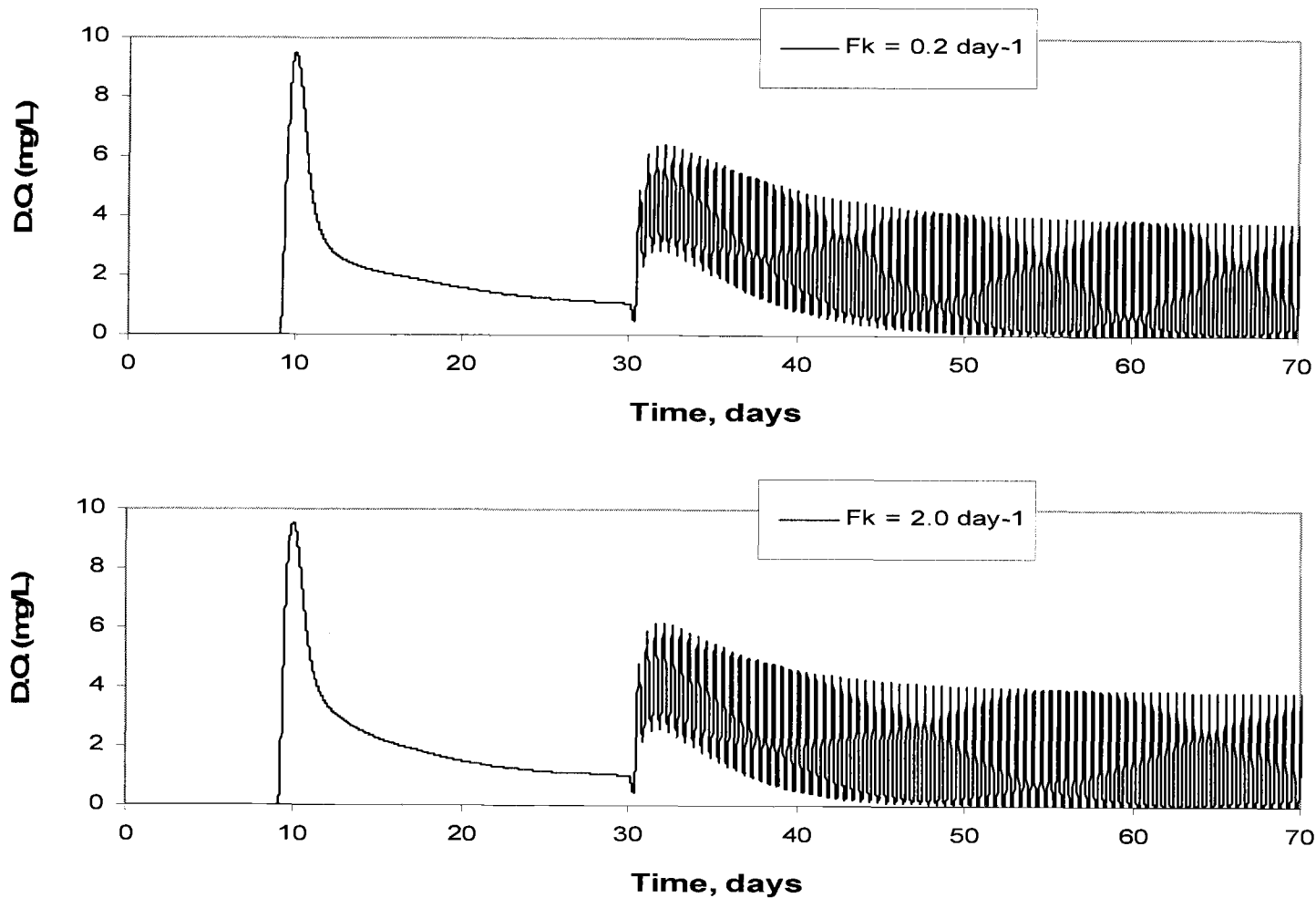


Figure 5.14a Comparison of butane utilization at S1 (1m) for equilibrium ( $F_k = 2.0 \text{ day}^{-1}$ ) and non-equilibrium ( $F_k = 0.2 \text{ day}^{-1}$ ) sorption with elongated butane and oxygen pulsing durations.



**Figure 5.14b** Comparison of oxygen utilization at S1 (1m) for equilibrium ( $F_k = 2.0 \text{ day}^{-1}$ ) and non-equilibrium ( $F_k = 0.2 \text{ day}^{-1}$ ) sorption with elongated butane and oxygen pulsing durations.

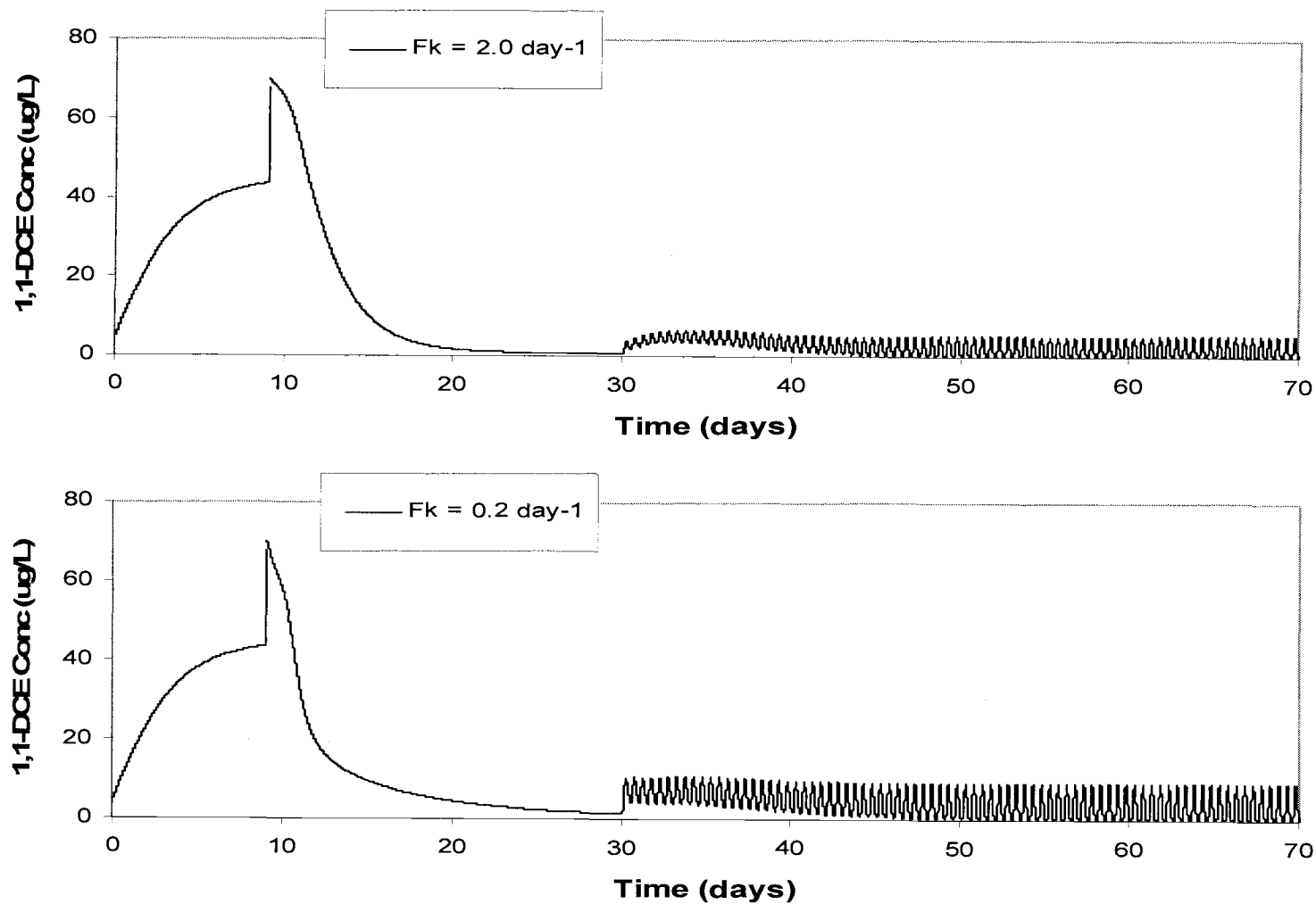


Figure 5.14c Comparison of 1,1-DCE transformation at S1 (1m) for equilibrium ( $F_k = 2.0 \text{ day}^{-1}$ ) and non-equilibrium ( $F_k = 0.2 \text{ day}^{-1}$ ) sorption with elongated butane and oxygen pulsing durations.

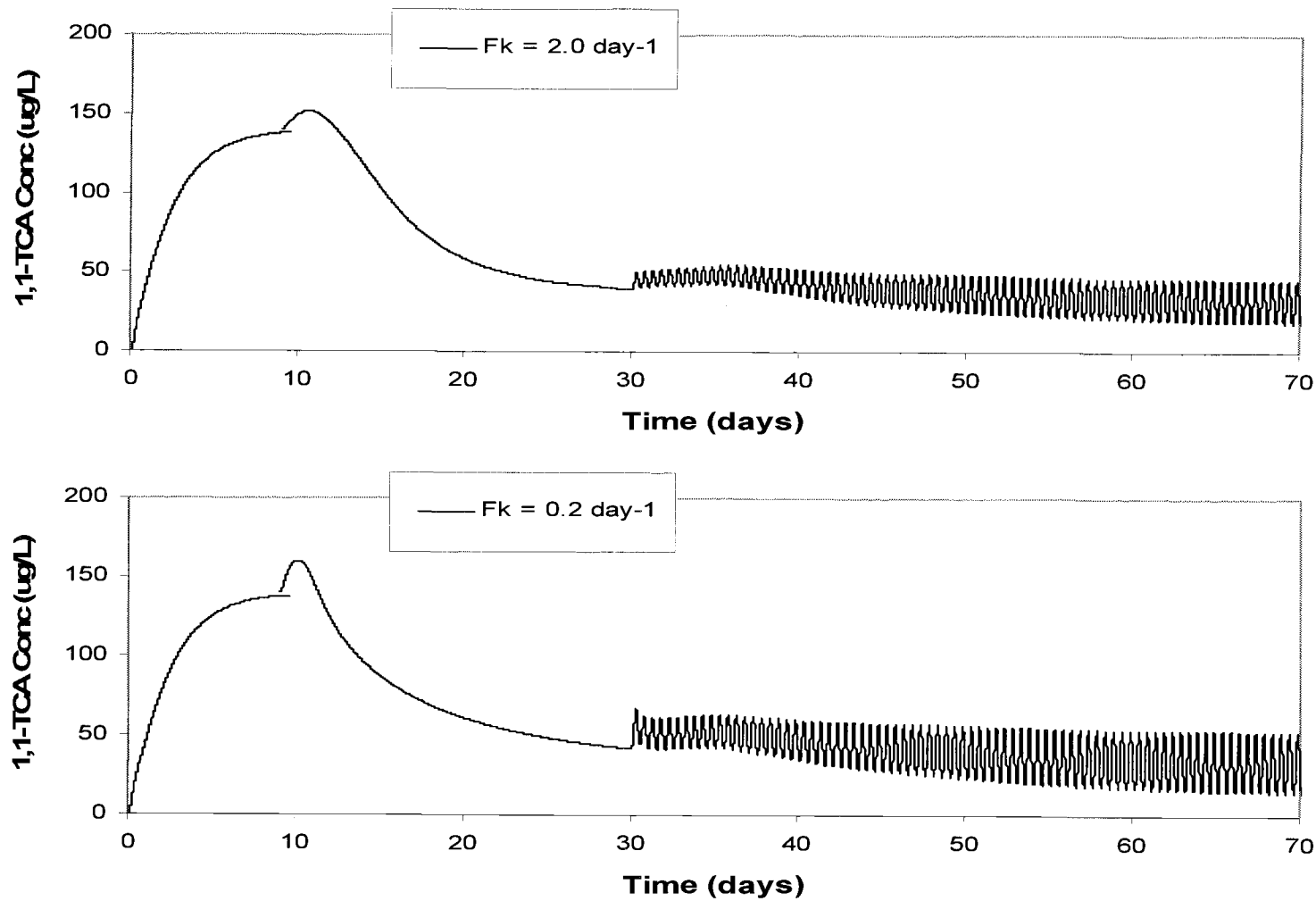


Figure 5.14d Comparison of 1,1,1-TCA transformation at S1 (1m) for equilibrium ( $F_k = 2.0 \text{ day}^{-1}$ ) and non-equilibrium ( $F_k = 0.2 \text{ day}^{-1}$ ) sorption with elongated butane and oxygen pulsing durations.



## 5.6 SUMMARY OF FIELD MODELING

Simulations for flow and sorption using the transport model showed a good match to the field breakthrough data. The transport values determined from these simulations were incorporated into the combined model to simulate biotransformation and transport of the field data.

Bioaugmentation in the field showed similar results to the laboratory data when adequate butane and oxygen were delivered to the test zone. 1,1-DCE was quickly degraded with 1,1-DCA and 1,1,1-TCA lagging behind. The lag in transformation follows the phenomena of strong butane inhibition on these CAHs. When butane and oxygen pulsing was elongated, not enough growth substrate was available to maintain an effective cometabolic population, and transformation ceased. Upon the reintroduction of shorter pulsing cycles, 1,1-DCE transformation was restored, although transformation of 1,1-DCA and 1,1,1-TCA never returned. This was most likely due to either a change in the microbial profile of the culture within the test zone, or an extreme product toxicity of 1,1-DCE. 1,1-DCE transformation likely resulted from increased butane addition upon return to the shorter pulsing.

The model simulations reproduced many of these trends. During shorter injection pulsing of butane and oxygen, 1,1-DCE was quickly transformed. 1,1-DCA and 1,1,1-TCA were inhibited by butane, as transformation of these CAHs did not occur until a good portion of butane had been utilized. Elongating the butane and oxygen pulsing durations in the model reduced the amount of butane available to the organisms, and transformation ceased. However, the model predicted that upon restoring the shorter pulsing cycles, 1,1-DCA and slight 1,1,1-TCA transformation should have occurred. This discrepancy from the actual field data suggests that there was a shift in the microbial community with time.

Other inaccurate matches between the field data and model output were due to perturbations in the field system, such as inconsistent delivery of butane and oxygen to the site and heterogeneities within the test zone. Also, the bioaugmented culture was an

enrichment from that used by Kim et al. (in press) from which many of the parameter values were taken. As the laboratory tests and modeling showed, there may be variations in other parameters not studied here that would affect the simulations.

From these model simulations, improvements can be made for future bioremediation projects. Simulations indicated that maintaining short pulsing cycles of butane and oxygen were required in order to maintain CAH transformation and butane utilization. A less drastic elongation in cycling durations may have allowed further distribution of the microbes from the injection well without losing transformation. Column studies could be performed in advance to better determine sorption parameters and the microbial distribution within an aquifer setting.

The importance of this model, despite such complexities, is that trends observed in the field were well simulated, and the model permitted an analysis of the complex interaction of transport, biostimulation, and the transformation kinetics of cometabolism. This permitted us to determine what may have happened when changes were made in the pulsing duration, or the effect of different 1,1-DCE transformation capacities.

## CHAPTER 6

### CONCLUSIONS

---

The overall goal of this study was to model results of a field demonstration where a butane-utilizing culture was bioaugmented and then biostimulated in-situ to promote the cometabolism of a CAH mixture of 1,1-DCE, 1,1-DCA, and 1,1,1-TCA. The model used kinetic parameter values defined from laboratory experiments. An existing transport model was modified to include inhibition and product toxicity influences on biotransformation.

The most significant contributions of this work included incorporation of inhibition kinetics into the biotransformation/transport model and demonstration of the sensitivity of the model parameters. Overall, comparison to laboratory and field data indicated that there is potential in using this strategy to predict and improve bioremediation strategies. There were, however, many complications that are difficult to explain, and thus continued efforts are needed to provide better model and field demonstrations.

General conclusions of this study are that:

- 1) the enrichment culture was successfully bioaugmented into aquifer groundwater/solid microcosms, showing that it was capable of cometabolically transforming 1,1-DCE, 1,1-DCA, and 1,1,1-TCA with butane as the primary growth substrate.
- 2) the bioaugmented culture in both media and microcosm experiments quickly transformed 1,1-DCE, while 1,1-DCA and 1,1,1-TCA were more slowly transformed. The rates of these latter CAHs increased when butane concentrations were reduced, indicating strong inhibitory effects by butane as shown by Kim et al. (*in press*).
- 3) transformation in microcosms was maintained for up to five cycles of butane and CAH additions over a period of almost 100 days.

- 4) the trends were very reproducible, as observed in dual sets of triplicate bioaugmented microcosms and eight media reactors.
- 5) microcosms that were not bioaugmented (those containing stimulated indigenous microorganisms) showed no ability to transform the CAHs when fed butane, indicating that it was the bioaugmented culture which provided this transformation.
- 6) the biotransformation model could simulate the order of CAH transformation and butane utilization that was observed in laboratory experiments.
- 7) bioaugmentation in the field resulted in successful biotransformation of the CAH mixture when adequate butane and oxygen were delivered to the site. The results were similar to the laboratory observations.
- 8) the combined biotransformation/transport model did a fairly good job in simulating field breakthrough experiments, allowing approximation of flow, dispersion, and sorption occurring within the test zone.
- 9) the combined biotransformation/transport model successfully simulated CAH transformation observed in the field, when adequate butane and oxygen were available.
- 10) when longer butane/oxygen pulsing durations occurred and less butane was injected, the combined model showed that transformation would cease. This is consistent with the field data.
- 11) the combined model showed that returning the injection system to shorter butane/oxygen cycles (allowing more butane being delivered to the site) should have restored transformation of all three CAHs. These results differed from actual field data, in which only 1,1-DCE transformation was restored.
- 12) most likely a change in the microbial profile within the test zone or an extreme 1,1-DCE product toxicity caused the transformation of 1,1-DCA and 1,1,1-TCA not to return.

- 13) inaccuracies of both the Stella and transport models demonstrated the complexity in understanding and simulating combined mechanisms which influence biotransformation.
- 14) the ability of both the Stella and transport models to simulate butane inhibition and the order of CAH transformation suggests that there is great potential in using laboratory studies to understand and improve in situ bioremediation.

Modeling biotransformation observed in the laboratory proved complicated, especially since the initial parameter values used were defined specifically for the culture studied by Kim et al. (*in press*). Although our culture was enriched from this culture, laboratory experiments (such as 1,1-DCE transformation capacity) and necessary model adjustments (such as decay and 1,1,1-TCA transformation capacity) indicated that at least some of these values differed between the cultures. Because of the complexity of the system, it is difficult to know exactly which parameters differed. The interpretation of the data in this study would be simplified had the culture for which independent parameter values had been determined (i.e. Kim's culture) been the same as that studied for cometabolic biotransformation of the CAH mixture.

A major finding, was that a sensitivity analysis using the Stella model allowed simulation of the appropriate order and approximate rate for which transformation and utilization occurred. It is difficult to know why cell mass existing within the reactors at the beginning of each bioaugmentation period appeared to be greater than that predicted by decay within the model. It may have been that decay during the absence of significant butane was in fact less than that expected. It is also possible that other model parameters may have been inaccurate. For example, the transformation capacity may have been set too low, leaving too little biomass remaining.

It is the reproduction of the rates and order that suggests that the model has potential in predicting actual biotransformation data of a CAH mixture. Clearly, though, individual experiments specific to the culture of interest are required to better

define parameter values. Nevertheless, manipulation of the Stella model suggested that using independently defined parameter values to model a complex system is a viable option in predicting and understanding microbial cometabolic behavior.

Similar comments can be said regarding the combined biotransformation and transport model in predicting field experiments. Using the parameter values assigned from the laboratory experiments, the model accurately simulated the trends in transformation and butane and oxygen utilization observed in the field. These results followed those observed within the laboratory reactors, notably rapid transformation of 1,1-DCE followed by butane inhibited transformation of 1,1-DCA and 1,1,1-TCA. 1,1-DCE transformation in the absence of butane quickly inactivated transformation of these latter two CAHs, verifying the extreme product toxicity of 1,1,-DCE.

Complications for modeling the field biotransformation and transport data likely arose from heterogeneity within the aquifer test zone, a change in microbial community during prolonged biostimulation, and perturbations in delivering growth substrate and oxygen. Further complexities for modeling field data exist due to the additional influences of flow and sorption. Such additional intricacies can make trouble-shooting and determining mechanistic behavior quite complicated. Therefore, the use of laboratory data to define parameter input in simulating such mechanisms is a reasonable approach. The successful results in mimicking trends shown in this study support the potential for such extrapolation and call for continued research of this kind.

## BIBLIOGRAPHY

- Alvarez-Cohen, L., McCarty, P.L. 1991. Product Toxicity and Cometabolic Competitive Inhibition Modeling of Chloroform and Trichloroethylene Transformation by Methanotrophic Resting Cells. *Appl. Environ. Microbiol.* **57**:1031-1037.
- Alvarez-Cohen, L., Speitel, G.E. 2001. Kinetics of Aerobic Cometabolism of Chlorinated Solvents. *Biodeg.* **12**:105-126.
- Borden, R.C., Bedient, P.B. 1986. Transport of Dissolved Hydrocarbons Influenced by Oxygen-limited Biodegradation 1. Theoretical Development. *Wat. Res.* **22**(13):1973-1982.
- Broholm, K., Christensen, T. H., Jensen, B. 1992. Modeling TCE Degradation by a Mixed Culture of Methane-Oxidizing Bacteria. *Wat. Res.* **26**(9):1177-1185.
- Change, H.S., Alvarez-Cohen, L. 1995. Model for the Cometabolic Biodegradation of Chlorinated Organics. *EST.* **29**:2357-2367.
- Chang, H.S., Alvarez-Cohen, L. 1996. Biodegradation of Individual and Multiple Chlorinated Aliphatic Hydrocarbons by Methane-Oxidizing Cultures. *Appl. Environ. Microbiol.* **62**(9):3371-3377.
- Chang, W., Criddle, S.C. 1997. Experimental Evaluation of a Model for Cometabolism: Prediction of Simultaneous Degradation of Trichloroethylene and Methane by a Methanotrophic Mixed Culture. *Biotech. Bioeng.* **56**(5):492-501.
- Clement, T.P., Johnson, C.D., Sun, Y., Klecka, G.M., Bartlett, C. 2000. Natural Attenuation of Chlorinated Ethene Compounds: Model Development and Field-Scale Application at the Dover Site. *J. Contam. Hydro.* **42**(2-4):113-140.
- Domenico, P.A., Schwartz, F.W. 1990. *Physical and Chemical Hydrogeology*. John Wiley & Sons, Inc.
- Ely, R.L., Williamson, K.J., Guenther, R.B., Hyman, M.R., Arp, D.J. 1995. A Cometabolic Kinetics Model Incorporating Enzyme Inhibition, Inactivation, and Recovery: I. Model Development, Analysis and Testing. *Biotech. Bioeng.* **46**:218-231.
- Fetter, C.W., 1993. *Contaminant Hydrogeology*. Macmillan Publishing Company, New York.
- Freeze, R.A., Cherry, J.A. 1979. *Groundwater*. Prentice Hall, Inc. Englewood Cliffs, NJ.

## BIBLIOGRAPHY, CONTINUED

- Gossett, J. M. 1987. Measurement of Henry's Law Constants for C1 and C2 Chlorinated Hydrocarbons. *EST.* **21**(2):202-208.
- Hamamura, N., Page, C., Long, T., Semprini, L., Arp, D. 1997. Chloroform Cometabolism by Butane-Grown CF8, *Pseudomonas butanovora*, and *Mycobacterium vaccae* JOB5, and *Methylosinus trichosporium* OB3b. *AEM.* **63**(9): 3607-3613.
- Harmon, T.C., Semprini, L., Roberts, P.V. 1992. Simulating Solute Transport Using Laboratory-Based Sorption parameters. *J. of Enviro. Engr.* **118**(5):666-689.
- Hopkins, G.D., Munakata, J., Semprini, L., McCarty, P.L. 1993. Trichloroethylene Concentration Effects on Pilot Field-Scale In-Situ Groundwater Bioremediation by Phenol-Oxidizing Microorganisms. *EST.* **27**(12):2542-2547.
- Hopkins, G.D., McCarty, P.L. 1995. Field Evaluations of *In Situ* Aerobic Cometabolism of Trichloroethylene and Three Dichloroethylene Isomers Using Phenol and Toluene as the Primary Substrates. *EST.* **29**(6):1628-1637.
- Jitnuyanont, P., Sayavedra-Soto, L., Semprini, L. 2000. Bioaugmentation of Butane-Utilizing Microorganisms to Promote Cometabolism of 1,1,1-Trichloroethane in Groundwater Microcosms. *Biodeg.* **00**: 1-12.
- Kaluarachchi, J.J., Cvetkovic, V., Berglund, S. 2000. Stochastic Analysis of Oxygen- and Nitrate-Based Biodegradation of Hydrocarbons in Aquifers. *J. Contam. Hydro.* **41**(3-4):335-365.
- Keenan, J.E., Strand, S.E., Stensel, H.D. 1994. Degradation Kinetics of Chlorinated Solvents by a Propane Oxidizing Enrichment Culture. *Bioremediation of Chlorinated and Polycyclic Aromatic Hydrocarbon Compounds*. Lewis Publishers, Boca Raton, FL. pgs. 1-13.
- Kim, Y., Semprini, L., Arp, D. 1997. Aerobic Cometabolism of Chloroform and 1,1,1-Trichloroethane by Butane-Grown Microorganisms. *Bioremediation Journal.* **1**(2):135-148.
- Kim, Y. 2000. Aerobic Cometabolism of Chlorinated Aliphatic Hydrocarbons by a Butane-Grown Mixed Culture: Transformation Abilities, Kinetics, and Inhibition. *PhD Dissertation. Oregon State University. Department of Civil, Construction, and Environmental Engineering.*



## BIBLIOGRAPHY, CONTINUED

- Kim, Y., Arp, D., Semprini, L. 2000. Chlorinated Solvent Cometabolism by Butane-Grown Mixed Culture. *J. of Enviro. Engr.* **Oct**: 934-942.
- Kim, Y., Arp, D., Semprini, L. 2002. A Combined Method for Determining Inhibition Type, Kinetic Parameters, and Inhibition Coefficients for Aerobic Cometabolism of 1,1,1-Trichloroethane by a Butane-Grown Mixed Culture. *Biotech. Bioeng.* **77**(5):564-576.
- Kim, Y., Arp, D., Semprini, L. *in press*. Kinetic and Inhibition Studies for the Aerobic Cometabolism of 1,1,1-Trichloroethane, 1,1-Dichloroethylene, and 1,1-Dichloroethane by a Butane-Grown Mixed Culture. *Biotech. Bioeng.*
- Kindred, J.S., Celia, M.A. 1989. Contaminant Transport and Biodegradation 2. Conceptual Model and Test Simulations. *Wat. Res.* **25**(6): 1149-1159.
- Lee, S.B., Strand, S.E, Stensel, H.D. 2000. Sustained Degradation of Trichloroethylene in a Suspended Growth Gas Treatment Reactor by an Actinomycetes Enrichment. *EST.* **34**(15):3261-3268.
- Mackay and Shiu, 1981. Review of Henry's Law Constants for Chemicals of Environmental Interest. *J. Phys. Chem. Ref. Data*, **10**(4):1175-1199.
- MacQuarrie, K.T.B., Sudicky, E.A., Frind, E.O. 1990. Simulation of Biodegradable Organic Contaminants in Groundwater 1. Numerical Formulation in Principal Directions. *Wat. Res.* **26**(2):207-222.
- Material Safety Data Sheets (MSDS), 2001. Chemical and Other Safety Information. The Physical and Theoretical Chemistry Laboratory. Oxford University. <http://physchem.ox.ac.uk/MSDS/>
- McCarty, P.L., Goltz, M.N., Hopkins, G.D., Dolan, M.E., Allan, J.P., Kawakami, B.T., Carrothers, T.J. 1998. Full-Scale Evaluation of *In Situ* Cometabolic Degradation of Trichloroethylene in Groundwater through Toluene Injection. *EST.* **32**(1):88-100.
- Rittmann, B.E, McCarty, P.L. 2001. Environmental Biotechnology: Principles and Applications. *McGraw-Hill Companies, Inc. New York City, NY.*
- Rungakamol, D. 2001. Aerobic Cometabolism of 1,1,1-Trichloroethane and Other Chlorinated Aliphatic Hydrocarbons by Indigenous and Bioaugmented Butane-Utilizers in Moffett Field Microcosms. *Masters Thesis. Oregon State University. Department of Civil, Construction, and Environmental Engineering.*

## BIBLIOGRAPHY, CONTINUED

- Schäfer, D., Schäfer, W., Kinzelback, W. 1998. Simulation of Reactive Processes Related to Biodegradation in Aquifers 1. Structure of the Three-Dimensional Reactive Transport Model. *J. Cont. Hydro.* **31**:167-186.
- Semprini, L., McCarty, P.L. 1991. Comparison between Model Simulations and Field Results for In-Situ Bioremediation of Chlorinated Aliphatics: Part 1. Biostimulation of Methanotrophic Bacteria. *Ground Water*. **29**(3):365-374.
- Semprini, L., McCarty, P.L. 1992. Comparison between Model Simulations and Field Results for In-Situ Bioremediation of Chlorinated Aliphatics: Part 2. Cometabolic Transformations. *Ground Water*. **30**(1):37-44.
- Shim, H., Ryoo, D., Barbieri, P., Wood, T.K. 2001. Aerobic Degradation of Mixtures of Tetrachloroethylene, Trichloroethylene, Dichloroethylenes, and Vinyl Chloride by Toluene-*o*-Xylene Monooxygenase of *Pseudomonas stutzeri* OX1. *Appl. Microbiol. Biotechnol.* **56**:265-269.
- Sipkema, E. M., de Koning, W., Klaassien, J.G., Janseen, D.B., Antonie A.C.M.B. 2000. NADH-Regulated Metabolic Model for Growth of *Methylosinus trichosporium* OB3b. Model Presentation, Parameter Estimation, and Model Validation. *Biotechnol. Prog.* **16**(2):176-188.
- Squillace, P.J., Scott, J.C., Moran, M.J., Nolan, B.T., Kolpin, D.W. 2002. VOCs, Pesticides, Nitrate, and their Mixtures in Groundwater Used for Drinking Water in the United States. *EST.* **36**(9):1923-1930.
- Strand, S.E., Bjelland, M., Stensel, H.D. 1990. Kinetics of Chlorinated Hydrocarbon Degradation by Suspended Cultures of Methane-Oxidizing Bacteria. *Res. J. Water Pollut. Control Fed.* **62**:124-129.
- Sun, Y., Petersen, J.N., Clement, T.P., Hooker, B.S. 1998. Effect of Reaction Kinetics on Predicted Concentration Profiles during Subsurface Bioremediation. *J. Cont. Hydro.* **31**:359-372.
- Unice, K.M., Logan, B.E. 2000. Insignificant role of Hydrodynamic Dispersion on Bacterial Transport. *Jour. Enviro. Engr.* **126**(6):491-500.
- United States Environmental Protection Agency (EPA). 1990. Office of Research and Development. Basics of Pump-and-Treat Ground-Water Remediation Technology. Document #: EPA-600/8-90/003.

## BIBLIOGRAPHY, CONTINUED

United States Environmental Protection Agency (EPA). 2001. Integrated Risk Information System (IRIS). [www.epa.gov/iris/](http://www.epa.gov/iris/)

United States Geological Survey. 1998. Modeling Solute-Transport and Biodegradation with BIOMOC. *USGS Fact Sheet*. **095-98**.

Vogel, T., McCarty, P.L., 1987. Abiotic and Biotic Transformations of 1,1,1-Trichloroethane under Methanogenic Conditions. *EST*. **21**(12):1208-1213.

Waddill, D.W., Widdowson, M.A. 1998. Three-Dimensional Model for Subsurface Transport and Biodegradation. *J. Enviro. Engr.* **124**(4):336-344.

Westrick, J.J., Mello, J.W., Thomas, R.F. 1984. The Groundwater Supply Survey. *AWWA*. **76**:52-59.

## APPENDICES

APPENDIX A  
NOMENCLATURE AND UNITS FOR  
BIOTRANSFORMATION/TRANSPORT MODEL

A.1 MASSES AND CONCENTRATIONS

ED = electron donor (butane)

EA = electron acceptor (oxygen)

$C_D$  = aqueous concentrations of butane; mg /L

$C_A$  = aqueous concentration of oxygen; mg /L

$C_{DCE}$  = aqueous concentration of 1,1-DCE; mg /L

$C_{DCE}^*$  = sorbed phase concentration of 1,1-DCE; mg DCE/kg soil

$C_{DCA}$  = aqueous concentration of 1,1-DCA; mg /L

$C_{DCA}^*$  = sorbed phase concentration of 1,1-DCA; mg DCA/kg soil

$C_{TCA}$  = aqueous concentration of 1,1,1-TCA; mg /L

$C_{TCA}^*$  = sorbed phase concentration of 1,1,1-TCA; mg TCA/kg soil

$X$  = aqueous concentration of cells; mg/L

$X_0$  = initial aqueous concentration of cells; mg/L

A.2 OXYGEN CONSUMPTION PARAMETERS

$F_a$  = stoichiometric ratio of electron acceptor per electron donor utilized for cell synthesis; mg EA/mg ED

$d_c$  = cell decay oxygen demand; mg  $O_2$ /mg cells

$f_d$  = fraction of biodegradable cells

A.3 KINETIC PARAMETERS

$Y$  = cell yield; mg cells/mg butane

$b$  = cell decay coefficient; day<sup>-1</sup>

$k_{mD}$  = maximum utilization rate of butane; mg butane/mg cells/day

APPENDIX A, CONTINUED  
NOMENCLATURE AND UNITS FOR  
BIOTRANSFORMATION/TRANSPORT MODEL

$K_{sD}$  = half-saturation constant of butane; mg butane/L

$K_{sA}$  = half-saturation constant of oxygen; mg  $O_2$ /L

$k_{mDCE}$  = maximum utilization rate of 1,1-DCE; mg DCE/mg cells/day

$K_{sDCE}$  = half-saturation constant of 1,1-DCE; mg DCE/L

$k_{mDCA}$  = maximum utilization rate of 1,1-DCA; mg DCA/mg cells/day

$K_{sDCA}$  = half-saturation constant of 1,1-DCA; mg DCA/L

$k_{mTCA}$  = maximum utilization rate of 1,1,1-TCA; mg TCA/mg cells/day

$K_{sTCA}$  = half-saturation constant of 1,1,1-TCA; mg TCA/L

#### A.4 INHIBITION CONSTANTS

$K_{lu,BUT,DCE}$  = constant for noncompetitive inhibition of 1,1-DCE by butane;  
mg butane/L

$K_{lc,BUT,DCE}$  = constant for competitive inhibition of 1,1-DCE by butane;  
mg butane/L

$K_{lc,DCA,DCE}$  = constant for competitive inhibition of 1,1-DCE by 1,1-DCA;  
mg DCA/L

$K_{lc,TCA,DCE}$  = constant for competitive inhibition of 1,1-DCE by 1,1,1-TCA;  
mg TCA/L

$K_{lu,BUT,DCA}$  = constant for noncompetitive inhibition of 1,1-DCA by butane;  
mg butane/L

$K_{lc,DCE,DCA}$  = constant for competitive inhibition of 1,1-DCA by 1,1-DCE;  
mg DCE/L

$K_{lc,DCE,DCA}$  = constant for competitive inhibition of 1,1-DCA by 1,1,1-TCA;  
mg TCA/L

APPENDIX A, CONTINUED  
NOMENCLATURE AND UNITS FOR  
BIOTRANSFORMATION/TRANSPORT MODEL

$K_{Iu,BUT,DCA}$  = constant for noncompetitive inhibition of 1,1,1-TCA by butane; mg butane/L

$K_{Ic,DCA,TCA}$  = constant for noncompetitive inhibition of 1,1,1-TCA by 1,1-DCA; mg DCA/L

$K_{Ic,DCE,TCA}$  = constant for competitive inhibition of 1,1,1-TCA by 1,1-DCE; mg DCE/L

$K_{Ic,DCE,BUT}$  = constant for competitive inhibition of butane by 1,1-DCE; mg DCE/L

$K_{Ic,DCA,BUT}$  = constant for competitive inhibition of butane by 1,1-DCA; mg DCA/L

$K_{Ic,TCA,BUT}$  = constant for competitive inhibition of butane by 1,1,1-TCA; mg TCA/L

#### A.5 PRODUCT TOXICITY PARAMETERS

$Tc_{DCE}$  = transformation capacity of 1,1-DCE; mg DCE/mg cells

$Tc_{DCA}$  = transformation capacity of 1,1-DCA; mg DCA/mg cells

$Tc_{TCA}$  = transformation capacity of 1,1-TCA; mg TCA/mg cells

#### A.6 TRANSPORT PARAMETERS

$Q$  = average groundwater flow;  $m^3/day$

$D_h$  = hydrodynamic dispersion coefficient;  $m^2/day$

$\phi$  = aquifer porosity

$\rho_b$  = bulk density of the aquifer solids; kg/L

$k_{dDCE}$  = 1,1-DCE partition coeff. between aq. and sorbed phases; L/kg

$k_{dDCA}$  = 1,1-DCA partition coeff. between aq. and sorbed phases; L/kg

APPENDIX A, CONTINUED  
NOMENCLATURE AND UNITS FOR  
BIOTRANSFORMATION/TRANSPORT MODEL

$k_{dTCA}$  = 1,1,1-TCA partition coefficient between aq. and sorbed phases;

L/kg

$F_{kDCE}$  = 1,1-DCE rate coeff. for mass transfer between aq. and sorbed phases;

day<sup>-1</sup>

$F_{kDCA}$  = 1,1-DCA rate coeff. for mass transfer between aq. and sorbed phases;

day<sup>-1</sup>

$F_{kTCA}$  = 1,1,1-TCA rate coeff. for mass transfer between aq. and sorbed phases;

day<sup>-1</sup>



## APPENDIX B

### STELLA BIOTRANSFORMATION MODEL FOR BATCH REACTORS

The model introduced by Kim et al. (in press) allowed for simulation of cometabolic biotransformation within a reactor. Butane, the three CAHs, and microbial mass were tracked over time in a liquid/headspace batch reactor system. Because mass transfer of a compound may occur between the liquid and gas within a batch system, mass balances between the phases must be included to calculate total mass consumed for any time period. The following equations, therefore, take on a similar form to those presented in Chapter 2, with masses being determined rather than aqueous concentrations.

Another difference between the Stella biotransformation model and the transport code defined in Chapter 2 includes the omission of mixed inhibition of CAHs on butane and other CAHs in the Stella code. The Stella model also assumes that oxygen is adequately available. Nomenclature and units are provided in Appendix C. The equations are solved simultaneously for a specified time interval to determine mass of each compound and cell concentration within the reactor at any time.

APPENDIX B, CONTINUED  
STELLA BIOTRANSFORMATION MODEL FOR BATCH REACTORS

### B.1 BUTANE UTILIZATION

The primary growth substrate for this model follows that presented in equation 2.13 (Section 2.3), omitting the influence of the electron acceptor and transport. Butane utilization is calculated assuming that biotic reactions occur only in the aqueous phase. The rate of butane mass utilized is defined as:

$$\frac{dM_{BUT}}{dt} = -Xk_{mBUT}V_L^* \quad (B.1)$$

$$\left( \frac{C_{BUT}}{K_{sBUT} \left( 1 + \frac{C_{DCE}}{K_{Ic,DCE,BUT}} + \frac{C_{DCA}}{K_{Ic,DCA,BUT}} + \frac{C_{TCA}}{K_{Ic,TCA,BUT}} \right) + C_{BUT}} \right)$$

Total mass of any compound is related to the aqueous concentration by a mass balance between the gaseous and aqueous phases (Appendix C):

$$C_L = M / (HccV_G + V_L) \quad (B.2)$$

APPENDIX B, CONTINUED  
STELLA BIOTRANSFORMATION MODEL FOR BATCH REACTORS

Rearranging equation B.2 and substituting in a term for the Henry's constant and volumes, the aqueous concentration can be calculated:

$$C_L = M\alpha \quad (\text{B.3})$$

$$\text{where: } \alpha = (V_L + V_G H_{cc})^{-1} \quad (\text{B.4})$$

Equation B.3 is substituted into equation B.1 to determine butane utilization. Total mass is converted from  $\mu\text{mol}$  to  $\text{mg}$  using the molecular weight of each compound (Table 1.1, Section 1.2) for comparing model output to laboratory data.

## B.2 TRANSFORMATION OF CAHs

Transformation of 1,1-DCE, 1,1,-DCA, and 1,1,1-TCA are calculated similar to that described for butane utilization. The mass consumed over time follows equation 2.15 (Section 2.3), omitting the terms for transport and oxygen utilization. Partitioning between the aqueous and gaseous phases is included in determining mass lost over a specific time interval. All transformation is assumed to occur in the liquid within the reactor:

APPENDIX B, CONTINUED  
STELLA BIOTRANSFORMATION MODEL FOR BATCH REACTORS

$$\frac{dM_1}{dt} = -XV_L \left( \frac{k_{m1}}{1 + C_{BUT}/K_{lu,BUT,1}} \right) * \left( \frac{C_1}{\frac{K_{s1}}{1 + C_{BUT}/K_{lu,BUT,1}} \left( 1 + C_{BUT}/K_{lc,BUT,1} + C_2/K_{lc,2,1} + C_3/K_{lc,3,1} \right) + C_1} \right) \quad (B.5)$$

where:  $M_1$  = mass of compound being transformed ( $\mu\text{g}$ )

other parameters as defined for equation 2.15 (Section 2.3)

Equation B.3 is substituted into equation B.5 to account for partitioning.

### B.3 MICROBIAL GROWTH AND DECAY

The concentration of cells grown and lost over a specific time interval is a function of cell yield, decay, and product toxicity. All reactions are assumed to occur in the aqueous phase.

$$\frac{dX}{dt} = Y \frac{dM_{BUT}}{dt} \frac{1}{V_L} - bX - \frac{1}{V_L} \left( \frac{1}{T_{cDCE}} \frac{dM_{DCE}}{dt} + \frac{1}{T_{cDCA}} \frac{dM_{DCA}}{dt} + \frac{1}{T_{cTCA}} \frac{dM_{TCA}}{dt} \right) \quad (B.6)$$

APPENDIX C  
NOMENCLATURE AND UNITS FOR  
STELLA BIOTRANSFORMATION MODEL

C.1 MASSES AND CONCENTRATIONS

$M_{\text{BUT}}$  = total mass of butane;  $\mu\text{mol}$

$M_{\text{DCE}}$  = total mass of 1,1-DCE;  $\mu\text{mol}$

$M_{\text{DCA}}$  = total mass of 1,1-DCA;  $\mu\text{mol}$

$M_{\text{TCA}}$  = total mass of 1,1,1-TCA;  $\mu\text{mol}$

$C_{\text{D}}$  = aqueous concentrations of butane;  $\mu\text{mol /L}$

$C_{\text{DCE}}$  = aqueous concentration of 1,1-DCE;  $\mu\text{mol /L}$

$C_{\text{DCA}}$  = aqueous concentration of 1,1-DCA;  $\mu\text{mol /L}$

$C_{\text{TCA}}$  = aqueous concentration of 1,1,1-TCA;  $\mu\text{mol /L}$

$X$  = aqueous concentration of cells;  $\text{mg/L}$

$X_0$  = initial aqueous concentration of cells;  $\text{mg/L}$

C.2 KINETIC PARAMETERS

$Y$  = cell yield;  $\text{mg cells}/\mu\text{mol butane}$

$b$  = cell decay coefficient;  $\text{hr}^{-1}$

$k_{\text{mD}}$  = maximum utilization rate of butane;  $\mu\text{mol butane}/\text{mg cells}/\text{hr}$

$K_{\text{sD}}$  = half-saturation constant of butane;  $\mu\text{mol butane/L}$

$k_{\text{mDCE}}$  = maximum utilization rate of 1,1-DCE;  $\mu\text{mol DCE}/\text{mg cells}/\text{hr}$

$K_{\text{sDCE}}$  = half-saturation constant of 1,1-DCE;  $\mu\text{mol DCE/L}$

$k_{\text{mDCA}}$  = maximum utilization rate of 1,1-DCA;  $\mu\text{mol DCA}/\text{mg cells}/\text{hr}$

$K_{\text{sDCA}}$  = half-saturation constant of 1,1-DCA;  $\mu\text{mol DCA/L}$

$k_{\text{mTCA}}$  = maximum utilization rate of 1,1,1-TCA;  $\mu\text{mol TCA}/\text{mg cells}/\text{hr}$

$K_{\text{sTCA}}$  = half-saturation constant of 1,1,1-TCA;  $\mu\text{mol TCA/L}$

APPENDIX C, CONTINUED  
NOMENCLATURE AND UNITS FOR  
STELLA BIOTRANSFORMATION MODEL

C.3 INHIBITION CONSTANTS

$K_{Iu,BUT,DCE}$  = constant for noncompetitive inhibition of 1,1-DCE by butane;  
 $\mu\text{mol butane/L}$

$K_{Ic,BUT,DCE}$  = constant for competitive inhibition of 1,1-DCE by butane;  
 $\mu\text{mol butane/L}$

$K_{Ic,DCA,DCE}$  = constant for competitive inhibition of 1,1-DCE by 1,1-DCA;  
 $\mu\text{mol DCA/L}$

$K_{Ic,TCA,DCE}$  = constant for competitive inhibition of 1,1-DCE by 1,1,1-TCA;  
 $\mu\text{mol TCA/L}$

$K_{Iu,BUT,DCA}$  = constant for noncompetitive inhibition of 1,1-DCA by butane;  
 $\mu\text{mol butane/L}$

$K_{Ic,DCE,DCA}$  = constant for competitive inhibition of 1,1-DCA by 1,1-DCE;  
 $\mu\text{mol DCE/L}$

$K_{Ic,TCA,DCA}$  = constant for competitive inhibition of 1,1-DCA by 1,1,1-TCA;  
 $\mu\text{mol TCA/L}$

$K_{Iu,BUT,TCA}$  = constant for noncompetitive inhibition of 1,1,1-TCA by  
butane;  $\mu\text{mol butane/L}$

$K_{Ic,DCE,TCA}$  = constant for competitive inhibition of 1,1,1-TCA by 1,1-DCE;  
 $\mu\text{mol DCE/L}$

$K_{Ic,DCA,TCA}$  = constant for competitive inhibition of 1,1,1-TCA by 1,1-DCA;  
 $\mu\text{mol DCA/L}$

$K_{Ic,DCE,BUT}$  = constant for competitive inhibition of butane by 1,1-DCE;  
 $\mu\text{mol DCE/L}$

APPENDIX C, CONTINUED  
NOMENCLATURE AND UNITS FOR  
STELLA BIOTRANSFORMATION MODEL

$K_{Ic,DCA,BUT}$  = constant for competitive inhibition of butane by 1,1-DCA;  
 $\mu\text{mol DCA/L}$

$K_{Ic,TCA,BUT}$  = constant for competitive inhibition of butane by 1,1,1-TCA;  
 $\mu\text{mol TCA/L}$

C.4 PRODUCT TOXICITY PARAMETERS

$T_{cDCE}$  = transformation capacity of 1,1-DCE;  $\mu\text{mol DCE/mg cells}$

$T_{cDCA}$  = transformation capacity of 1,1-DCA;  $\mu\text{mol DCA/mg cells}$

$T_{cTCA}$  = transformation capacity of 1,1-TCA;  $\mu\text{mol TCA/mg cells}$

C.5 MASS TRANSFER PARAMETERS FOR AQUEOUS TO GASEOUS PHASES

$V_L$  = volume of liquid in reactor; L

$V_G$  = volume of gas in reactor; L

$H_{ccBUT}$  = dimensionless Henry's constant for partitioning of butane  
between aqueous and gaseous phases

$H_{ccDCE}$  = dimensionless Henry's constant for partitioning of 1,1-DCE  
between aqueous and gaseous phases

$H_{ccDCA}$  = dimensionless Henry's constant for partitioning of 1,1-DCA  
between aqueous and gaseous phases

$H_{ccTCA}$  = dimensionless Henry's constant for partitioning of 1,1-TCA  
between aqueous and gaseous phases

APPENDIX D  
MOFFETT FIELD SOIL CORES USED FOR MICROCOSMS

Core material was taken from Moffett Field Test Facility, CA and refrigerated until used. Table D.1 provides the specific locations from which the samples were obtained.

**Table D.1 Core Material used in Microcosms**

Location	Depth (ft)
SU39 – PP2	15.5-16
SU39 – PP5	16-16.5
SU39 – PP6	15-15.5
SU39 - FP2	15.5-16
SU39 - FP3	14.5-15
SU39 - FP3	16-16.5
SU39 - 17	15.5-16
SU39 - 17	17.5-18



## APPENDIX E

### DERIVATION OF MASS TRANSFER OF VOLATIVE COMPOUNDS IN A BATCH REACTOR

In a batch reactor, volatile compounds will partition between aqueous and gaseous phases. At equilibrium conditions, the mass balance for both phases representing total mass in the reactor are defined by:

$$M = C_G V_G + C_L V_L \quad (E.1)$$

where: M = total mass in reactor

$C_G$  = concentration in gaseous phase

$V_G$  = gaseous volume in reactor

$C_L$  = Concentration in liquid phase

$V_L$  = liquid volume in reactor

Gaseous and aqueous concentrations are related by Henry's constant,  $H_{cc}$ :

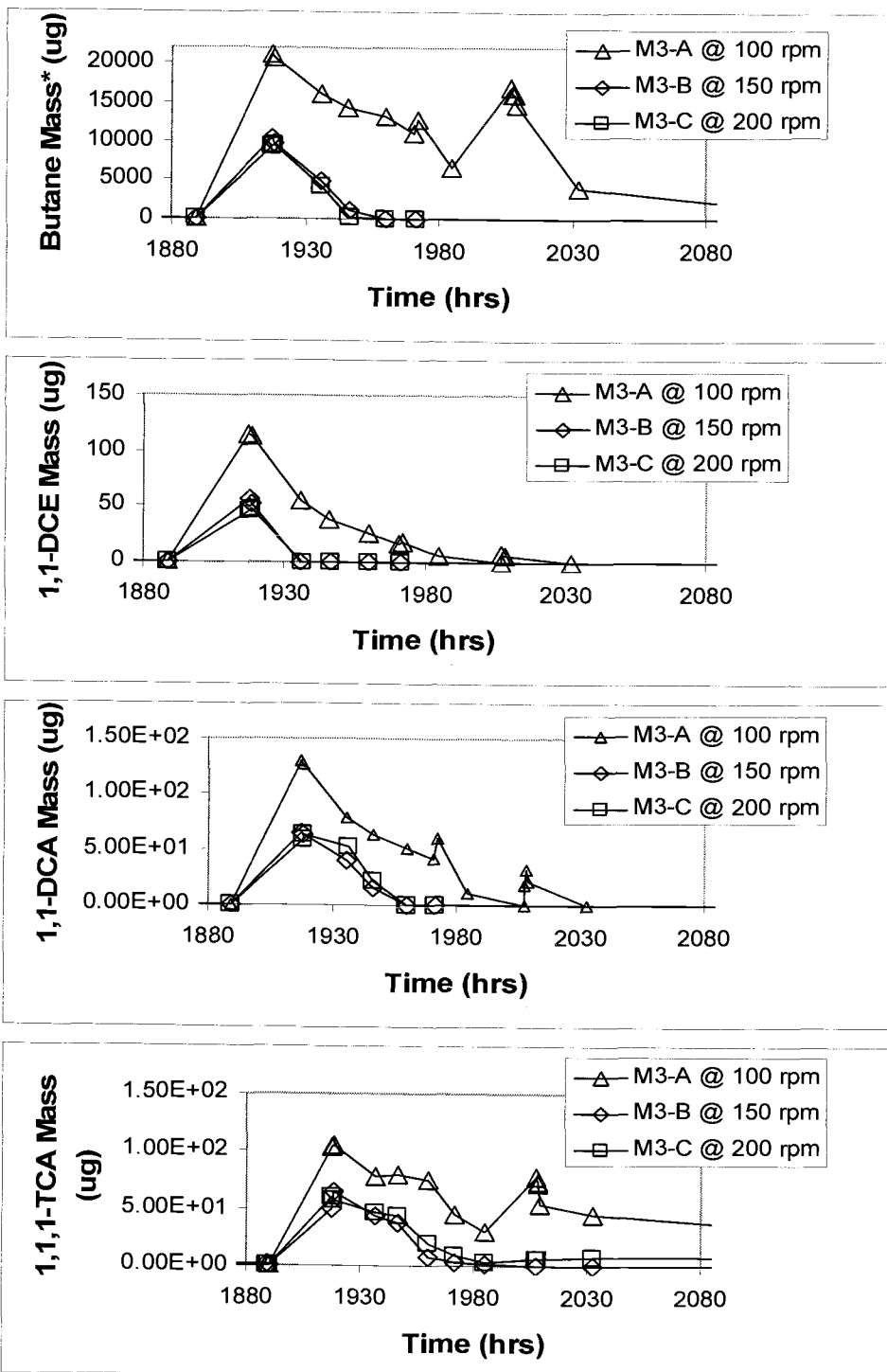
$$H_{cc} = C_G / C_L \quad C_G = H_{cc} C_L \quad C_L = C_G / H_{cc} \quad (E.2)$$

Substituting this relationship into equation C.1, the mass balance becomes:

$$M = C_L (H_{cc} V_G + V_L) \quad (E.3) \quad M = C_G (V_G + V_L / H_{cc}) \quad (E.4)$$

The relationships allowed for comparison of laboratory data and simulation output. Simulations using Kim et al.'s (2000) model made use of equations E.3 and E.4 to track total mass with partitioning. Laboratory data was converted from gaseous concentrations to total mass using equation E.4.

# APPENDIX F MASS TRANSFER LIMITATION IN M3 MICROCOSMS



\*Butane is reported as mass in the gaseous phase of the reactor.

## APPENDIX G MASS TRANSFER LIMITATION MODEL

Kim et al. (2000) derived the following equations to describe mass transfer limitation between the aqueous and gaseous phases of a compound within a reactor:

$$\frac{dS_G}{dt} = -K_{La} \left( \frac{S_G}{H_{cc}} - \frac{M_s}{V_L} + \frac{S_G V_G}{V_L} \right) \frac{V_L}{V_G} \quad (\text{G.1})$$

$$\frac{dS_L}{dt} = -K_{Ga} \left( H_{cc} S_L - \frac{M_s}{V_G} + \frac{S_L V_L}{V_G} \right) \frac{V_G}{V_L} \quad (\text{G.2})$$

where:  $S_G$  = gaseous conc. of substrate ( $\mu\text{mol/L}$ )

$S_L$  = aqueous conc. of substrate ( $\mu\text{mol/L}$ )

$M_s$  = total mass of substrate in aqueous and gaseous phases ( $\mu\text{mol}$ )

$V_L$  = aqueous volume (L)

$V_G$  = gaseous volume (L)

$K_{La}$  = mass transfer rate coeff. from gaseous to liquid phase ( $\text{hr}^{-1}$ )

$K_{Ga}$  = mass transfer rate coeff. from liquid to gaseous phase ( $\text{hr}^{-1}$ )

$H_{cc}$  = dimensionless Henry's constant of substrate

Equation G.2 was incorporated into equation B.1 (Appendix B) for early simulations of our culture's biotransformation behavior. The resulting equation for butane utilization with mass transfer limitation is:

APPENDIX G, CONTINUED  
MASS TRANSFER LIMITATION MODEL

$$\frac{dM_{BUT}}{dt} = -Xk_{mBUT}V_L \quad (G.3)$$

$$\left( \frac{C_{BUT}}{K_{sBUT} \left( 1 + \frac{C_{DCE}}{K_{lc,DCE,BUT}} + \frac{C_{DCA}}{K_{lc,DCA,BUT}} + \frac{C_{TCA}}{K_{lc,TCA,BUT}} \right) + C_{BUT}} \right) - K_{Ga} \left( H_{ccBUT} C_{BUT} - \frac{M_B}{V_G} + \frac{C_{BUT} V_L}{V_G} \right) \frac{V_G}{V_L}$$

where:  $K_{Ga}$  = mass transfer rate coeff. for gaseous to liquid phase ( $\text{hr}^{-1}$ )

other parameters as defined in Appendix C

As with equation B.1, a mass balance is incorporated into equation G.3 to relate total mass between the aqueous and gaseous phases of the reactor to the aqueous concentration. The relationship is:

$$C_L = M\alpha \quad (G.4)$$

$$\text{where: } \alpha = (V_L + V_G H_{cc})^{-1} \quad (G.5)$$

Equation G.4 is substituted into equation G.3 to determine butane utilization on a total mass basis. Total mass is converted from  $\mu\text{mol}$  to  $\text{mg}$  using the molecular weight of each compound (Table 1.1, Section 1.2) for comparing model output to laboratory data.

# APPENDIX H BIOTRANSFORMATION/TRANSPORT MODEL INPUT FOR FLOW (Q) DETERMINATION

**Table H.1 Input Values for Flow Determination at S1 (1m)**

Solute Transport and Degradation Model									
Input Parameters Listing									
Flow Determination @ S1									
			ED	Bromide					
			CAH#1	-					
			CAH#2	-					
LINE #									
1	DHI	QLI							
	m2/d	m3/d							
	0.31	1							
2	PORI	THICK	WIDTH						
	-	m	m						
	0.333	1.5	1						
3	IMAX	NSTOP	NT	HT	XMAX				
	# spatial nodes	iteration	ec. iteration	d/iteration	tot dist				
	25	33330	15	0.0003	2.4				
4	CPSD1	CPSD2	CPSA1	CPSA2	CPD2	CPD3	CPD4	CPD5	
	mg/l	mg/l	mg/l	mg/l	mg/l	mg/l	mg/l	mg/l	
	0	150	0	150	150	150	150	150	
5	DENB	FK	KD	WELRAD					
	kg/L		L/kg	m					
	1.6	200	0.69	1					
6	CXAI	K	KSD	KSA	K2	KS2			
	mg/l	mg/mg-d	mg/l	mg/l	mg/mg-d	mg/l			
	0	0	3.48	1	6.5	0.14			
7	K22	KD2	FK2	KS22					
	mg/mg-d	L/kg		mg/l					
	0.64	0.5	200	1.63					
8	KHAL								
	mg/l								
	800								
9	Y	YE	B	BI	TC	TC2			
	mg cells/mg l	e c/e d	1/d	1/d	mg/mg	mg/mg			
	0.790	0.5	0	0.1	0.0504	0.11			
10	D	FD	CDOD						
	g ea/g ed :tn degra cej ea/g cells								
	4	0.8	1.42						
11	IRAD	ICON	IPRINT	IDBRK	ICXAI				
	radial coord?		print data?	ode for ru	mg/L				
	2	2	1	11	0				
12	PT0	PT1	PT2	PT3	PULSE1	PULSE2	PULSE3	PULSE4	PULSE5
	days of pulsing cycles				days: 1st pulse=>1st pulse time, 2nd pulse=> 2nd pulse time				
					T<PT0				
	10	31	31	31	10	10	10	10	10
13	CS2PI0	CS2PI1	CS2PI2	CS2PI3	CS2PI4	CS2PI5			
	Initial Conc in Aquifer 2nd Inj C1 1st Inj C1 3rd Inj C1 Initial C1 in Aquifer								
	mg/l	mg/l	mg/l	mg/l	mg/l	mg/l			
	0	0	0	0	0	0			
14	CS2PI3	CS2PI4							
	mg/l	mg/l							
	4th Inj C1	5th Inj C1							
	0	0							
15	PS1	PS2	PS3	PS4	PS5				
	d	d	d	d	d				
	21	40	41	42	43				
16	PS21	PS22	PS23						
	d	d	d						
	21	40	41						
17	CS22PI	CS22PI0	CS22PI1	CS22PI2	CS22PI3				
	mg/l	mg/l	mg/l	mg/l	mg/l				
	C2 in Aquifer 1st Inj C2 2nd Inj C2 3rd Inj C2 4th Inj C2								
	mg/l	mg/l	mg/l	mg/l	mg/l				
	0	0	0	0	0				
18	KIC1D	KIC2D	KIU1D	KIU2D	KICD1	KIC21			
	Inhibition of former on latter								
	mg/L	mg/L	mg/L	mg/L	mg/L	mg/L			
	0.843	41.786	800	800	0.019	2.27			
19	KIUD1	KIUD2	KIUD3	KIUD4	KIUD5				
	mg/L	mg/L	mg/L	mg/L	mg/L	mg/L			
	0.4002	800	800	0.107	0.029	800			

Input data for modeling flow in Figure 5.3 (Section 5.2)

# APPENDIX H, CONTINUED BIOTRANSFORMATION/TRANSPORT MODEL INPUT FOR FLOW (Q) DETERMINATION

**Table H.2 Input Values for Flow Determination at S3 (4m)**

Solute Transport and Degradation Model Input Parameters Listing Flow Determination @ S3									
				ED	Bromide				
				CAH#1	-				
				CAH#2	-				
LINE #									
1	DHI	QLI							
	m2/d	m3/d							
	0.31	1.5							
2	PORI	THICK	WIDTH						
	-	m	m						
	0.333	1.5	1						
3	IMAX	NSTOP	NT	HT	XMAX				
	# spatial nodes	iterations	iteration d/iteration	tot dist					
	25	33330	15	0.0003	8				
4	CPSD1	CPSD2	CPSA1	CPSA2	CPD2	CPD3	CPD4	CPD5	
	mg/l	mg/l	mg/l	mg/l	mg/l	mg/l	mg/l	mg/l	
	0	150	0	0	150	150	150	150	
5	DENB	FK	KD	WELRAD					
	kg/L		L/kg	m					
	1.6	200	0.68	1					
6	CXAI	K	KSD	KSA	K2	KS2			
	mg/l	mg/mg-d	mg/l	mg/l	mg/mg-d	mg/l			
	0	0	3.48	1	6.5	0.14			
7	K22	KD2	FK2	KS22					
	mg/mg-d	L/kg		mg/l					
	0.64	0.5	200	1.63					
8	KHAL								
	mg/l								
	800								
9	Y	YE	B	BI	TC	TC2			
	mg cells/mg	e c/e d	1/d	1/d	mg/mg	mg/mg			
	0.790	0.5	0	0.1	0.0504	0.11			
10	D	FD	CDOD						
	g ea/g ed :tn degra	g ea/g cells							
	4	0.8	1.42						
11	IRAD	ICON	IPRINT	IDBRK	ICXAI				
	radial coord?		print data?	ode for ru	mg/L				
	2	2	1	17	0				
12	PT0	PT1	PT2	PT3	PULSE1	PULSE2	PULSE3	PULSE4	PULSE5
	days of pulsing	cyles			days: 1st pulse=>1st pulse time, 2nd pulse=> 2nd pulse time				
					T<PT0		T<PT1		T<PT2
	10	31	31	31	10	10	10	10	10
13	CS2PI0	CS2PI1	CS2PI2	CS2PI3	CS2PI4	CS2PI5			
	Initial Conc in Aquifer	2nd Inj C1	1st Inj C1	3rd Inj C1	Initial C1 in Aquifer				
	mg/l	mg/l	mg/l	mg/l	mg/l				
	0	0	0	0	0				
14	CS2PI3	CS2PI4							
	mg/l	mg/l							
	4th Inj C1	5th Inj C1							
	0	0							
15	PS1	PS2	PS3	PS4	PS5				
	d	d	d	d	d				
	21	40	41	42	43				
16	PS21	PS22	PS23						
	d	d	d						
	21	40	41						
17	CS22PI1	CS22PI2	CS22PI3	CS22PI4	CS22PI5				
	mg/l	mg/l	mg/l	mg/l	mg/l				
	C2 in Aquifer	1st Inj C2	2nd Inj C2	3rd Inj C2	4th Inj C2				
	0	0	0	0	0				
18	KIC1D	KIC2D	KIU1D	KIU2D	KICD1	KIC21			
	Inhibition of former on latter								
	mg/L	mg/L	mg/L	mg/L	mg/L	mg/L			
	0.843	41.786	800	800	0.019	2.27			
19	KIUD1	KIUD2	KICD1	KIUD1	KIUD2	KIUD3			
	mg/L	mg/L	mg/L	mg/L	mg/L	mg/L			
	0.4002	800	800	0.107	0.029	800			

Input data for modeling flow in Figure 5.3 (Section 5.2)

# APPENDIX I BIOTRANSFORMATION/TRANSPORT MODEL INPUT FOR MASS TRANSFER RATE COEFF. DETERMINATION ( $F_k$ )

**Table I.1 Input Values for  $F_k$  at S1 (1m)**

Solute Transport and Degradation Model											
Input Parameters Listing											
Fk Determination @ S1											
ED											
CAH#1 DCE											
CAH#2 TCA											
LINE #											
1	DHI	QLI									
	m2/d	m3/d									
	0.31	1									
2	PORI	THICK	WIDTH								
	-	m	m								
	0.333	1.5	1								
3	IMAX	NSTOP	NT	HT	XMAX						
#	spatial nodes	iterations	sec. iteration	d/iteration	tot dist						
	25	33330	15	0.0003	2.4						
4	CPSD1	CPSD2	CPSA1	CPSA2	CPD2	CPD3	CPD4	CPD5	CPA3	CAP2	CPA3
	mg/l	mg/l	mg/l	mg/l	mg/l	mg/l	mg/l	mg/l	mg/l	mg/l	mg/l
	0	0	0	0	0	0	0	0	0	0	0
5	DENB	FK	KD	WELRAD							
	kg/L		L/kg	m							
	1.8	2	0.69	1							
6	CXAI	K	KSD	KSA	K2	KS2					
	mg/l	mg/mg-d	mg/l	mg/l	mg/mg-d	mg/l					
	12	3.48	1.11	1	6.5	0.14					
7	K22	KD2	FK2	KS22							
	mg/mg-d	L/kg		mg/l							
	0.64	0.5	2	1.63							
8	KHAL	PA1	PA2								
	mg/l	mg/l	mg/l								
	800	0	0								
9	Y	YE	B	BI	TC	TC2					
mg cells/mg l	e c/e d	1/d	1/d	mg/mg	mg/mg						
	0.790	0.5	0.1	0.1	0.0504	0.11					
10	D	FD	CDOD								
	g ea/g ed :tn degra ce g ea/g cells										
	4	0.8	1.42								
11	IRAD	ICON	IPRINT	IDBRK	ICXAI						
radial coord?	print data?		ode for rui		mg/L						
	2	2	1	11	0						
12	PT0	PT1	PT2	PT3	PULSE1	PULSE2	PULSE3	PULSE4	PULSE5	PULSE6	
	days of pulsing cyles				days: 1st pulse=>1st pulse time, 2nd pulse=> 2nd pulse time						
					T<PT0	T<PT2		T<PT3			
	9	31	31	31	0.01	0.042	0.083	1	0.083	1	
13	CS2PI0	CS2PI1	CS2PI2	CS2PI3	CS2PI4	CS2PI5					
	Initial Conc in Aquifer	2nd inj C1	1st inj C1	3rd inj C1	Initial C1 in Aquifer						
	mg/l	mg/l	mg/l	mg/l	mg/l	mg/l					
	0	0	0.045	0.045	0.045	0.005					
14	CS2PI3	CS2PI4									
	mg/l	mg/l									
	0.045	0.045									
15	PS1	PS2	PS3	PS4	PS5						
	d	d	d	d	d						
	21	40	41	42	43						
16	PS21	PS22	PS23								
	d	d	d								
	21	40	41								
17	CS22PI	CS22PI0	CS22PI1	CS22PI2	CS22PI3						
	mg/l	mg/l	mg/l	mg/l	mg/l						
	C2 in Aquifer	1st Inj C2	2nd Inj C2	3rd inj C2	4th inj C2						
	0	0.14	0.175	0.175	0.175						
18	KIC1D	KIC2D	KIU1D	KIU2D	KICD1	KIC21					
	Inhibition of former on latter										
	mg/L	mg/L	mg/L	mg/L	mg/L	mg/L					
	0.843	41.786	800	800	0.019	2.27					
19	KIUD1	KIUD2	KICD2	KIC12	KIUD2	KIU12					
	mg/L	mg/L	mg/L	mg/L	mg/L	mg/L					
	0.4002	800	800	0.107	0.029	800					

*Input data for modeling sorption in Figure 5.5 (Section 5.3)*

# APPENDIX J BIOTRANSFORMATION/TRANSPORT MODEL INPUT FOR TRANSFORMATION AT S1

**Table J.1 Input Values for 1,1-DCE and 1,1,1-TCA Simulation at S1.**

Solute Transport and Degradation Model Input Parameters Listing TCA vs DCE										ED CAH#1 CAH#2	BUTANE DCE TCA
LINE #	DH m2/d	QU m3/d									
1	0.31	1									
2	POR	THICK	WIDTH								
	-	m	m								
	0.333	1.5	1								
3	IMAX	NSTOP	NT	HT	XMAX						
	# spatial nodes	tot iterations	rec. iters.	days/iteration	tot dist						
	25	220000	30	0.0003	2.4						
4	CPSD1	CPSD2	CPSA1	CPSA2	CPD2	CPD3	CPD4	CPD5	CPA2	CPA3	CPA4
	mg/l	mg/l	mg/l	mg/l	mg/l	mg/l	mg/l	mg/l	mg/l	mg/l	mg/l
	0	35	25	0	35	35	35	20	5	18	25
5	DENB	FK	KD	WELRAD							
	kg/L		L/kg	m							
	1.6	2	0.69	1							
6	CXAI	K	KSD	KSA	K2	KS2					
	mg/l	mg/mg-d	mg/l	mg/l	mg/mg-d	mg/l					
	0.05	3.46	1.11	1	6.5	0.14					
7	K22	KD2	FK2	KS22							
	mg/mg-d	L/kg		mg/l							
	0.64	0.5	2	1.63							
8	KH-AL	PA1	PA2	PA3							
	mg/l	days	days	days							
	800	14	21	31							
9	Y	YE	B	BI	TC	TC2					
	mg cells/mg ed	e ole d	1/d	1/d	mg cells/mg C1	mg cells/mg C2					
	0.79	0.5	0.1	0	60	9					
10	D	FD	CDOD								
	g ea/g ed		g ea/g cells								
	4	0.8	1.42								
11	IRAD	ICON	IPRINT	IDBRK	ICXAI						
	radial coord?		print data?	node for run	mg/L						
	2	2	1	11	1						
12	PT0	PT1	PT2	PT3	PULSE1	PULSE2	PULSE3	PULSE4	PULSE5	PULSE6	PULSE7
	d	d	d	d		days: 1st pulse=>1st pulse time, 2nd pulse=>2nd pulse time, etc.					
					T<PT0	T<PT2	T<PT3	T<PT3	T<PT3	T<PT3	T<PT3
	11	14	21	31	0.01	0.042	0.063	1	0.042	1	0.01
13	CSDP10	CSAP10	CS2P1	CS2P10	CS2P12	CS2					
	CD in Aquifer	CA in Aquifer	2nd C1 Inj	1st C1 Inj	3rd C1 Inj	C1 in Aquifer					
	mg/l	mg/l	mg/l	mg/l	mg/l	mg/l					
	0	0	0.055	0.055	0.055	0.07					
14	CS2P13	CS2P14									
	4th C1 Inj	5th C1 Inj									
	mg/l	mg/l									
	0.055	0.055									
15	PS1	PS2	PS3	PS4	PS5						
	d	d	d	d	d						
	21	40	41	42	43						
16	PS21	PS22	PS23								
	d	d	d								
	21	40	41								
17	CS22P1	CS22P10	CS22P1	CS22P2	CS22P3						
	C2 in Aquifer	1st C2 Inj	2nd C2 Inj	3rd C2 Inj	4th C2 Inj						
	mg/l	mg/l	mg/l	mg/l	mg/l						
	0.14	0.14	0.175	0.175	0.175						
18	KIC1D	KIC2D	KIU1D	KIU2D	KICD1	KIC21					
	mg/L	mg/L	mg/L	mg/L	mg/L	mg/L					
	0.843	41.796	800	800	0.019	2.27					
19	KIUD1	KIUD21	KICD2	KIC12	KIUD2	KIU12					
	mg/L	mg/L	mg/L	mg/L	mg/L	mg/L					
	0.4002	800	800	0.107	0.029	800					

Initial microbial distribution is tabulated in Appendix L.

Input data for modeling biotransformation in Figure 5.9 (Section 5.5)



# APPENDIX J, CONTINUED BIOTRANSFORMATION/TRANSPORT MODEL INPUT FOR TRANSFORMATION AT S1

**Table J.2 Input Values for 1,1-DCE and 1,1-DCA Simulation at S1.**

Solute Transport and Degradation Model Input Parameters Listing DCA vs DCE									
		ED CAH#1 CAH#2		BUTANE DOE DCA					
LINE #									
1	DH1 m2/d	QU1 m3/d							
	0.31	1							
2	POR1	THICK m	WIDTH m						
	0.333	1.5	1						
3	IMAX	NSTOP	NT	HT	XMAX				
	# spatial nodes	tot iterations	rec. iters.	days/iteration	tot dist				
	25	220020	30	0.0003	2.4				
4	CPSD1 mg/l	CPSD2 mg/l	CPSA1 mg/l	CPSA2 mg/l	CPD2 mg/l	CPD3 mg/l	CPD4 mg/l	CPD5 mg/l	CPA2 mg/l
	0	35	25	0	35	35	35	20	5
5	DENB kg/L	FK	KD L/kg	WELRAD m					
	1.8	2	0.69	1					
6	CXAI mg/l	K	KSD mg/l	KSA mg/l	K2 mg/mg-d	KS2 mg/l			
	0.05	3.46	1.11	1	6.5	0.14			
7	K22 mg/mg-d	KD2 L/kg	FK2	KS22 mg/l					
	1.16	0.5	2	1.9					
8	KHAL mg/l	PA1 days	PA2 days	PA3 days					
	800	14	21	31					
9	Y mg cells/mg ed	YE e of e d	B 1/d	BI 1/d	TC mg cells/mg C1	TC2 mg cells/mg C2			
	0.79	0.5	0.1	0	60	9			
10	D g ea/g ed	FD	ODOD g ea/g cells						
	4	0.8	1.42						
11	IRAD radial coord?	ICON	IPRINT print data?	IDBRK node for run	ICXAI mg/L				
	2	2	1	11	1				
12	PT0 d	PT1 d	PT2 d	PT3 d	PULSE1	PULSE2	PULSE3	PULSE4	PULSE5
						days: 1st pulse=>1st pulse time, 2nd pulse=>2nd pulse time, etc.			
	11	14	21	31	0.01	0.042	0.063	1	0.042
					T<PT0		T<PT2	T<PT3	T>PT3
13	CSDP10 mg/l	CSAP10 mg/l	CS2P1 mg/l	CS2P10 mg/l	CS2P12 mg/l	CS21 mg/l			
	0	0	0.055	0.055	0.055	0.07			
14	CS2P13 4th C1 Inj mg/l	CS2P14 5th C1 Inj mg/l							
	0.055	0.055							
15	PS1 d	PS2 d	PS3 d	PS4 d	PS5 d				
	21	40	41	42	43				
16	PS21 d	PS22 d	PS23 d						
	11	25	51						
17	CS22P1 C2 In Aquifer mg/l	CS22P10 1st C2 Inj mg/l	CS22P1 2nd C2 Inj mg/l	CS22P2 3rd C2 Inj mg/l	CS22P3 4th C2 Inj mg/l				
	0.15	0.2	0.1	0.175	0.15				
18	KIC1D mg/L	KIC2D mg/L	KIUD mg/L	KIUD2 mg/L	KICD1 mg/L	KIC21 mg/L			
	0.843	39.88	800	800	0.019	1.781			
19	KIUD1 mg/L	KIUD21 mg/L	KICD2 mg/L	KIC12 mg/L	KIUD2 mg/L	KIUD12 mg/L			
	0.4002	800	800	0.343	0.232	800			

*Initial microbial distribution is tabulated in Appendix L.*

*Input data for modeling biotransformation in Figure 5.9 (Section 5.5)*

APPENDIX K  
PARAMETER DESCRIPTIONS FOR BIOTRANSFORMATION/TRANSPORT  
MODEL\*

*\*Parameter in parentheses denote that presented in Appendix A*

B (b)	Cell Decay Coefficient ( $\text{day}^{-1}$ )
BI	Enzyme Decay Coeff. ( $\text{day}^{-1}$ ); set to 0 for ED continually present
CDOD ( $d_c$ )	Cell Decay Oxygen Demand (g EA/g cells)
CPD2-5	Injected Concentration of ED at Various Pulsing Times (mg/L)
CPSA1	1 <sup>st</sup> Injection Concentration of EA Substrate (mg/L)
CPSA2	2 <sup>nd</sup> Injection Concentration of EA Substrate (mg/L)
CPSD1	1 <sup>st</sup> Injection Concentration of ED Substrate (mg/L)
CPSD2	2 <sup>nd</sup> Injection Concentration of ED Substrate (mg/L)
CS22PI	Initial Aq. Conc. of CAH#2 within Aquifer (mg/L)
CS22PI0	1 <sup>st</sup> Injection Conc. of CAH#2 (mg/L)
CS22P1-3	2 <sup>nd</sup> , 3 <sup>rd</sup> , & 4 <sup>th</sup> Injection Conc. of CAH#2 (mg/L)
CS2I	Initial Aq. Conc. of CAH #1 within Aquifer (mg/L)

APPENDIX K, CONTINUED  
PARAMETER DESCRIPTIONS FOR TRANSPORT MODEL

CS2PI	2nd Injection Concentration of CAH #1 (mg/L)
CS2PI0	1 <sup>st</sup> Injection Conc. of CAH #1 (mg/L)
CS2PI2	3 <sup>rd</sup> Injection Conc. of CAH #1 (mg/L)
CS2PI3	4 <sup>th</sup> Injection Conc. of CAH #1 (mg/L)
CS2PI4	5 <sup>th</sup> Injection Conc. of CAH #1 (mg/L)
CSAPI0	Initial Aq. Conc. of EA within Aquifer (mg/L)
CSDPI0	Initial Aq. Conc. of ED within Aquifer (mg/L)
CXAI (X <sub>0</sub> )	Initial Uniform Distributed Biomass (mg/L)
D (F <sub>a</sub> )	EA/ED Utilization for Biomass Synthesis (g EA/g ED)
DENB (ρ <sub>b</sub> )	Density of Solids for Retardation Calculation (kg/L)
DHI (D <sub>h</sub> )	Dispersion Coeff. (input parameter) (m <sup>2</sup> /day)
FD (f <sub>d</sub> )	Fraction of Degrading Cells (0.8 per literature)
FK (F <sub>k1</sub> )	Mass Transfer Rate Sorption Parameter for CAH#1 (day <sup>-1</sup> )

APPENDIX K, CONTINUED  
PARAMETER DESCRIPTIONS FOR TRANSPORT MODEL

FK2 ( $F_{k2}$ )	Mass Transfer Rate Sorption Parameter for CAH#2 ( $\text{day}^{-1}$ )
HT	Time Step for Calculating Values (days/iteration) (Time Step = $NT \cdot HT$ ) (Total Simulation Time = $NSTOP \cdot HT$ )
ICXAI	Whether or Not There is Initially Distributed Biomass (yes =1)
IDBRK	Location (Node) for which Data is Recorded/Printed
IMAX	No. of Spatial Nodes within Test Zone, spacing = $(IMAX-1)/XMAX$
IPRINT	Whether or not to Print (yes = 1)
IRAD	Determines whether Radial Coords. are Used (yes = 1)
K ( $k_{mD}$ )	Maximum Utilization Rate of ED (mg/mg/d)
K2 ( $k_{m1}$ )	Maximum Utilization Rate of CAH#1 (mg/mg/d)
K22 ( $k_{m2}$ )	Maximum Utilization Rate of CAH#2 (mg/mg/d)
KD ( $k_{d1}$ )	Sorption Coeff of CAH#1 (L/kg)
KD2 ( $k_{d2}$ )	Sorption Coeff of CAH#2 (L/kg)

APPENDIX K, CONTINUED  
PARAMETER DESCRIPTIONS FOR TRANSPORT MODEL

KHAL ( $K_{HAL}$ ) Haldane's Constant (a measure of ED's toxicity, high # => low tox.)

KIC1D( $K_{ic1D}$ ) Competitive Inhibition Constant of CAH#1 on ED (mg/L)

KIC2D( $K_{ic2D}$ ) Competitive Inhibition Constant of CAH#2 on ED (mg/L)

KIU1D( $K_{iu1D}$ ) Noncompetitive Inhibition Constant of CAH#1 on ED (mg/L)

KIU2D( $K_{iu2D}$ ) Noncompetitive Inhibition Constant of CAH#2 on ED (mg/L)

KICD1( $K_{icD1}$ ) Competitive Inhibition Constant of ED on CAH#1 (mg/L)

KIC21( $K_{ic21}$ ) Competitive Inhibition Constant of CAH#2 on CAH#1 (mg/L)

KIUD1( $K_{iuD1}$ ) Noncompetitive Inhibition Constant of ED on CAH#1 (mg/L)

KIU21 ( $K_{iu21}$ ) Noncompetitive Inhibition Constant of CAH#2 on CAH#1

KICD2( $K_{icD2}$ ) Competitive Inhibition Constant of ED on CAH#2 (mg/L)

KIC12 ( $K_{ic12}$ ) Competitive Inhibition Constant of CAH#1 on CAH#2 (mg/L)

KIUD2( $K_{iuD2}$ ) Noncompetitive Inhibition Constant of ED on CAH#2 (mg/L)

KIU12 ( $K_{iu12}$ ) Noncompetitive Inhibition Constant of CAH#1 on CAH#2 (mg/L)

APPENDIX K, CONTINUED  
PARAMETER DESCRIPTIONS FOR TRANSPORT MODEL

KS2 ( $K_{s1}$ )	Half-Saturation Coeff for CAH#1 (mg/L)
KS22 ( $K_{s2}$ )	Half-Saturation Coeff. of CAH#2 (mg/L)
KSA ( $K_{sA}$ )	Half-Saturation Coeff for EA (mg/L)
KSD ( $K_{sD}$ )	Half-Saturation Coeff for ED (mg/L)
NSTOP	Total # of Iterations
NT	Iteration Step at which to Record/Print values (Time Step = NT*HT)
PORI ( $\phi$ )	Porosity (input parameter)
PS1-5	Time @ which Inj. (boundary) Conc. changes for CAH#1 (days)
PS21-3	Time @ which Inj. (boundary) Conc. changes for CAH#2 (days)
PT0-3	Time @ which ED Injection (boundary) Conc. & pulse duration change (days)
PULSE 1-6	Pulsing Duration for injecting ED, odd #s (days) Pulsing Duration for injecting ED and EA (total cycle!), even #s (days)
QLI (Q)	Volumetric Flow Rate ( $m^3/day$ )

APPENDIX K, CONTINUED  
PARAMETER DESCRIPTIONS FOR TRANSPORT MODEL

TC ( $T_{c1}$ )	Transformation Capacity of CAH#1 (mg cells/mg CAH#1) Yes! This is inverse of standard TC (mg substrate/mg cells)
TC2 ( $T_{c2}$ )	Transformation Capacity of CAH#2 (mg cells/mg CAH#2) Yes! This is inverse of standard TC (mg substrate/mg cells)
THICK	Aquifer Thickness (m)
WIDTH	Aquifer Width (m)
XMAX	Total Simulation Distance (m)
Y	Cell Yield (mg cells/mg ED)
YE	ec/ed Yield for Oxygen Consumption

APPENDIX L  
INITIAL MICROBIAL DISTRIBUTION ASSUMED WITHIN AQUIFER FOR  
BIOAUGMENTATION MODELING\*

**Table L.1 Initial Microbial Distribution for Biotransformation Simulations.**

<b>Dist (m)</b>	0	0.1	0.2	0.3	0.4	0.5	0.6	0.7	0.8
<b>Conc (mg/L)</b>	12.0	6	3	2	1	.5	.25	.125	.06
<b>Dist (m)</b>	0.9	1.0	1.1	1.2	1.3	1.4	1.5	1.6	1.7
<b>Conc (mg/L)</b>	.03	.02	.01	.01	.01	.005	.0025	.001	.0005
<b>Dist (m)</b>	1.8	1.9	2.0	2.1	2.2	2.3	2.4		
<b>Conc (mg/L)</b>	.0005	.0005	.0005	.0005	.0005	.0005	.0005		

---

*\*Used for modeling in Section 5.5.*



APPENDIX M  
1,1-DCE TRANSFORMATION CAPACITY ( $T_{CDCE}$ ) INPUT VALUES FOR  
SENSITIVITY ANALYSIS OF BIOTRANSFORMATION/TRANSPORT MODEL

**Table M.1  $T_{CDCE}$  Input Values for Sensitivity Analysis.**

<u>mg 1,1-DCE/ mg cells*</u>	<u>mg cells/mg 1,1-DCE**</u>
0.0167	60
0.025	40
0.05	20

*\*Conventional units used for transformation capacity*

*\*\*Units used for input with biotransformation/transport model*

# APPENDIX N BIOTRANSFORMATION/TRANSPORT MODEL INPUT FOR VARIED FIRST ORDER MASS TRANSFER SORPTION RATE AND PULSING DURATIONS

**Table N.1 Input Values for Variations in Mass Transfer Sorption Rate and Butane and Oxygen Pulsing Durations.**

Solute Transport and Degradation Model											
Input Parameters Listing											
Fk variation and longer pulse durations											
ED											
CAH#1											
CAH#2											
DCE											
TCA											
LINE #											
1	DHI	QLI									
	m2/d	m3/d									
	0.31	1									
2	PORI	THICK	WIDTH								
	-	m	m								
	0.333	1.5	1								
3	IMAX	NSTOP	NT	HT	XMAX						
	# spatial nodes	iteration	ec. iteration	d/iteration	tot dist						
	25	2200020	30	0.0003	2.4						
4	CPSD1	CPSD2	CPSA1	CPSA2	CPD2	CPD3	CPD4	CPD5	CPA2	CPA3	CPA4
	mg/l	mg/l	mg/l	mg/l	mg/l	mg/l	mg/l	mg/l	mg/l	mg/l	mg/l
	0	35	25	0	35	35	35	35	25	25	25
5	DENB	FK	KD	WELRAD							
	kg/L		L/kg	m							
	1.6	2.0	0.2	0.69	1						
6	CXAI	K	KSD	KSA	K2	KS2					
	mg/l	mg/mg-d	mg/l	mg/l	mg/mg-d	mg/l					
	0.6	3.48	1.11	1	6.6	0.14					
7	K22	KD2	FK2	KS22							
	mg/mg-d	L/kg		mg/l							
	0.64	0.5	2.0	0.2	1.83						
8	KHAL	PA1	PA2	PA3							
	mg/l	mg/l	mg/l	mg/l							
	800	14	21	31							
9	Y	YE	B	BI	TC	TC2					
	mg cells/mg l	e c/e d	1/d	1/d	mg/mg	mg/mg					
	0.790	0.5	0.1	0	60.0000	9					
10	D	FD	CDOD								
	g ea/g ed	tn degra	ce g ea/g cells								
	4	0.8	1.42								
11	IRAD	ICON	IPRINT	IDBRK	ICXAI						
	radial coord?	print data?			ode for run	mg/L					
	2	2	1	11	0						
12	PT0	PT1	PT2	PT3	PULSE1	PULSE2	PULSE3	PULSE4	PULSE5	PULSE6	PULSE7 PULSE8
	days of pulsing cycles				days: 1st pulse=>1st pulse time, 2nd pulse=> 2nd pulse time						
					T<PT0 T<PT2 T<PT3 T>PT3						
	21	22	23	24	0.01	0.042	0.125	0.6	0.125	0.5	0.125 0.5
13	CSDPI0	CSAPI0	CS2PI	CS2PI0	CS2PI2	CS2I					
	Initial Conc in Aquifer 2nd inj C1 1st inj C1 3rd inj C1 Initial C1 in Aquifer										
	mg/l	mg/l	mg/l	mg/l	mg/l	mg/l					
	0	0	0.065	0.065	0.065	0.07					
14	CS2PI3	CS2PI4									
	mg/l	mg/l									
	4th inj C1 5th inj C1										
	0.065	0.065									
15	PS1	PS2	PS3	PS4	PS5						
	d	d	d	d	d						
	21	40	41	42	43						
16	PS21	PS22	PS23								
	d	d	d								
	21	40	41								
17	CS22PI	CS22PI0	CS22PI	CS22P2	CS22P3						
	mg/l	mg/l	mg/l	mg/l	mg/l						
	C2 in Aquifer 1st Inj C2 2nd Inj C2 3rd inj C2 4th inj C2										
	0.14	0.14	0.175	0.175	0.175						
18	KIC1D	KIC2D	KIU1D	KIU2D	KICD1	KIC21					
	Inhibition of former on latter										
	mg/L	mg/L	mg/L	mg/L	mg/L	mg/L					
	0.843	41.786	800	800	0.019	2.27					
19	KIUD1	KIU21	KICD2	KIC12	KIUD2	KIU12					
	mg/L	mg/L	mg/L	mg/L	mg/L	mg/L					
	0.4002	800	800	0.107	0.029	800					

Input data for modeling biotransformation in Figure 5.14 (Section 5.5.5)